University of Canterbury

Doctoral Thesis

Model-Based Decision Support in Glycaemic Control

Author:
Liam Fisk

Supervisor:
Dr. J. Geoffrey Chase

A thesis submitted in fulfilment of the requirements for the degree of Doctor of Philosophy

in the

Centre for Bioengineering
Mechanical Engineering

August 2014

Declaration of Authorship

I, Liam Fisk, declare that this thesis titled, 'Model-Based Decision Support in Glycaemic Control' and the work presented in it are my own. I confirm that:

- This work was done wholly or mainly while in candidature for a research degree at this University.
- Where any part of this thesis has previously been submitted for a degree or any other qualification at this University or any other institution, this has been clearly stated.
- Where I have consulted the published work of others, this is always clearly attributed.
- Where I have quoted from the work of others, the source is always given. With the exception of such quotations, this thesis is entirely my own work.
- I have acknowledged all main sources of help.
- Where the thesis is based on work done by myself jointly with others, I have made clear exactly what was done by others and what I have contributed myself.

Signed: _____

Date: _____

"Which would you prefer: a descriptive model backed by physiological evidence or a monkey who simply tells you the right answer?"

J. Geoffrey Chase

UNIVERSITY OF CANTERBURY

Abstract

College of Engineering
Mechanical Engineering

Doctor of Philosophy

Model-Based Decision Support in Glycaemic Control

by Liam Fisk

Model-based decision support relies on a series of mathematical models and methods to convert raw clinical data into actionable recommendations. High clinical burden associated with measurement, and clinically significant outcomes, make glycaemic control an area where considerable benefit is possible. However, few glycaemic control protocols have been successful in critical care, and fewer exist for outpatient management of diabetes. Challenges faced include high levels of uncertainty and noise, limited measurements, and risk of iatraogenic low blood glucose events. This thesis aims to develop a successful glycaemic control framework, STAR, beyond the critical care environment, and set the stage for an outpatient glycaemic control protocol that individuals with diabetes can use to inform their day-to-day glucose management decisions. To achieve this goal, appropriate models and methods are developed, and validated against both clinical and *in-silico* data.

Acknowledgements

I would like to thank the Center for Bioengineering, and specifically Jennifer Dickson. Instead of just soundproofing my cubicle, they all put up with my rambling, and the conversations I've had there have been illuminating. Jenn, if I hadn't had you to discuss ideas with, the whole experience would have been rather isolating. I also thank you for the potluck lunches - it was rather a genius idea to conscript the hordes of international students to cook for us.

Also, I'd like to thank the three then-postdocs for keeping me in line: Aaron Le Compte, Paul Docherty, and Chris Pretty. Aaron was the reason I did a Ph.D. at all - his sheer competence was inspiring, and he spent over a year answering every question I could muster, and teaching me whatever skills I needed. Aaron, you gave me your time no matter how busy you were, or how basic my questions became, and I appreciate that more than I can express.

On the other hand, Paul taught me something very specific: If it looks stupid, but it works, it ain't stupid. Under his tutelage I learned to get a prototype up and running as quickly as possible, and this approach taught me more about mathematics in a month than I had learned to date. Most of this thesis was born of a single conversation with Paul, and to him I credit my new-found ability to understand mathematics papers. Paul, I enjoyed our conversations and thank you for the skills you taught me. I believe what I learned from you is one of the most valuable skills I now possess.

And Chris, you gave me perspective. Like Aaron, you have that overarching competence that is reflected in both word and deed, and you balance a critical eye with an ability to recognise positive aspects. That being said, I do pity some of the students who submitted those lab reports.

Next, my studies wouldn't have been the same without Dr Geoffrey Shaw. Being involved in the ICU was perhaps one of the most valuable experiences I've had, and was central to showing me the potential of engineering. You were a constant font of ideas and energy, and your trust was empowering. And I learned about a vast range of topics just by sitting in the same room as you.

Above all, I would like to thank Professor Geoffrey Chase. He gave me a myriad of opportunities, and afforded me a great deal of freedom in my research. His door was always open for discussions, even if the flood of emails was reaching critical mass.

Because of Geoff, I'm leaving my Ph.D. the same way I started - uncertain of what to do next - but with a range of experiences that have given me insight. This insight has

given me confidence in my abilities, a belief that I will be able to contribute no matter what I decide to do, and a desire to understand the world around me. His omnivorous approach to research changed my perspective of academic pursuits, and his inclusive approach to credit was a lesson in itself. And of course, I appreciate the time he spent with a troublesome student.

My family is a constant in an uncertain future, and for that I thank them all. To Matt: you brought me back into the fold, and I appreciate what our relationship has become. To James and Ella: I'm seeing you both grow, and now I can see the people you might be in the future. Keep going where you are headed, and you'll both be something special. To Mum and Dad: I wouldn't be here without your support, and each of you is an inspiration in your own way. Between you, you've taught me empathy, integrity, and to look for meaning.

Lastly, Yeri Kim. The story of my Ph.D. has been as much a story of our relationship, and we have both grown during these years. There have been both parallels and contrasts between our experience of doctoral studies, but it was comforting to be walking the same path as a loved one. I can't imagine having done this without you, Yeri, and I hope I can also help you to achieve your goals.

Contents

List of Figures

List of Tables

Abbreviations

AGC	**A**ccurate **G**lycaemic **C**ontrol
ATP	**A**denosine **T**ri**P**hosphate
BG	**B**lood **G**lucose
BMI	**B**ody **M**ass **I**ndex
CDF	**C**umulative **D**ensity **F**unction
DISST	**D**ynamic **I**nsulin **S**ensitivity and **S**ectretion **T**est
ECF	**E**xtra**C**ellular **F**luid
FPG	**F**asting **P**lasma **G**lucose
ICING	**I**ntensive **C**ontrol **I**nsulin-**N**utrition-**G**lucose
ICU	**I**ntensive **C**are **U**nit
IFG	**I**mpaired **F**asting **G**lucose
IGT	**I**mpaired **G**lucose **T**olerance
IMGU	**I**nsulin **M**ediated **G**lucose **U**ptake
IQR	**I**nter-**Q**uartile **R**ange
IV	**I**ntra**V**enous
IVGTT	**IV G**lucose **T**olerance **T**est
MPC	**M**odel **P**redictive **C**ontrol
NGT	**N**ormal **G**lucose **T**olerance
NIMGU	**N**on-**I**nsulin **M**ediated **G**lucose **U**ptake
NPH	**N**eutral **P**rotamine **H**agedorn
OGTT	**O**ral **G**lucose **T**olerance **T**est
PDF	**P**robability **D**ensity **F**unction
PID	**P**roportional-**I**ntegral-**D**erivative
RMS	**R**oot **M**ean **S**quared
SDE	**S**tochastic **D**ifferential **E**quation

SPRINT	**S**pecialised **R**elative **I**nsulin and **N**utrition **T**ables
STAR	**S**tochastic **TAR**geted glycaemic control
T1DM	**T**ype **1** **D**iabetes **M**ellitus
T2DM	**T**ype **2** **D**iabetes **M**ellitus

Symbols

S_I	model-based insulin sensitivity	$\mathrm{L.mU^{-1}.min^{-1}}$
G_x	internal glucose process noise	$\mathrm{mmol.L^{-1}.min^{-1}}$

For Yeri

Chapter 1

Introduction

The problem of hyperglycaemia begins with acute care and ends with management of diabetes. Diabetes is a general term for a range of metabolic conditions, each resulting in chronic hyperglycaemia [1]. Hyperglycaemia is defined as elevated blood glucose concentrations (BG), and can be caused by a wide range of metabolic dysfunctions. Not only is hyperglycaemia the root cause of long term complications in diabetes [2], but the condition has also been correlated with morbidity and mortality in a hospital setting [3]. While critically ill patients may also be diabetic, the physiological stress of injury can cause significantly elevated BG [4]. This research attempts to link model-based insulin therapy in a hospital setting with out-patient management of diabetes. To achieve this, both *in-silico* and real-world data sets are used to develop mathematical models and methods for prediction and dose-optimisation algorithms.

1.1 Glucose homoeostasis

While an exhaustive review of glucose homoeostatic mechanisms is not necessary, a broad overview is useful to establish the physiological context of this work. In the human body, the main dietary energy sources are carbohydrates and fats [5]. Oxidation of these compounds produces adenosine triphosphate (ATP), which is then available for use within cells. The substrates that are not immediately oxidised after absorption are stored, with carbohydrates stored as glycogen, and fats as triglycerides. As glycaemic control is by definition management of blood glucose, fatty acid concentrations are not considered in this work.

After carbohydrate consumption and absorption into circulation, complex carbohydrates are reduced to monosaccharides by the liver. The only monosaccharides present in physiological relevant concentrations are glucose or fructose [6]. The major monosaccharide transporters are the facilitated diffusion GLUT transporters, with GLUT-5 targeting fructose and the remaining 6 targeting glucose. The majority of GLUT family receptors are located on the cell surface, though a portion of GLUT-4 is associated with intracellular vesicles, and is recruited to the cell surface in response to insulin. After transport, the molecules are oxidised to produce ATP.

Postprandial glucose oxidation is approximately 10 $g.hr^{-1}$ [5]. All remaining glucose is converted to glycogen through glycogenesis, a process which consumes 5% of the total energy content. Glycogen storage occurs in both hepatic and muscle tissues, where hepatic tissues have high glycogen affinity and muscle tissues have much lower affinities. However, the relative total tissue masses mean the total glycogen stored in muscle tissue is around 3 to 4 times greater than that in hepatic tissues.

Future glucose demand is thus met through a combination of glycogenolysis and gluconeogenesis. Glycogenolysis is the production of glucose from stored glycogen, and gluconeogenesis is the production of glucose from other substrates. Gluconeogenesis occurs mainly in the liver and kidneys, with renal glucose balance typically zero, but able to compensate for compromised hepatic production [7].

A complex signalling relationship exists between the liver and pancreas. A number of hormones that are secreted by the pancreas directly into the hepatic portal vein, entering the liver in high concentrations. Briefly, alpha cells secrete the hormone glucagon, which promotes endogenous glucose production [8] by activating glycogen phosphorylase in liver hepatocytes, an enzyme that hydrolyses glycogen in glycogenolysis. In contrast, beta cells secrete insulin, which promotes glycogenesis in hepatocytes [9]. Additionally, insulin increases glucose transport in fat and muscle cells by stimulating the translocation of the transporter GLUT4 from intracellular sites to the plasma membrane [10]. The most significant contributors to glucose homoeostasis are summarised in Figure 1.1.

1.1.1 Glucose dysregluation

The mechanism by which the human body maintains euglycaemia is complex, and dysregulation can occur. Compensatory mechanisms exist, such as increased insulin secretion in the face of insulin resistance, or upregulation of gluconeogenesis in the kidney when hepatic glucose production is insufficient. However, both acute and chronic dysregulation occur, with clinically significant effects. Chronic dysregulation is broadly labelled as diabetes mellitus.

Initial signs of chronic impairment are impaired fasting glucose (IFG) and impaired glucose tolerance (IGT). IFG is defined as fasting plasma glucose (FPG) levels between

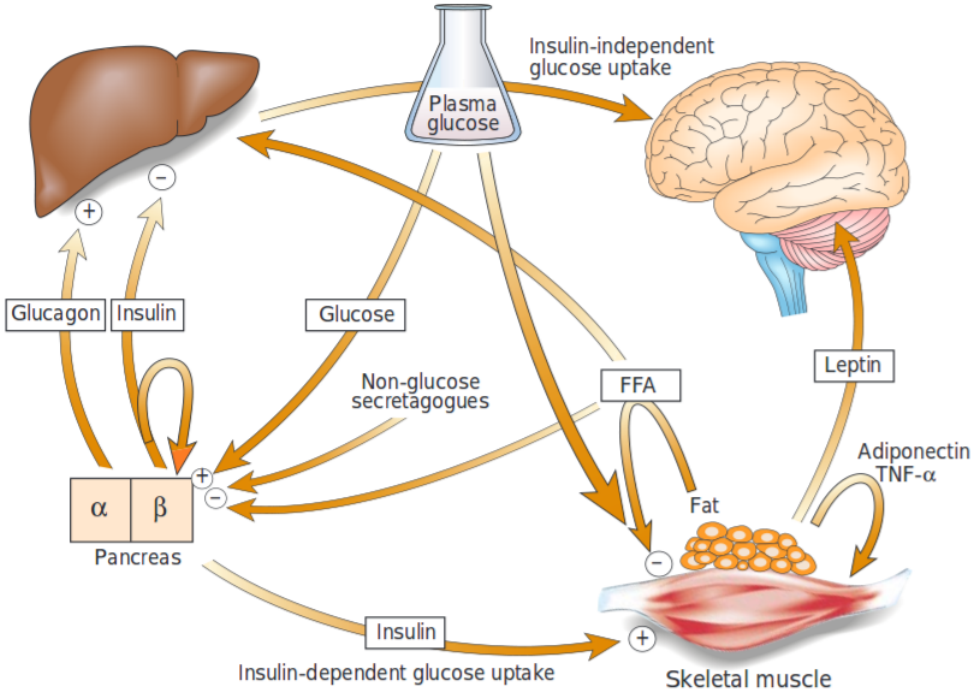

FIGURE 1.1: *Main mechanisms of glucose homoeostasis, reproduced from [10].*

5.6 mmol.L^{-1} and 6.9 mmol.L^{-1}, while IGT is defined as BG between 7.8 mmol.L^{-1} and 11.0 mmol.L^{-1} 2 hours after ingesting 75g of glucose orally, as part of the oral glucose tolerance test (OGTT) [1]. Values exceeding these ranges are currently used as diagnostic criteria for diabetes mellitus.

The two major categories of diabetes mellitus are type 1 (T1DM) and type 2 (T2DM). T1DM accounts for approximately 5% to 10% of all cases, and is characterised by cellular-mediated autoimmune destruction of the β-cells of the pancreas [1]. Absolute insulin deficiency thus results. In contrast, T2DM encompasses individuals who have insulin resistance and usually have relative (rather than absolute) insulin deficiency. These individuals comprise 90% to 95% of those with diabetes. Other genetic defects, diseases, and chemicals can cause diabetes mellitus. It is estimated diabetes affects at least 285 million people worldwide, and it was estimated that diabetes accounted for

12% of global health expenditures in 2010, or at least $376 billion [11].

The primary symptom in diabetes mellitus is high blood glucose concentrations (hyperglycaemia). Individuals suffering from marked hyperglycaemia experience polyuria, polydipsia, weight-loss (sometimes with polyphagia), and blurred vision. Acute, life-threatening consequences of uncontrolled glycaemia are hyperglycaemia with ketoacidosis or the non-ketotic hyperosmolar syndrome. Longer term complications include retinopathy with potential loss of vision; nephropathy leading to renal failure; peripheral neuropathy with risk of foot ulcers, amputations, and Charcot joints; and autonomic neuropathy causing gastrointestinal, genitourinary, and cardiovascular symptoms and sexual dysfunction. Patients with diabetes have an increased incidence of atherosclerotic cardiovascular, peripheral arterial, and cerebrovascular disease. Hypertension and abnormalities of lipoprotein metabolism are often found in people with diabetes. Impairment of growth and susceptibility to certain infections may also accompany chronic hyperglycaemia [1].

Administration of exogenous insulin lowers BG, and can produce hypoglycaemia. Mild hypoglycaemic events can induce unpleasant symptoms, while severe hypoglycaemia can cause neurological impairments. Symptoms include anxiety, palpitations, tremor, sweating, hunger, and paresthesias, while neurological impairments include behavioural changes, cognitive dysfunction, seizures, and coma. Additionally, focal neurological deficits can occur. Although severe prolonged hypoglycaemia can cause permanent brain damage, typically complete recovery is made [12].

Recurrent hypoglycaemia is the norm in T1DM. When maintaining glycaemic control, plasma glucose levels may be less than 2.8 to 3.3 mmol.L^{-1} 10% of the time. Typically, two episodes of symptomatic hypoglycaemia occur per week. An estimated 2% to 4% of

deaths of people with T1DM have been attributed to hypoglycaemia. The rates of severe hypoglycaemia in T2DM are roughly 10% of those in T1DM, even during aggressive insulin therapy. However, quantitative data from patients with T2DM treated to near-euglycaemia with rigorous ascertainment of hypoglycaemia are not available [12].

In critical illness, even non-diabetic individuals can experience acute or chronic hyperglycaemia. Stress-induced hyperglycaemia affects 30-50% of critically ill patients, and increases morbidity and mortality [4, 13]. While BG is difficult to control using insulin due to hypoglycaemic risk [14], both extremes, as well as glycemic variability, have been independently linked to increased morbidity and mortality [15–17].

1.2 Management of diabetes

Management of diabetes is a difficult task, with a variety of goals and management strategies. The American Diabetes Association recommends a glycated hemoglobin (HbA1C) A1C level less than 7%. Historic data from the United States between 1988 and 1995 showed 43% of individuals with diabetes in the United States had an HbA1C level greater than 8.0%, with 18% greater than 9.5%, and 24% of the insulin-treated patients had poor control. More than 50% of those with T1DM used only 1 to 2 insulin injections per day, and many patients with T2DM did not achieve adequate control using twice-daily neutral protamine Hagedorn (NPH insulin) [18].

Mechanism of management varies between individuals and form of diabetes. Due to absolute insulin deficiency, T1DM individuals require insulin for survival. During early stages, residual β cell function enables some individuals to remain on basal bolus insulin therapy only. This therapy involves once- or twice- daily injections of long-acting insulin (e.g. NPH or glargine). More severe insulin deficiency requires a physiologic insulin

regime, where basal and prandial insulin doses are used to mimic a normal secretion pattern [18]. Current research on an artificial pancreas is ongoing, where continuous glucose monitors and closed loop control algorithms are used to automate glycaemic control [19]. While no commercial product currently exists, several are in development. However, the artificial pancreas has high associated costs, adding to the already substantial financial burden of diabetes.

Management of T2DM is much more variable. T2DM differs from T1DM in that insulin resistance is typically a significant factor, and oral medications are thus useful. Initially, insulin sensitisers (e.g. metformin) or secretagogues (e.g. sulfonylurea) may be sufficient to normalise BG. As the disease progresses, basal insulin replacement is required, and as β cell function declines physiologic insulin regimes are followed. Combination insulin/oral medication regimes can be effective in reducing weight gain and incidence of hypoglycaemia for similar control [18].

1.3 Glycaemic control in acute care

Treating hyperglycaemia in critical illness is substantially different from managing diabetes. Nutrition inputs are highly regulated, frequent BG measurements can be taken, and exercise/other lifestyle factors are not a factor. Insulin administration is typically intravenous (IV), and nutrition can be administered enterally or parenterally. While greater certainty about exogenous inputs exists, the patient can have extremely variable BG due to their compromised state.

Accurate glycemic control (AGC) can reduce morbidity and mortality in critical illness [20–22], but has proven difficult to achieve safely and consistently [23–25]. Higher nursing workloads due to high density glucose readings are impractical in many units [26, 27].

Hand-held glucometers are easier for measurement, but their larger errors can add additional difficulty for some AGC protocols. Finally, clinical compliance determines much of the efficacy of any AGC method, with quality of glycemic control thus also limited by the confidence and compliance of nursing staff [27, 28].

A range of strategies have been implemented to guide insulin therapy, ranging from ad-hoc to algorithmic, and from conventional to intensive insulin therapy. As mentioned previously, these initiatives have been met with varying success, and thus no definitive solution has been agreed upon. Indeed, much debate still centres around the need for AGC, as hypoglycaemia can mitigate any benefits gained from treating hyperglycaemia, and control strategies have historically performed poorly [14].

Perhaps the most common method is the sliding scale. This methodology is conceptually simple, but is particularly rigid and cannot manage inter-patient variability. Attempting intensive insulin therapy guided by a sliding scale has led to poor outcomes in the past, with trials halted due to high incidence of hypoglycaemia and protocol violations [29]. Combining multiple sliding scales (dynamic sliding scale) based on prior glycaemic responses has led to much improved results [22, 30]. This control strategy is potentially an optimal combination of simplicity and power, but is still rigid and must be tailored for each intensive care unit (ICU).

More traditional control strategies that have been implemented include linear control. A proportional-integral-derivative (PID) controller uses a linearised model and modern control theory to optimise infusion rates. However, measurement sparsity and noise, plant non-linearities, and other factors have meant expert systems have failed to significantly outperform ad-hoc treatment [31].

A more suitable application of modern control theory has been model predictive control, or MPC [32]. This methodology involves predicting and calculating a long-term optimal control strategy at each measurement, but only implementing the first step in this control strategy. MPC lends itself well to both open-loop and closed-loop control, and has been demonstrated to be equivalent to or better than standard care [33].

Finally, another successful strategy has been model-based heuristic control [34]. A combination of deterministic and stochastic models are used to predict likely ranges of outcomes for any insulin/nutrition pair. A series of heuristic rules are used to eliminate unsatisfactory insulin/nutrition pairs, and the remaining set of pairs are ranked according to clinically specified criteria. The optimal insulin/nutrition pair is thus selected for each possible measurement interval, and implemented by the attending nurse.

1.4 Summary

Glucose homoeostasis is a complex system that is compromised in diabetes mellitus and can be affected by critical illness. Hyperglycaemia has a variety of associated morbidities, which can be mitigated by successful insulin therapy. However, insulin therapy is associated with an increased risk of hypoglycaemia, and has been difficult to achieve consistently in either acute or chronic hyperglycaemia. A range of treatment options exist for management of diabetes, but application of quantitative control is difficult and thus decision support is lacking. In contrast, many different quantitative strategies have been applied in critical illness, but have been met by limited success. This research aims to progress model-based heuristic control in the ICU, and extend the utility of this control strategy into hospital ward/outpatient management of diabetes.

Chapter 2

Improved Virtual Trial Methodology to Investigate Changes to DKA Insulin Therapy Protocol

2.1 Introduction

Virtual trials [35] are a valuable tool for *in-silico* development of glycaemic control algorithms. However, certain metabolic derangements cause periods where current model dynamics are not relevant, and thus validity of virtual trials is compromised. One case is during the initial stages of treatment of diabetic ketoacidosis (DKA), where blood glucose (BG) is extremely high, and response to insulin is limited.

DKA occurs when glucose metabolism is compromised by insufficient available insulin [36]. Fats are used in place of glucose, producing ketones, and lack of insulin inhibits ketone metabolism. Thus DKA leads to accumulation of ketones in blood and urine. Untreated, DKA leads to prolonged hyperglycaemia, and can cause cerebral edema, myocardial infarction, and kidney failure. DKA is a medical emergency, with therapy focused on correcting hyperglycaemia with intravenous insulin. Therapy often involves hourly BG measurements, which is particularly disruptive for patients overnight. This chapter investigates whether extending measurement interval to two hours is possible without compromising patient safety.

The key steps in a virtual trial are: A) fitting the underlying "true" parameter profile, B) using a protocol to choose the new treatment, and C) using the "true" parameter profile to solve for the resulting virtual BG measurement. From a virtual trial standpoint, investigating potential changes to clinical practice is challenging. During the initial stages of insulin therapy, BG is well above typical values for critically ill patients. Model dynamics are thus profoundly different [37].Correctly fitting the data is the critical step for a representative virtual trial, as failure to fit translates directly to loss of information and lesser virtual trial confidence. Due to low data density in a real-world glycaemic control setting only one parameter, insulin sensitivity (S_I), can be reliably identified [38]. Previously, this parameter has been represented as a series of rectangle functions, non-zero only on the relevant hour [39].

The Intensive Control Insulin-Nutrition-Glucose (ICING) model [40] is capable of describing glucose-insulin dynamics with BG$\leq$12mmol.L^{-1}, when hypoglycaemia is a real risk. However, the pharmacodynamic surface and fitting methods do not allow a high quality virtual patient to be generated in higher "severe" hyperglycaemic ranges [37]. Simply using the ICING model to generate an S_I profile from clinical DKA data leads

to an ill-fitting initial period, where the model is incapable of sustaining extremely high BG. Simulating a virtual trial with this S_I profile will thus cause artificially rapid normalisation of BG.

This chapter describes a method for adapting the ICING model into a simplified interpretation stochastic differential equation (SDE), where S_I is represented as a series of *b-spline* basis functions with increased local support. A process noise term, G_x, captures the variation that a regularised S_I profile cannot fit, and can natively preserve the initial high BG period of DKA therapy. Additionally, patients are typically conscious, and have been known to eat small meals during insulin therapy, which can distort the fitting S_I profile. A regularised S_I profile limits the resulting effect, with the unobserved nutrition intake primarily captured by G_x.

2.2 Methods

2.2.1 ICING model

The ICING model defines glucose and insulin kinetics and dynamics in critically ill patients [40]

$$\dot{I} = \frac{U_x + (1 - x_L)U_n}{V_I} - n_I(I - Q) - n_K I - n_L \frac{I}{1 + \alpha_G I} \tag{2.1}$$

$$\dot{Q} = n_I(I - Q) - n_C \frac{Q}{1 - \alpha_G Q} \tag{2.2}$$

$$\dot{G}(t) = -p_G G - S_I(t)\frac{G(t)Q(t)}{1 - \alpha_G Q(t)} + \frac{1}{V_G}\left(P_{EGP} - P_{CNS} + P_N(t) + \max\left(P_{max}, d_2 P_2(t)\right)\right) \tag{2.3}$$

$$P_2(t) = d_1 P_1(t) - \max\left(P_{max}, d_2 P_2(t)\right) \tag{2.4}$$

$$P_1(t) = P(t) - d_1 P_1(t) \tag{2.5}$$

where $G(t)$ [mmol.L^{-1}] is the total plasma glucose, $I(t)$ [mU.L^{-1}] is the plasma insulin, and interstitial insulin is represented by Q(t) [mU.L^{-1}]. Exogenous insulin input is represented by $U_{ex}(t)$ [mU.min^{-1}], and glucose-dependent endogenous insulin production is estimated with U_{en} [mU.min^{-1}] [41]. $S_I(t)$ [L.mU^{-1}.min^{-1}] is the identified insulin sensitivity profile, $P_1(t)$ [mmol] represents the glucose in the stomach and $P_2(t)$ [mmol] represents glucose in the gut. Enteral glucose input is denoted $P(t)$ [mmol.min^{-1}], while parenteral glucose input is denoted $P_N(t)$ [mmol.min^{-1}]. All model constants are shown in Table 2.1.

TABLE 2.1: ICING constant model parameters

Variable	Description	Value
p_G	Non-insulin mediated uptake	0.006 min^{-1}
n_I	Insulin transport rate	0.006 min^{-1}
n_K	Renal clearance	0.0542 min^{-1}
n_L	Hepatic clearance	0.1578 min^{-1}
n_C	Interstitial clearance	0.006 min^{-1}
d_1	Stomach clearance	0.0151 min^{-1}
d_1	Gut clearance	0.00301 min^{-1}
P_{max}	Maximal gut clearance	6.11 mmol.min^{-1}
P_{EGP}	Endogenous glucose production	1.16 mmol.min^{-1}
P_{CNS}	Nervous system glucose disposal	0.3 mmol.min^{-1}
x_L	First-pass hepatic extraction	0.67
V_I	Insulin volume of distribution	4.0 L
V_G	Glucose volume of distribution	13.3 L
α_I	Saturation of hepatic insulin clearance	0.0017 L.mU^{-1}
α_G	Saturation of insulin-mediated glucose uptake	0.01538 L.mU^{-1}

2.2.2 Parameter Identification

A simple version of the integral-based fitting method will be introduced via a differential equation with an unknown linear parameter, θ:

$$\dot{x} = f_0(t, x) + \theta f_1(t, x) \tag{2.6}$$

where x is the conserved quantity, θ the unknown constant parameter, $f_1(t, x)$ is the function corresponding to this parameter, and $f_0(t, x)$ contains the remaining known parameters and functions. The model estimate of x at time t is:

$$x_{mod}(t) = x_0 + \int_{t_0}^{t} f_0 \mathrm{d}t + \theta \int_{t_0}^{t} f_1 \mathrm{d}t \tag{2.7}$$

Assuming multiple data points, a residual error (ϵ) will occur. The error at the i^{th} measurement, $\epsilon_i = x_{mod}(t_i) - x(t_i)$, is:

$$\epsilon_i = -x(t_i) + x_0 + \int_{t_0}^{t_i} f_0 \mathrm{d}t + \theta \int_{t_0}^{t_i} f_1 \mathrm{d}t \tag{2.8}$$

which, provided the integrals can be numerically estimated, can be minimised using least squares for n measurements:

$$\begin{bmatrix} \int_{t_0}^{t_1} f_1 \mathrm{d}t \\ \vdots \\ \int_{t_0}^{t_n} f_1 \mathrm{d}t \end{bmatrix} \theta = \begin{bmatrix} x(t_1) - x_0 - \int_{t_0}^{t_1} f_0 \mathrm{d}t \\ \vdots \\ x(t_n) - x_0 - \int_{t_0}^{t_n} f_0 \mathrm{d}t \end{bmatrix} \tag{2.9}$$

If measured data is dense enough, or appropriate assumptions used, these integrals can be fully formed without further computation, and the linear system solved directly using least squares [39]. If sparse data or noise causes these integrals to be poorly approximated

by the available data, this approach can be applied iteratively, where new parameters produce a modified solution, which is then used to update the integrals [42].

These methods were developed for clinical data comprised of intermittent 1 and 2 hour measurement intervals, a distinct parameter value was fitted for each hour interval. Thus, θ was described as m piecewise-constant functions, where:

$$\theta(t) = \sum_{j=1}^{m} \gamma_j g_j(t) \tag{2.10}$$

where γ_j is the j^{th} θ value and $g_j(t)$ is a rectangle function, non-zero on a single hour interval. This description of θ is equivalent to a 0^{th} order uniform *b-spline* basis [43] with $m+1$ knots, each an hour apart. Equation (2.7) thus expands to:

$$x_{mod}(t) - x_0 = \int_{t_0}^{t} f_0 \mathrm{d}t + \gamma_1 \int_{t_0}^{t} g_1 f_1 \mathrm{d}t + \ldots + \gamma_m \int_{t_0}^{t} g_m f_1 \mathrm{d}t \tag{2.11}$$

Accordingly, Equation (2.9) becomes:

$$\hat{A}_{1,(n,m)} \hat{\Gamma}_{(m,1)} = \hat{b}_{1,(n,1)} \tag{2.12}$$

where $\hat{\Gamma}_{(m,1)} = [\gamma_1, \ldots, \gamma_m]^\top$, and:

$$\hat{A}_{1,(n,m)} = \begin{bmatrix} \int_{t_0}^{t_1} g_1 f_1 \mathrm{d}t & \ldots & \int_{t_0}^{t_1} g_m f_1 \mathrm{d}t \\ \vdots & \ddots & \vdots \\ \int_{t_0}^{t_n} g_1 f_1 \mathrm{d}t & \ldots & \int_{t_0}^{t_n} g_m f_1 \mathrm{d}t \end{bmatrix} \tag{2.13}$$

$$\hat{b}_{1,(n,1)} = \begin{bmatrix} x(t_1) - x_0 - \int_{t_0}^{t_1} f_0 \mathrm{d}t \\ \vdots \\ x(t_n) - x_0 - \int_{t_0}^{t_n} f_0 \mathrm{d}t \end{bmatrix} \tag{2.14}$$

If $m + 1 > n$, the linear system is clearly indeterminate. Such a case almost always occurs with this type of clinical data, as 2 hour BG measurements are common [22]. To circumvent this issue, data can be re-sampled hourly, an assumption that introduces fitting error if measurements are offset and can force unusual parameter spikes if additional glucose is added parenterally close to a re-sampled measurement.

A continuous profile would therefore be beneficial, and controlling the order of the basis and knot locations provides a natural method for regularising the shape of the S_I profile. However, using a knot at each measurement forces the shape of the S_I profile to reach a stationary point in the middle of the measurement period, as well as forcing all changes to be the direct result of changes in S_I.

2.2.3 Insulin sensitivity profile

Previously, due to low data density, all dynamic changes were lumped into the S_I profile. This raw S_I profile showed a number of clinically important trends [44–46] highlighting the importance of S_I. Clearly, the model-based metric evolves over time, and sudden rises greatly increase the risk of hypoglycaemia when patients are undergoing intensive insulin therapy, as injected insulin has an amplified effect on BG, and insulin dose is selected based on data indicating a prior (reduced) effect of insulin.

Variability in S_I exists due to changes in patient state, measurement noise, and mismodelled dynamics. Some literature suggests the major effect of intensive insulin therapy is the suppression of hepatic glucose production [47], though the relationship between

plasma insulin and endogenous glucose production is poorly understood. Pulsatile delivery, intraportal concentrations, and arteriovenous concentration gradients are all thought to have an effect, amongst other factors. However, quantifying the relationship between the liver and insulin is impossible using the data available at the bedside in critical care. It is sufficient to say that the relationship changes, and thus not all changes in patient state can truly be labelled "insulin-dependent".

This research regularises the S_I profile to restrict the frequency of large or sudden "insulin-dependent" state changes that result from a wide range of possible variations by utilising the generalisable description of a *b-spline* [43] basis. Figure 2.1 compares the current 0^{th} order basis with 60 minute knot widths with an equivalent proposed 2^{nd} order basis with 240 minute knot widths. The local support provided by a 2^{nd} order description regularises the profile, restricting the hour-to-hour changes in S_I. Typical clinical DKA data has hourly BG measurements, due to current clinical practice standards.

2.2.4 Noise profile

Regularising the S_I profile highlights a bias vs. variance tradeoff, as multiple measures per function introduces fitting error with real data. As the S_I profile becomes smoother, greater error is introduced. Thus, additional fitting is required to prevent information being lost in the generation of virtual patients. Such information loss would result in virtual trials showing unintended artificial improvement or degradation. Returning to Equation (2.6), a zero-mean internal noise (process noise, $\phi(t)$) can be added:

$$\dot{x} = \phi(t) + f_0(t, x) + \theta f_1(t, x) \tag{2.15}$$

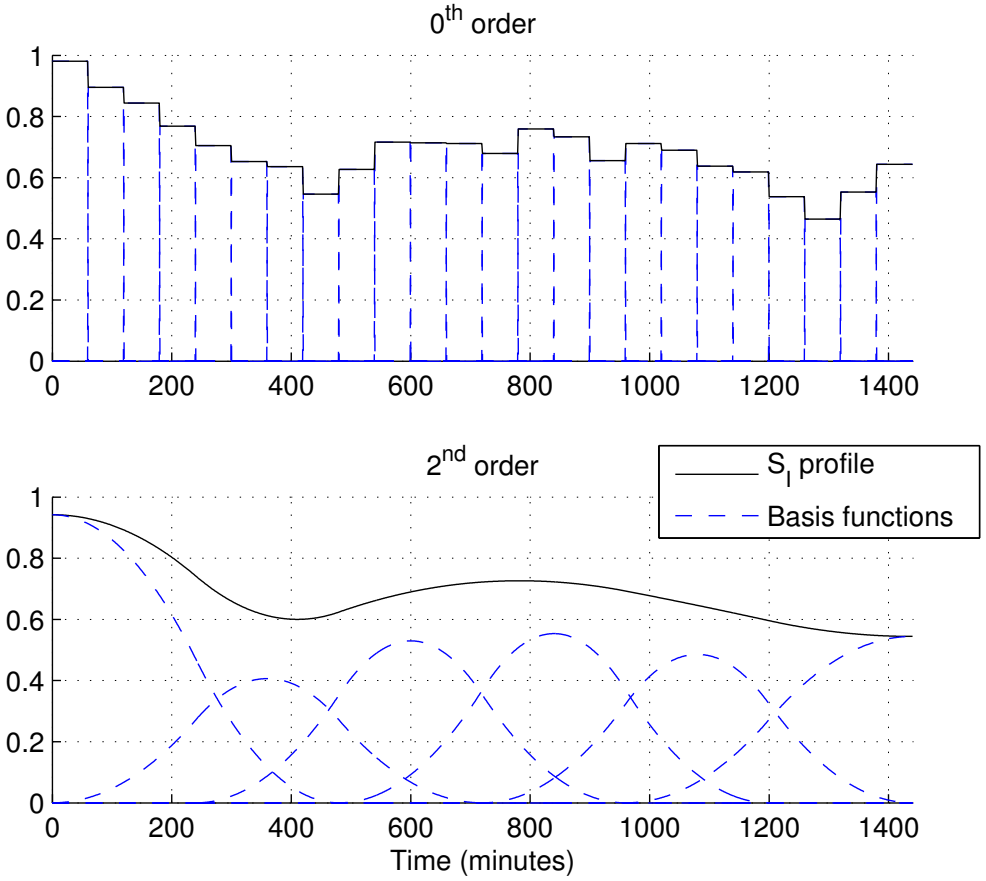

FIGURE 2.1: *Comparison of the current 0^{th} order basis (60 minute knot widths) with a proposed 2^{nd} order basis (240 minute knot widths).*

Typically, $\phi(t)$ would take the form of a Wiener process [48]. However, the added computational intensity associated with the increased resolution, and non-deterministic forward simulation, is not necessary in this application. In this simple SDE, $\phi(t)$ becomes the integral of a Wiener process between two measurements, and captures unmodelled dynamics and measurement noise that cannot be incorporated by the now-regularised S_I profile. Thus, $\phi(t)$ is a piecewise-constant function, individual values of which can be fitted using:

$$\begin{bmatrix} \hat{A}_{1,(n,m)} & \hat{A}_{2,(n,n)} \end{bmatrix} \begin{bmatrix} \hat{\Gamma}_{(m,1)} \\ \hat{\Phi}_{(n,1)} \end{bmatrix} = \hat{b}_{1,(n,1)} \tag{2.16}$$

where $\hat{\Phi}_{(n,1)} = [\phi_1, \ldots, \phi_n]^\top$ (ϕ_i is the i^{th} value of the piecewise constant $\phi(t)$), and:

$$\hat{A}_{2,(n,n)} = \begin{bmatrix} -(t_1 - t_0) & 0 & \ldots & 0 \\ -(t_1 - t_0) & -(t_2 - t_1) & \ldots & 0 \\ \vdots & \vdots & \ddots & \vdots \\ -(t_1 - t_0) & -(t_2 - t_1) & \ldots & -(t_n - t_{n-1}) \end{bmatrix} \tag{2.17}$$

As $n + m > n$ when $m > 0$ this system is always rank-deficient. However, the definition of $\phi(t)$ as zero-mean noise can be utilised to fill the rank of the system. As zero-mean noise, $\int_{t_0}^{t_n} \phi(t)\mathrm{d}t = 0$, and by the definition of the basis functions, $\sum_{i=1}^{m} g_i(t) = 1 \ \forall$ t. Thus, $\phi(t) \equiv \sum_{i=1}^{m} \phi(t) g_i(t)$. If zero-mean is enforced over the area of local support for each component $\phi(t)g_i(t)$:

$$\int_{t_0}^{t_n} \phi(t) g_i(t)\mathrm{d}t = 0 \ \ \forall \ \ i = 1, \ldots, m \tag{2.18}$$

As $\phi(t)$ is constant between two measurements:

$$\phi_1 \int_{t_0}^{t_1} g_i(t)\mathrm{d}t + \ldots + \phi_n \int_{t_{n-1}}^{t_n} g_i(t)\mathrm{d}t = 0 \tag{2.19}$$

Thus, the system in Equation (2.16) can be made full rank, and can be solved for all variables:

$$\begin{bmatrix} \hat{A}_{1,(n,m)} & \hat{A}_{2,(n,n)} \\ \hat{0}_{(m,m)} & \hat{A}_{3,(m,n)} \end{bmatrix} \begin{bmatrix} \hat{\Gamma}_{(m,1)} \\ \hat{\Phi}_{(n,1)} \end{bmatrix} = \begin{bmatrix} \hat{b}_{1,(n,1)} \\ \hat{0}_{(m,1)} \end{bmatrix} \tag{2.20}$$

where:

$$\hat{A}_{3,(m,n)} = \begin{bmatrix} \int_{t_0}^{t_1} g_1(t)\mathrm{d}t & \ldots & \int_{t_{n-1}}^{t_n} g_1(t)\mathrm{d}t \\ \vdots & \ddots & \vdots \\ \int_{t_0}^{t_1} g_m(t)\mathrm{d}t & \ldots & \int_{t_{n-1}}^{t_n} g_m(t)\mathrm{d}t \end{bmatrix} \tag{2.21}$$

The new form of the ICING model is therefore:

$$\dot{G}(t) = G_x(t) - p_G G - S_I(t)\frac{G(t)Q(t)}{1-\alpha_G Q(t)} + \frac{1}{V_G}\left(P_{EGP} - P_{CNS} + P_N(t) + \max\left(P_{max}, d_2 P_2(t)\right)\right) \quad (2.22)$$

where $S_I(t) = \theta(t)$ consists of *b-spline* basis functions, and $G_x(t) = \phi(t)$ is the new stochastic element. During a virtual trial, $G_x(t)$ is treated as the observed realisation of the stochastic process, and used in conjunction with $S_I(t)$ to calculate deterministic outcomes to modified therapeutic inputs.

2.2.5 DKA Cohort

Hourly BG, insulin and dextrose infusion rates, bolus insulin doses, and patient details were collected for 74 patients admitted to Auckland City Hospital with type 1 diabetes in DKA. Available cohort details are shown in Table 2.2. Each patient commenced an insulin infusion between 1700-0100 hours according to the Auckland City Hospital DKA protocol, shown in Table 2.3. Typically, patients begin on Scale B, with higher scales reserved for very insulin insensitive or critically ill patients. The scale is increased/decreased after multiple measurements at the maximum/minimum BG range displayed. Once BG is <15mmol.L^{-1} on 2 consecutive tests, 10% dextrose is introduced at 80mL/hr.

2.2.6 Analyses

The intent of this research is to develop and implement a new fitting method to be used for virtual trials, and thus assess the likely impact of a shift to two-hourly BG

TABLE 2.2: DKA cohort details, presented as median [minimum - maximum] when appropriate.

	Cohort details
Episodes	74
Age (years)	26 [18 - 84]
Sex	39 male, 35 female
Episode length (hours)	12.0 [4.0 - 15.0]
Number of BG measures	12.0 [5.0 - 15.0]
Starting BG	23.4 [8.3 - 53.0]

TABLE 2.3: Insulin infusion rates specified by the Auckland City Hospital DKA protocol.

Scale	BG<5.0	5.0≤BG≤11.0	11.0≤BG≤17.0	BG>17.0
A	Stop	1U/hr	3U/hr	6U/hr
B	1U/hr	3U/hr	6U/hr	12U/hr
C	2U/hr	4U/hr	8U/hr	16U/hr
D	4U/hr	8U/hr	16U/hr	32U/hr
E	8U/hr	16U/hr	32U/hr	64U/hr

measurements for DKA patients at Auckland Hospital. Accordingly, two main categories of analyses were carried out. The first was to demonstrate the problem solved by the research, and thus justify the added complexity. The second analysis was to assess the likely impact of a change in protocol.

When fitting, convergence was assumed if maximum error was within 0.05 mmol.L^{-1} (within the minimum resolution of a glucometer). To speed iterations, the G_x profile was updated between iterations using the current S_I profile. Initially, clinical data was fit using the ICING model and standard methodology [39], yielding an hourly piecewise-constant S_I profile fitted non-iteratively to linearly-interpolated hourly BG measurements. The fit was analysed with error between BG measurements and modelled plasma glucose used to quantify how well a virtual trial would reproduce the original dataset. Fitting error in any patient indicates a virtual trial run using this patient could not

recreate the original observed data, and thus error is an important metric. The data was then fit using the new methodology, with S_I comprised of 2^{nd} order basis functions with 240 minute knot widths, and fitting error distributions compared.

Virtual trials were carried out using a) the current protocol using the original BG measurement timings, "1 hour: clinical", b) strict 1 hour BG measurements, "1 hour: strict", and c) a two-hourly adaptation "2 hour: strict". For the "1 hour: clinical" trial, the maximum scale was set to C as this scale was the highest scale observed in the data set. Clinically administered parenteral nutrition was not changed during any trial. Whole cohort BG statistics were used to assess performance and safety relative to the clinical data. For a fair comparison between protocols, results were resampled minute-wise and collated to give % time in each band.

2.3 Results

Figure 2.2 indicates fitting error is unacceptably high when using the original model and fitting method. Approximately 5% of BG measures correspond to a fitting error of over 5 mmol.L^{-1}, representing the areas where the unique metabolic processes in DKA dominate glucose metabolism. This error is completely ameliorated by the new methodology, with the simple SDE capturing sustained high BG periods the model could not otherwise maintain. All patient episodes converged (results not shown here), thus indicating the stability of the fitting methodology. Figure 2.2 shows it is possible to stably decompose patient BG, insulin, and nutrition data into a regularised S_I profile, and a piecewise constant process noise, G_x.

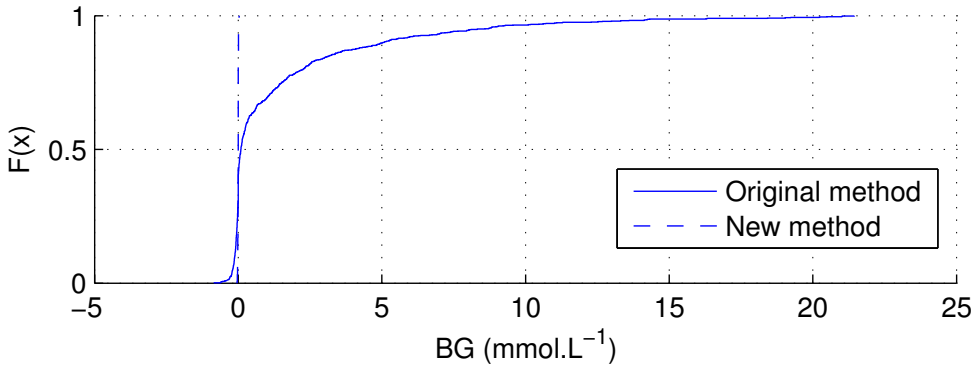

FIGURE 2.2: *Cumulative density function of fitting error across all BG measurements in the DKA cohort. Fitting error is dominated by high BG periods where the original method could not fit, and eliminated using the new methodology.*

An example of this decomposition can be seen in Figure 2.3. This patient was chosen due to the large spike in BG between t=400 and t=500 minutes, where clinicians believe the patient consumed an unknown quantity of food. Subplot (a) shows the original method failing to reach the peak BG, and the new method fitting the peak precisely. The corresponding fitted parameters are shown in subplot (b). The peaks of the original S_I profile are smoothed in the new fitting method, and S_I no longer reaches 0 during this unforeseen BG increase. The remaining variability is captured in the G_x profile.

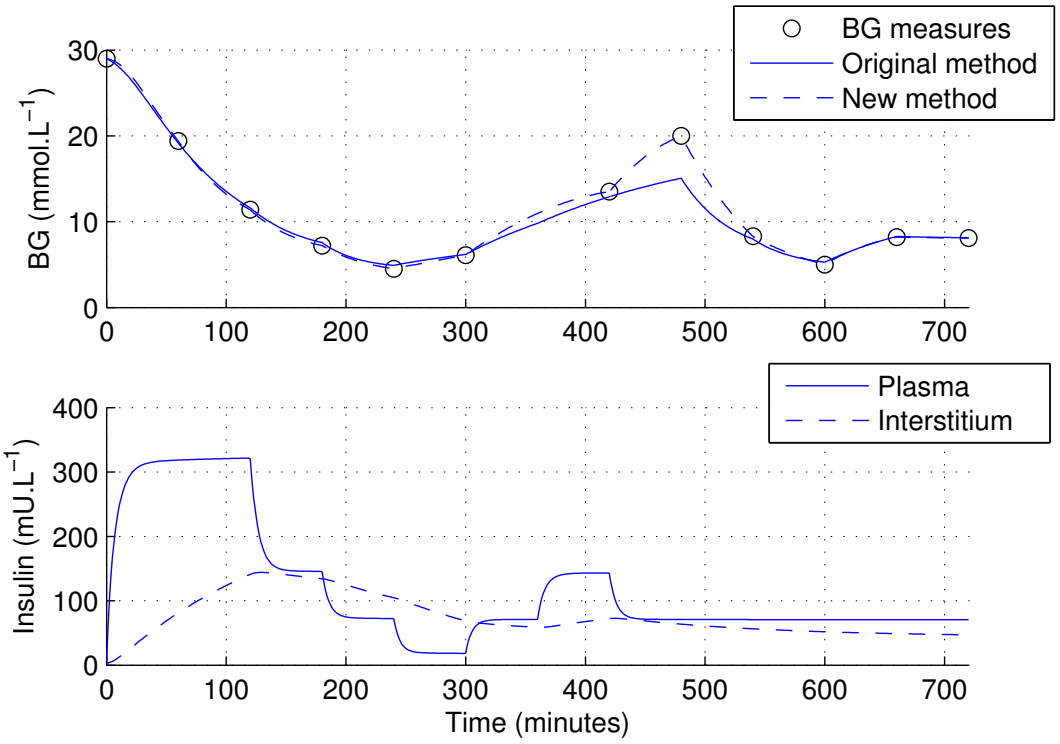

(a) BG data and model solutions

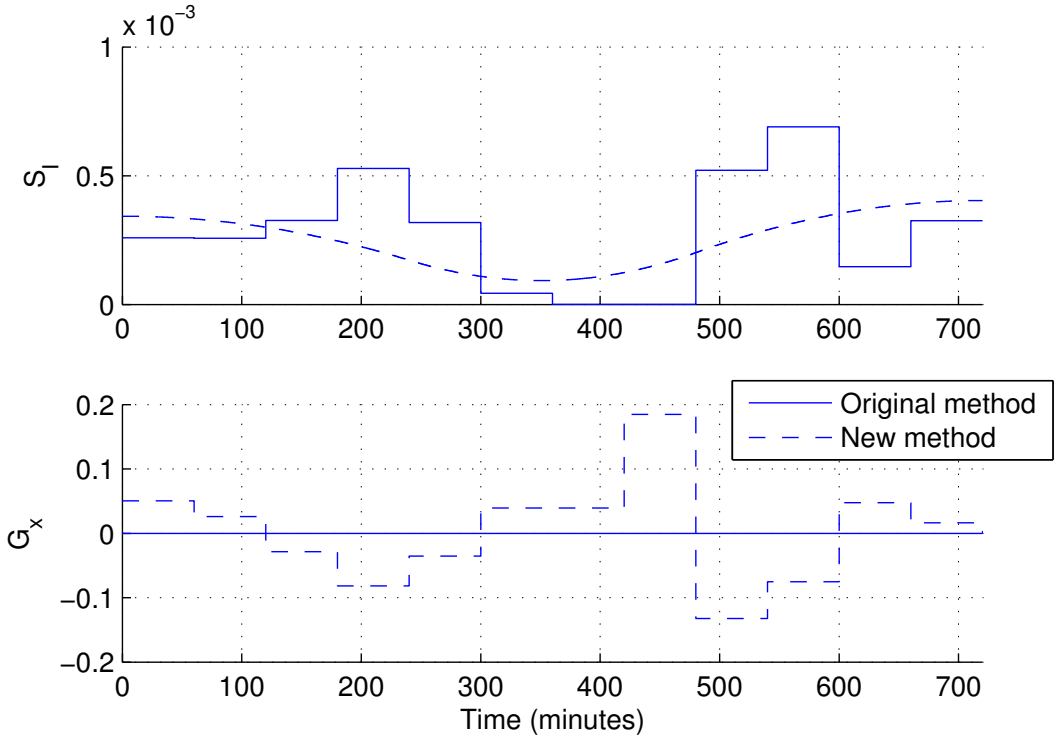

(b) Fitted profiles

FIGURE 2.3: *a) shows the raw data and fitted model solution to an individual patient with an unexpected spike in BG, and b) shows the fitted S_I and G_x profiles. The original method was incapable of reaching the large peak, while the new method fitted each data point by capturing the variation using the G_x profile.*

This feature will improve the validity of the virtual trial under these conditions. Using the new methodology, the virtual patient retains some sensitivity to insulin in such periods, where previously any dose of insulin during this period would have failed to have any effect. This is particularly important in critical illness, as BG is affected by a number of poorly understood metabolic processes that can become deranged. A direct balance between "noise" and "insulin-dependent" glycaemic responses can be struck using the new methodology.

Table 2.4 presents the results from each trial. Measures per day are greater than 24 for the "1 hour: strict" protocol as all patient episodes were under 15 hours, and the final measurement was timed to coincide with the last clinically available data point rather than maintaining a 1 hour interval. The results show only minor improvements if staff follow the current protocol to the letter, with possible reductions in hyperglycaemia and eliminating all minor hypoglycaemic (BG<4.0 mmol.L^{-1}) incidents.

Furthermore, increasing BG measurement intervals to 2 hours has a limited effect on results. Minor hypoglycaemic events have been increased relative to the "ideal" implementation of the current protocol, but are still below the current incidence in the clinical data. BG median and IQR does not change, and % time in band is slightly reduced. Overall, very little change in BG outcomes, both in performance and safety, should be expected if staff move to two-hour sampling overnight for patient comfort.

However, from a compliance standpoint there are differences between the clinical data and the "ideal" implementation of the protocol. Specifically, the upper quartile of BG is 2.1 mmol.L^{-1} higher for the clinical data, and the upper quartile of insulin infusion rates has been reduced from 8 to 6 U.hr-1. From Table 2.3 it is thus clear that increasing the scale from the default of B to C does not occur as often in practice as is theoretically

possible, which increases the BG IQR. Interestingly, the infusion rates recommended by the 2 hourly adaptation of the protocol match the clinical data closely, as scale increases take twice as long.

TABLE 2.4: Clinical and virtual trial results.

	Clinical data	1 hour - clinical	1 hour - strict	2 hour strict
Num BG Measurements:	803	803	883	488
Measures/day:	23.9	23.9	26.2	14.5
		Clinical summary		
% BG > 10 mmol/l	69.7	68.4	67.5	67.0
% BG in 8.0 - 10 mmol/l	15.2	17.9	19.3	19.5
% BG in 4.0-8.0 mmol/l	14.4	14.4	14.4	13.7
% BG < 4.0 mmol/l	1.00	0	0	0.4
% BG < 2.22 mmol/l	0	0	0	0
		Resampled summary		
Median [IQR] BG	12.4 [9.4 - 16.5]	11.9 [9.3 - 14.4]	11.9 [9.2 - 14.4]	11.9 [9.2 - 14.4]
% time > 10 mmol/l	69.0	68.3	68.1	68.1
% time in 8.0 - 10 mmol/l	15.6	18.7	18.7	18.8
% time in 4.0-8.0 mmol/l	13.9	13.1	13.2	12.7
% time < 4.0 mmol/l	0.6	0	0	0.3
% time < 2.22 mmol/l	0	0	0	0
		Therapy summary		
Median [IQR] Insulin (U/hr)	6.00 [3.00 : 6.00]	6.00 [3.00 : 8.00]	6.00 [3.00 : 8.00]	6.00 [3.00 : 6.00]
Median [IQR] Parenteral (g/hr)	6.00 [0.00 : 8.00]	6.00 [0.00 : 8.00]	6.00 [0.00 : 8.00]	6.00 [0.00 : 8.00]

2.4 Discussion

Unmodelled dynamics during DKA necessitate a new approach to virtual trial creation. Sustained extreme BG is impossible for the pharmacodynamic surface of the ICING model to achieve [37], leading to large fitting errors and reducing confidence in virtual trial results. Either a new glucose-insulin model or a new fitting methodology is required to address this issue.

A new model that describes glucose-insulin dynamics during DKA would be an ideal solution. However, this approach presents the difficulty of knowing when a patient is leaving the DKA state. Furthermore, hypoglycaemia is not a concern during DKA, as BG is well above the range where typical hour-to-hour changes could pose a serious risk. An adequate DKA protocol must therefore reduce patient BG to normal ranges without posing a hypoglycaemic risk as BG normalises.

As the current protocol is a simple sliding scale, and this study does not compare and contrast therapy choices during the period of BG normalisation, the presented methodology was adequate to ensure the data could be reproduced without the need to derive a new model and justify switching times. A two-hourly protocol could theoretically pose a hypoglycaemic risk with BG < 12 mmol.L^{-1}, a BG range that is well described by the ICING model. Due to the simplicity of the protocol, differences between one and two hour BG measurement intervals were minimal for both performance and safety, and thus clinicians can be confident in the decision to extend measurement intervals overnight.

Interestingly, as insulin rates recommended by the two-hourly protocol are actually closer to clinically administered values than the "ideal" implementation of the current protocol, nurses may actually be more comfortable with the longer measurement intervals. Currently, staff tend towards lowering the recommended infusion rate. As confidence

in the protocol leads to greater compliance [28], increasing measurement may have an unexpected benefit. However, overall compliance appears to be strong, with only small differences between clinical data and BG outcomes with perfect compliance.

This representation of S_I as a series of *b-splines* and a simple glucose SDE can also be used for fitting clinical data from outside the presented context. Direct control over the balance between noise and metabolic response has a natural application in critical care, but may also permit robust parameter identification in the hospital wards and outpatient diabetes therapy, where noise is intrinsically higher and data more sparse.

Additionally, S_I and G_x profiles could be used in a non-parametric prediction algorithm, replacing the computationally intensive stochastic model of STAR [34]. Such a non-parametric approach could feasibly be updated in real-time, improving the quality of glycaemic control for longer-stay ICU patients. Safety would be improved for more variable (higher noise) patients, and performance would be improved for more stable patients, neither of whom benefit from additional data using the current whole-cohort approach. The novel simplicity of this SDE permits stable parameter identification with a relatively computationally light algorithm, which permits use in real-time glycaemic control.

2.5 Summary

A robust parameter identification method was introduced, permitting identification of a smooth S_I profile, and capturing remaining variation in a simple stochastic element, G_x. This method extends the validity of a virtual trial to describing likely outcomes of a protocol change in DKA therapy in type-1 diabetes. Virtual trial results using this new methodology indicate that extending BG measurement interval from one to two hours

overnight will not compromise either patient safety or protocol performance. Thus, it is possible to retain the existing level of control without waking the patient every hour to take a capillary BG measurement.

Chapter 3

Non-Parametric Prediction with a Glucose SDE

3.1 Introduction

Virtual trials were a key technique used to develop the STAR (Stochastic Targeted [34]) and SPRINT (Specialised Relative Insulin and Nutrition Tables [22]) protocols *in-silico*. Avoiding physical trials during initial development enabled pre-informed protocols to be implemented in pilot studies, with the virtual trial results giving a high degree of confidence in safety and efficacy. Virtual trials also provide context analysing clinical trial results, as shown in [35], and Chapter 2. An indicative measure of compliance and performance can be provided by the comparison between virtual trial results and true observations. Virtual trials are thus an valuable tool for model-based control design.

Prior work developed the virtual trial methodology using the ICING (Intensive Control Insulin-Nutrition-Glucose [40]) model and integral-based fitting [39]. The available dataset was from the SPRINT analysis [22], collected from paper spreadsheets.

The ICU in Christchurch Hospital used a summary spreadsheet with hourly slots for measurements to be recorded, thus leading to hourly-binned data. Consequently, the integral-based fitting technique was carried out with an hourly piecewise-constant insulin sensitivity (S_I) profile, and linear interpolation was used to create intermediate BG estimates for 2-hourly intervals.

Implementation of the STAR protocol on a computerised tablet led to more precise timestamps being recorded for both BG measurement and therapy delivery. With BG measurement times often offset from the hour, and nutrition changes happening between measurements, the foundational use of piecewise-constant S_I and interpolated measurements introduced new difficulties. The nature of STAR prevented these inadequacies affecting real-time control, but the validity of virtual trials was degraded by the failure to fully fit the dataset. Simply fitting a single S_I value between measurements was an insufficient fix, as irregular intervals would degrade the mathematical correctness of the stochastic models [49] used by STAR to forecast likely changes.

Chapter 2 describes a robust fitting methodology capable of decomposing patient data into a continuous insulin sensitivity profile, S_I, and an internal noise term, G_x. This new methodology was designed to circumvent periods of unmodelled dynamics during diabetic ketoacidosis, where fitting error reduced virtual trial validity. However, the new methodology also solves the problem of irregular measurement timing, permitting future virtual trials to be carried out using the new data set.

The problem presented by the new fitting methodology is thus how to forecast likely glycaemic variability. Ideally, a glycaemic control protocol should adapt to suit the patient as more data becomes available. Approximately 20% of the STAR episodes observed to

date have been 72 hours or longer, thus accumulating a significant data set is not uncommon. However, while the current insulin-sensitivity is fitted and thus patient-specific, STAR forecasts changes in S_I using a whole-cohort stochastic model [49]. Creation of this model is extremely computationally expensive, taking approximately 20 minutes when parallelised and running on all cores of a quad-core CPU. A tablet computer lacks the computational power to carry out these computations in real time, and thus STAR is limited by the whole-cohort description of S_I variability.

The major reason the complicated mathematics behind the stochastic model were necessary was the discrete nature of the S_I profile. Kernel-density methods were thus required to generate a suitable probability density functions. Unfortunately, neither a variable-width or continuous S_I profile fit into the existing stochastic model paradigm. This reflects the fact the stochastic model was designed to describe the variability of S_I in the SPRINT cohort, and is fundamentally tied to the hourly S_I profile chosen to describe BG variability.

This chapter details a non-parameteric approach to generating predictions, using both S_I and G_x. Non-parametric methods were chosen due to relative simplicity, thus significantly reducing the computational burden. The non-parameteric approach can be updated in real-time by heavily weighting and superimposing the data observed when controlling the current patient on top of existing whole-cohort observed responses. The prediction methodology is validated by demonstrating coverage of the prediction bands is representative.

3.2 Methods

The ICING model and basis function SDE approach was used to fit patient data, as per Chapter 2. A 2^{nd} order basis with uniform 240 minute knot spacings were used to create a smooth S_I profile and piecewise-constant G_x profile. Fitting was considered converged when the max error between any BG measure and the corresponding model estimate was within 0.1 mmol.L^{-1}.

3.2.1 STAR Cohort

BG, insulin, and nutrition data was collected as part of routine use of the STAR protocol in Christchurch Hospital medical and surgical ICU between July 2011 and February 2013. For use in this study, datasets were split when a gap greater that 5 hours occurred between consecutive BG measurements. Observational ethics was granted by the National Ethics Advisory Committee. Available cohort details are shown in Table 3.1.

TABLE 3.1: STAR cohort details

	Cohort details
Episodes	207
Total hours	11538
Total BG measures	6517
Age (years)	61 [48 - 71]
Sex	66.2% male, 33.8% female
Length of episode (hours)	32 [15 - 68]
BG measures	19 [10 - 39]

3.2.2 Summary of prediction methodology

Firstly, S_I and G_x profiles were fitted using available patient data. Using these profiles, probability density functions (PDFs) were generated in the form of discretised matrices.

Finally, cumulative density functions (CDFs) were created by taking the cumulative sum of each PDF at each timepoint, and interpolated to give percentile bands. A simple example of the conversion of a S_I trace to a PDF is shown in Figures 3.1 and 3.2. The trace in Figure 3.1 is simply rounded based on the chosen discretisation, and the value of the PDF incremented by one in the relevant bin at each timepoint.

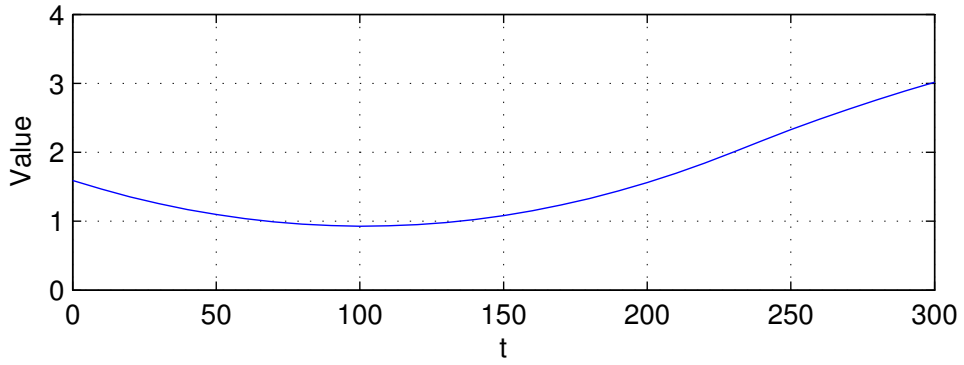

FIGURE 3.1: *Example trace.*

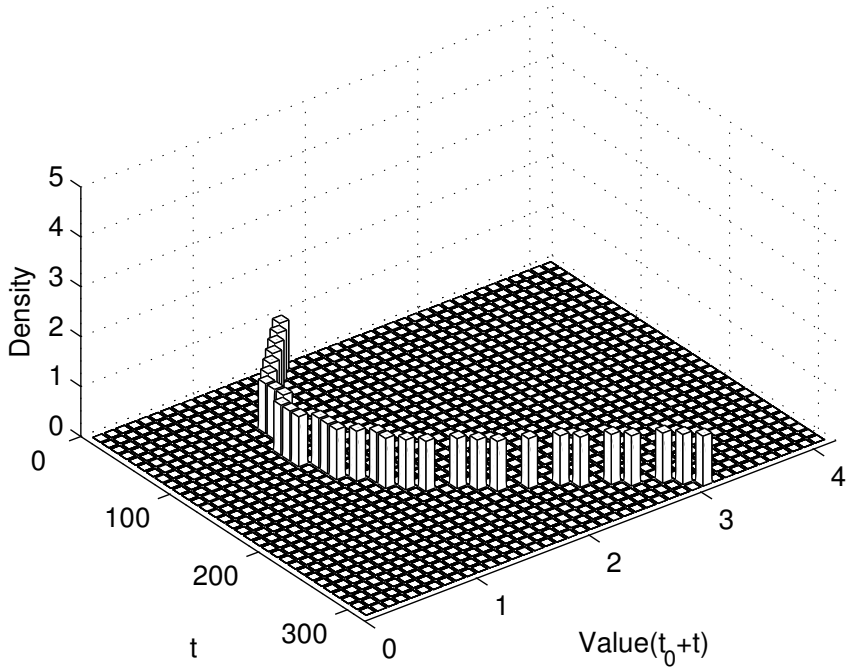

FIGURE 3.2: *Example trace converted to PDF form by discretising the trace and incrementing the PDF by one in the relevant bin at each timepoint.*

Both S_I and G_x were handled separately. As S_I future outcomes depends on the current

S_I, multiple PDFs were generated by binning S_I data, calculating percentiles, and unifying the set of percentiles into a single prediction surface. No such dependence exists for G_x, and thus a single PDF was created. When predicting, the 95$^{\text{th}}$ percentile of S_I and the 5$^{\text{th}}$ percentile of G_x were used to generate the 5$^{\text{th}}$ percentile BG outcome, as the two parameters have opposite effects on BG.

3.2.3 Insulin sensitivity prediction

A series of S_I ranges were used to generate separate PDFs, as significantly differing S_I variability has been observed over the range of S_I values [49]. The ranges were chosen by binning the observed S_I range such that each bin contained 5% of all observed S_I. Figure 3.3 shows the S_I levels in each bin.

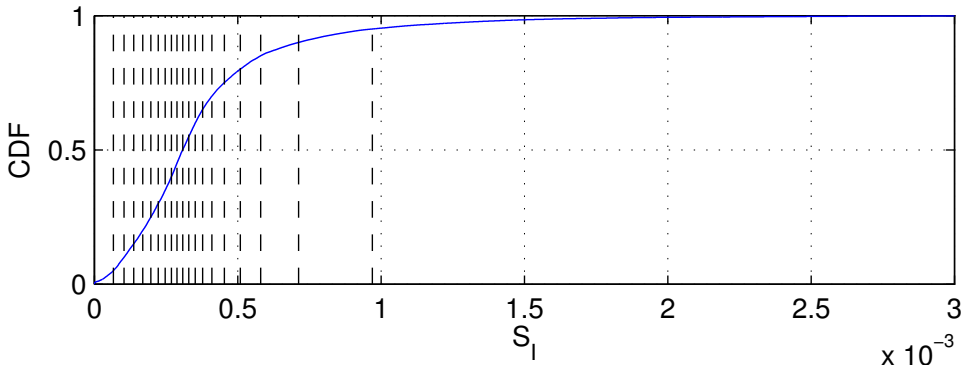

FIGURE 3.3: *Discretisation of S_I for stochastic models. The edge of each bin is shown with dashed lines, each containing 5% of the observed S_I values.*

The minute-wise S_I profiles in each of these bins was converted to ΔS_I to ensure all future S_I curves start from zero. This choice simplifies prediction, as the appropriate ΔS_I profile can simply be added to the current S_I level. Absolute ΔS_I was used in place of $\%\Delta S_I$ as extremely small S_I values will have a disproportionate $\%\Delta S_I$. These ΔS_I profiles were discretised to a series of integer grids as shown in Figure 3.2, with the final PDF for each bin appearing similar to Figure 3.4.

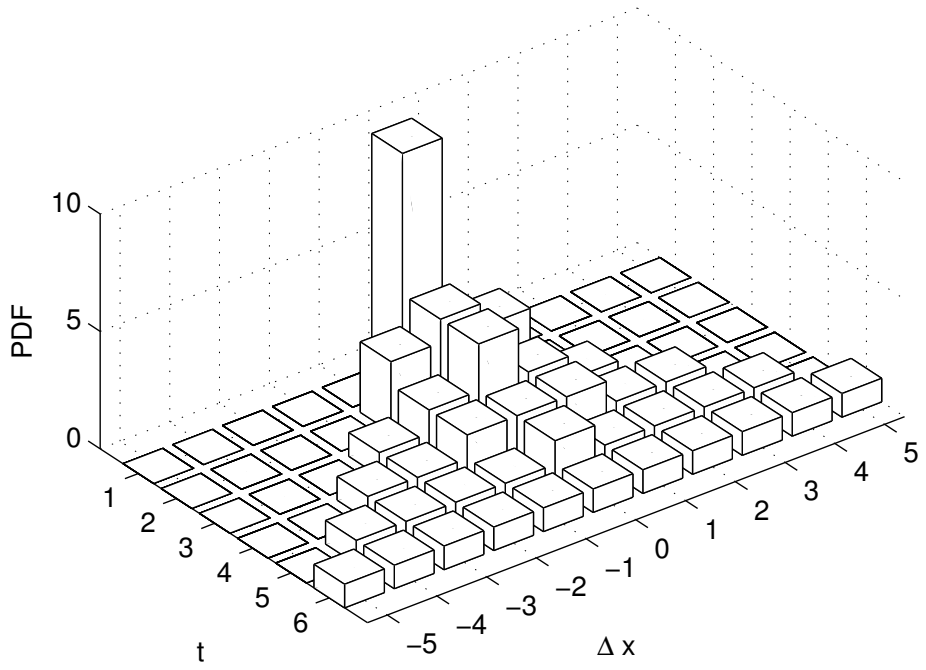

FIGURE 3.4: *Example discretised PDF, where t is the arbitrary unit of time in the future, while Δx is the arbitrary unit of change.*

Each S_I PDF matrix was discretised in steps of 1 minute in the x direction, and calculated from 0 to 300 minutes. The y direction was discretised in steps of $4{\times}10^{-6}$, and limits of the were chosen such that a maximum of 1% of all ΔS_I values would fall outside the limits on either side. These limits ranged from $\pm 2.6{\times}10^{-4}$ to $\pm 15{\times}10^{-4}$.

3.2.4 Noise prediction

In Figure 3.5, all fitted G_x values are plotted against measurement interval, prior BG measurement, and insulin/nutrition administered during the measurement interval. Graphically, the only factor that affects the variance of G_x is the measurement interval, which is congruent with the constraints introduced to G_x. Due to the choice of constraint, longer term changes in BG are mediated by S_I, while short term changes

will predominantly affect the G_x profile. Thus, it is sufficient to generate G_x percentiles based on measurement interval alone.

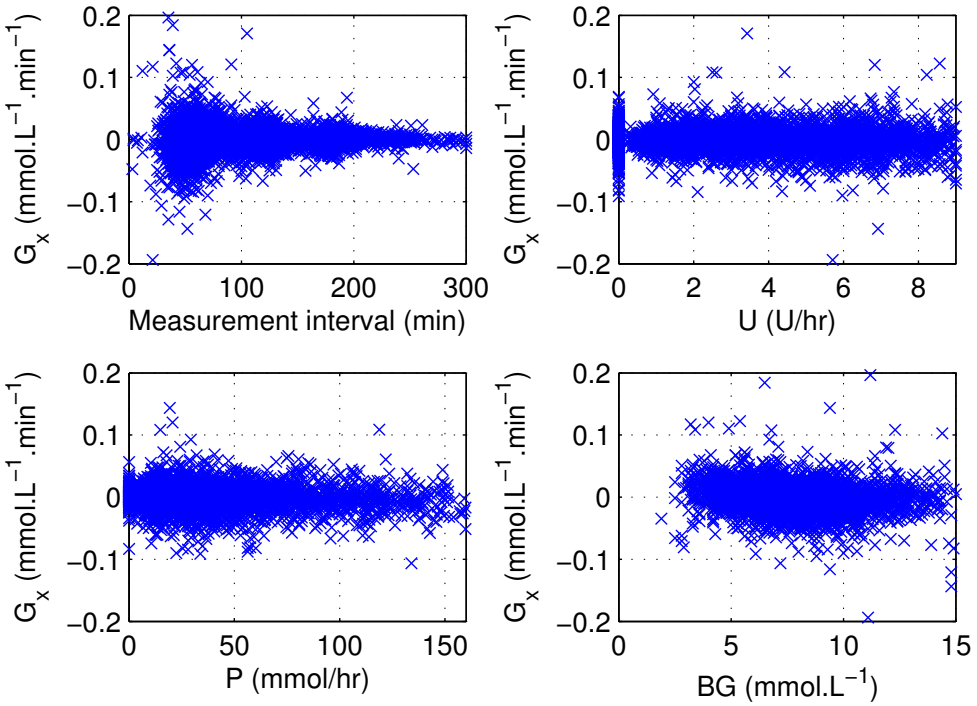

FIGURE 3.5: *Scatter diagram of all fitted G_x vales with a 2nd order basis, plotted against measurement interval, exogenous insulin, exogenous glucose, and initial BG. Hourly insulin is only indicative, as timing errors will affect the value when insulin is delivered in a bolus.*

The cumulative distribution of measurement intervals is shown in Figure 3.6. In order to generate PDFs in a similar manner to S_I, each G_x value was converted to a constant profile non-zero in the region $t_{lower} \leq t \leq t_{upper}$. This region was chosen to prevent the smaller G_x values at for longer intervals artificially tightening shorter predictions, and the sparse data at $t \approx 300$ from causing high variance for longer predictions. Values for t_{lower} and t_{upper} were defined using the CDF in Figure 3.6, where $F(t)$ is the value of the CDF at time t, and t_i is the duration of the measurement corresponding to the current G_x value:

$$\begin{aligned} t_{lower,i} &= F^{-1}(F(t_i) - 0.66) \\ t_{upper,i} &= F^{-1}(F(t_i) - 0.02) \end{aligned} \tag{3.1}$$

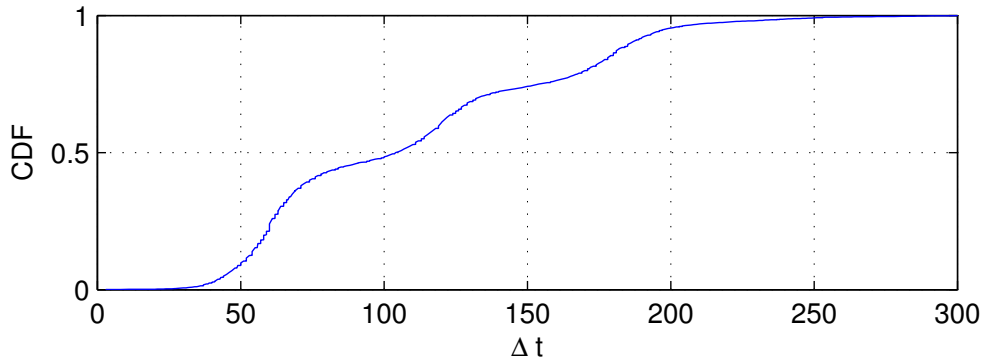

FIGURE 3.6: Noise CDF.

Thus, a non-parameteric description of the G_x PDF similar to the method presented for S_I can be obtained. The G_x PDF matrix was discretised in steps of 1 minute in the x direction, and calculated from 0 to 300 minutes as per S_I. The y direction was discretised in steps of $8{\times}10^{-4}$, with limits of ± 0.2.

3.2.5 Analyses

Using these two methods, PDFs and thus percentile bounds were generated for both S_I and G_x. The unification of these two distributions at the n^{th} percentile is assumed to be additive, where the n^{th} percentile BG outcome is calculated using the $(100-n)^{\text{th}}$ percentile S_I and G_x functions. In this way, 5^{th}, 25^{th}, 50^{th}, 75^{th}, and 95^{th} percentile BG outcomes were calculated for each measurement interval. The number of times the true BG measure at the end of the interval exceeded these percentiles was recorded, and compared to the expected value. Both whole-cohort and per-patient values were recorded.

To give context to the results, the original 60 minute piecewise-constant S_I method was also used to fit the STAR cohort. Stochastic models [49] were generated for 1-5 hours, and used to generate 5^{th}, 25^{th}, 50^{th}, 75^{th}, and 95^{th} percentile BG outcomes. The ability

of these BG outcomes to represent the true measurements was compared with the new methodology.

3.3 Results

Table 3.2 details how well the stochastic models self-validate against the true BG measurements. The original stochastic model coverage is poor with the new STAR data. The self-validation of the new method is markedly improved, with extremely closely matching whole-cohort percentiles. Per-patient values are also improved, particularly for the outer 5^{th} and 95^{th} percentiles. Whole-cohort predictive capability was strongest for the 5^{th}, 75^{th}, and 95^{th} percentiles, but was still approximately correct for the 25^{th} and 50^{th} percentiles. All whole-cohort values were within 4% (absolute) of the expected value, suggesting the S_I and G_x distributions can be effectively decoupled for prediction. Table 3.2 demonstrates the new prediction methodology is better suited to describing glycaemic variability in irregular data sets.

TABLE 3.2: Comparison of prediction band coverage. Results are presented as absolute % error between the percentile and the true percentage of BG measures that exceeded the percentile.

	Original method	New method
Percentile	*Whole-cohort*	
5^{th}	+6.3	0.0
25^{th}	+7.1	+3.7
50^{th}	+0.5	+3.0
75^{th}	-7.8	+1.8
95^{th}	-7.6	+0.9
	Per-patient median [IQR]	
5^{th}	+7.2 [-1.4 : +17.2]	-1.7 [-5.0 : +3.8]
25^{th}	+8.7 [-0.4 : +17.9]	+4.4 [-3.8 : +15.0]
50^{th}	0.0 [-6.2 : +8.5]	+4.0 [-2.4 : +12.5]
75^{th}	-8.2 [-15.5 : 0.0]	+3.9 [-5.0 : +12.5]
95^{th}	-6.9 [-18.1 : +0.7]	+5.0 [-1.2 : +5.0]

Two examples of the stochastic models generated with the Lin et al. method are shown in Figure 3.7. Their binned counterparts in the new method are presented in full as a

surface in Figure 3.8. The binned ΔS_I PDFs used to create these percentiles are not shown.

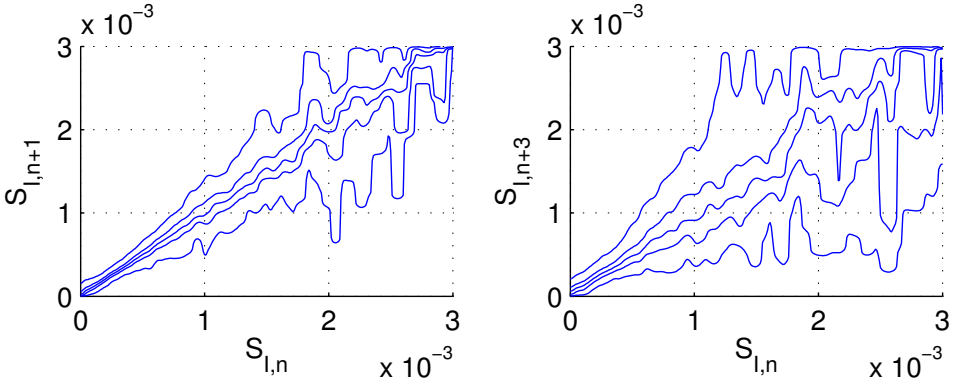

FIGURE 3.7: *Kernel-density stochastic model built from the STAR cohort data. Only 1 and 3 hours are shown for brevity.*

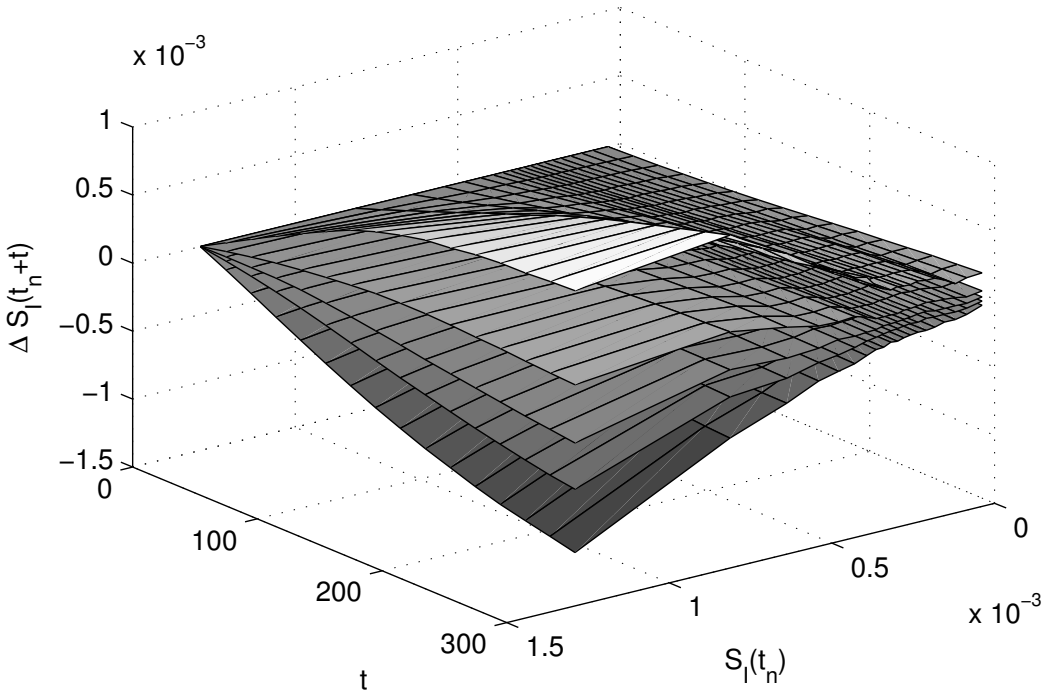

FIGURE 3.8: *From bottom to top: 5^{th}, 25^{th}, 50^{th}, 75^{th}, and 95^{th} S_I percentiles generated using the new non-parametric methodology, and combined into a single surface.*

The PDF surface from the G_x data is shown in Figure 3.9, with the corresponding percentiles shown in Figure 3.10. The magnitude of the 90^{th} percentile band for G_x ranged from approximately $\pm 10\%$ to $\pm 45\%$ of the ICING model parameter of endogenous

glucose production. In contrast, the 50^{th} percentile band ranged from approximately $\pm 3\%$ to $\pm 10\%$ endogenous glucose production.

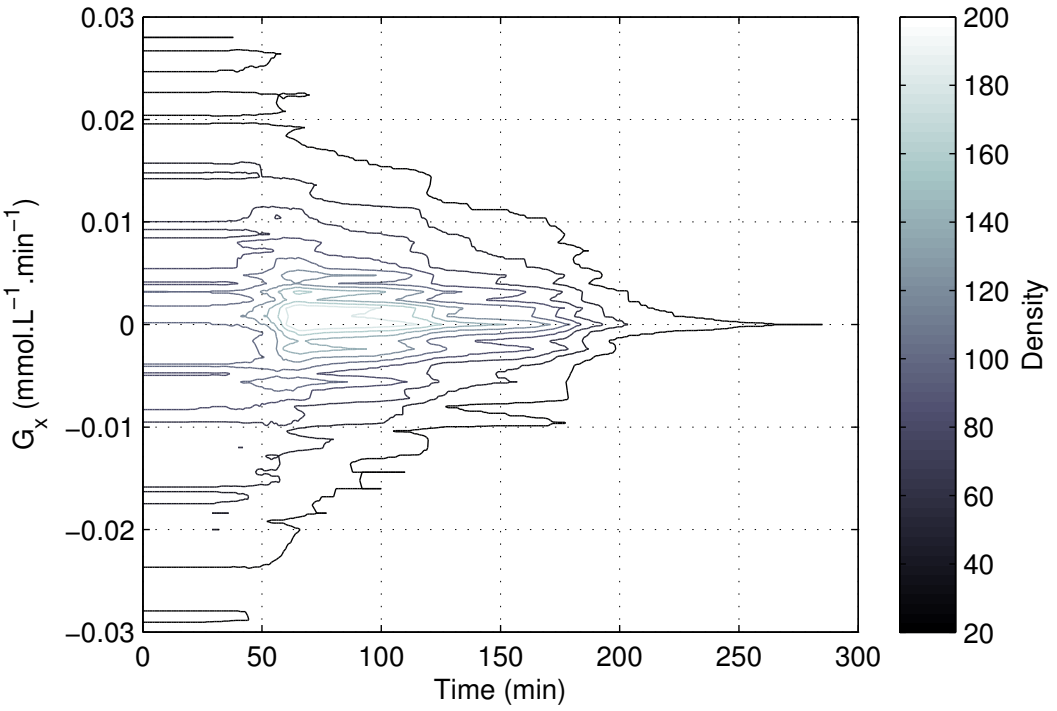

FIGURE 3.9: *Noise PDF matrix, used to generate the percentiles shown in Figure 3.10.*

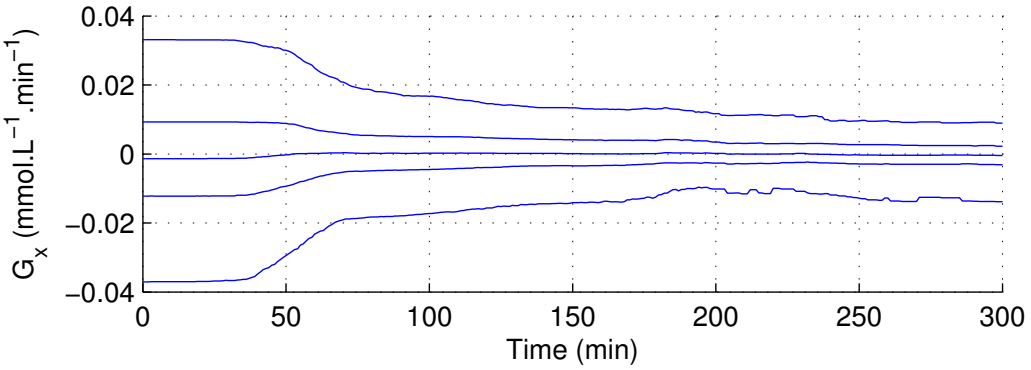

FIGURE 3.10: *5^{th}, 25^{th}, 50^{th}, 75^{th}, and 95^{th} noise percentiles generated using the PDF matrix in Figure 3.9.*

STAR makes treatment decisions based on the location and 90% range of BG outcomes. Accordingly, all 90% ranges have been presented for the original and new methods in Figures 3.11 and 3.12, respectively. The new methodology has dramatically more consistent BG prediction ranges across the board. While the minimum band width has

been raised somewhat, the maximum has been dropped significantly. The within- and without- band measurements were separated, and the CDFs for each subset suggest that BG is slightly more likely to exceed the band for lower measurement intervals. This feature is true for each method, but the new method reduces the magnitude of the effect. Figures 3.13 and 3.14 present the same results, but plotted against pre-measure S_I. Similar patterns appear to exist for both methods, and the CDFs show both methods are capable of correcting for current S_I level.

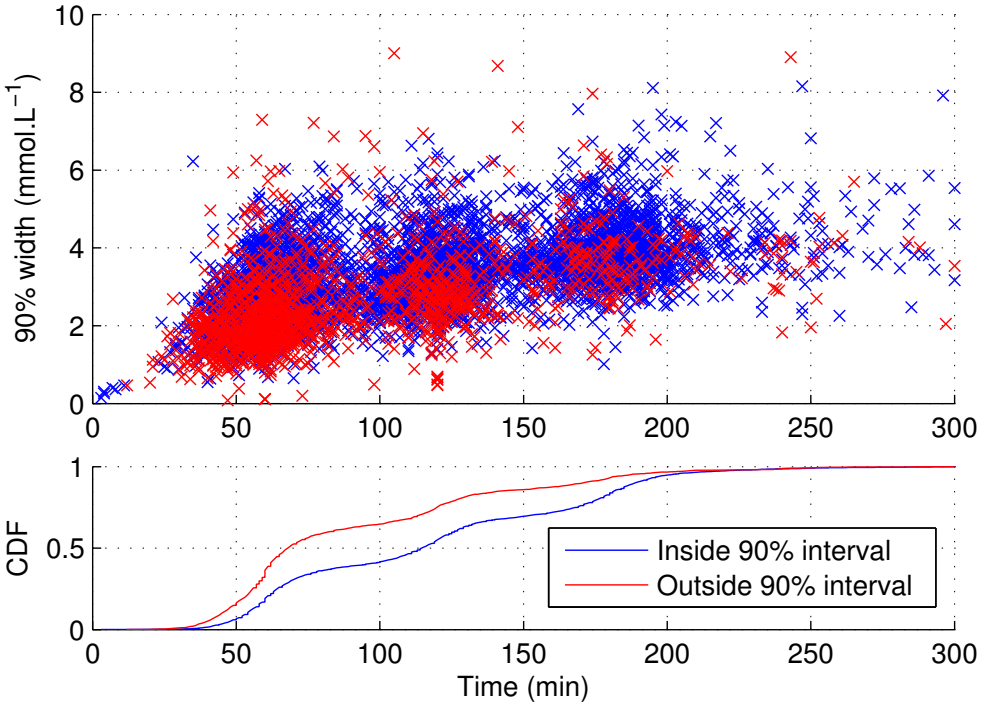

FIGURE 3.11: *BG prediction band widths and comparison of distributions.*

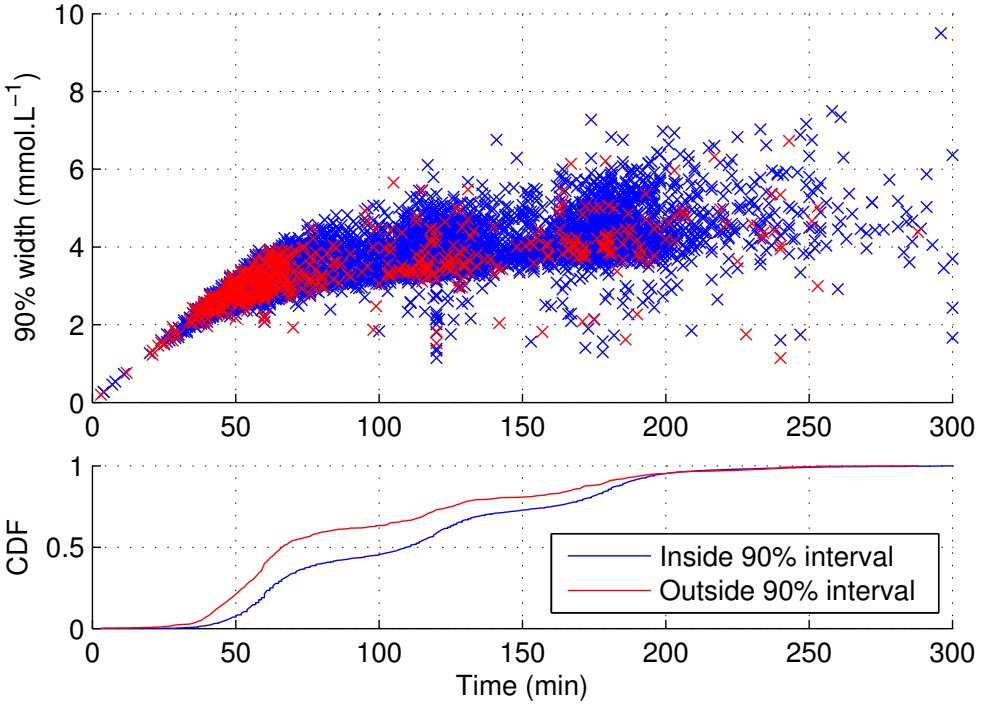

FIGURE 3.12: *BG prediction band widths and comparison of distributions.*

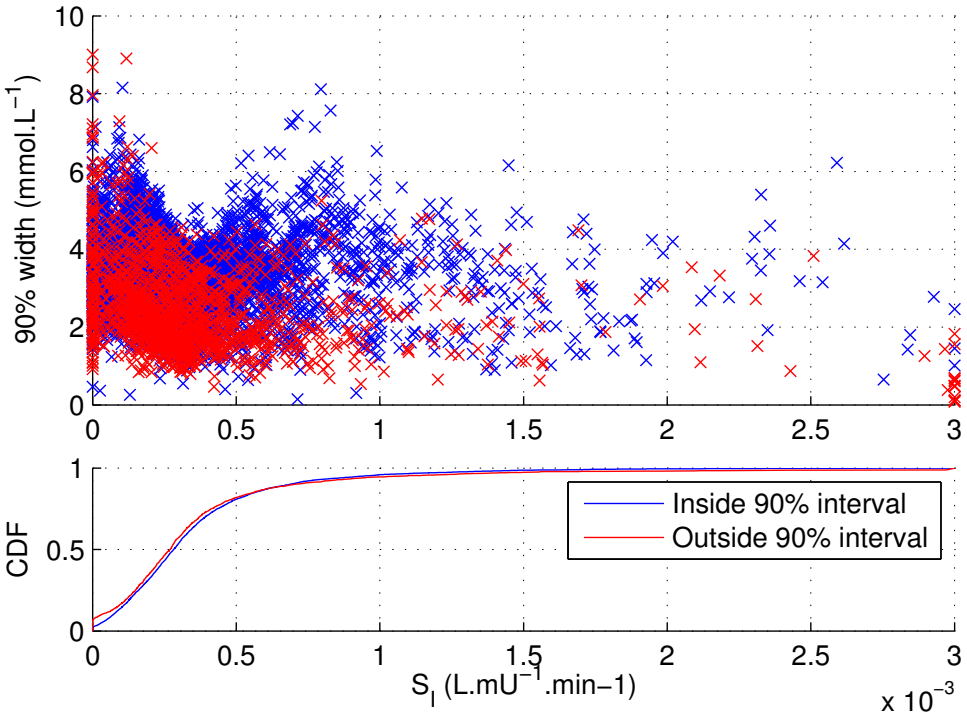

FIGURE 3.13: *BG prediction band widths from Figure 3.11 plotted against pre-measure S_I.*

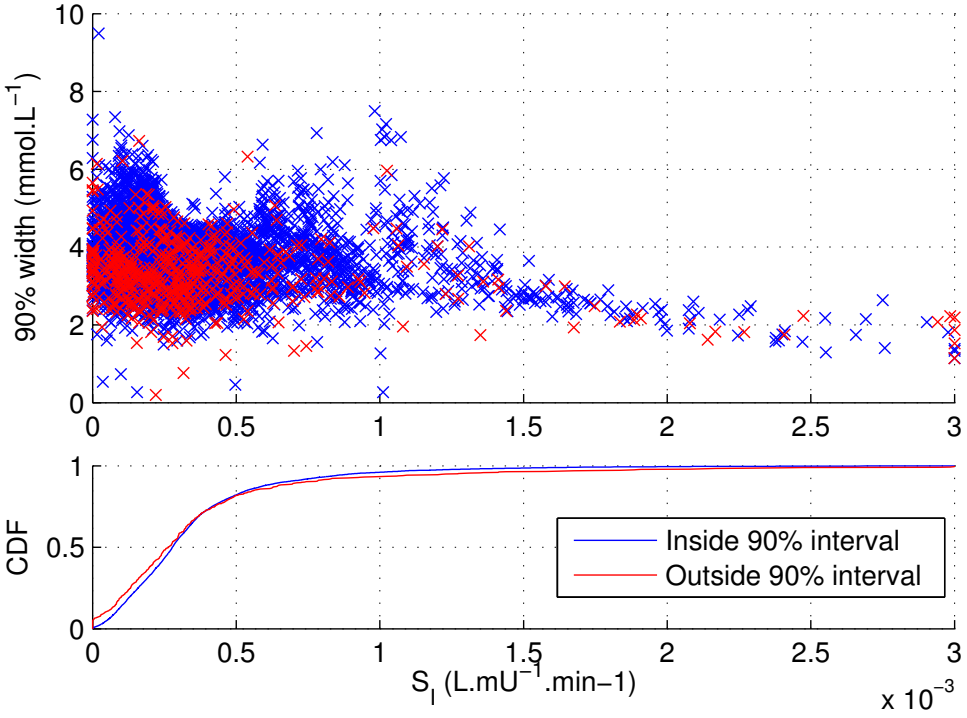

FIGURE 3.14: *BG prediction band widths from Figure 3.12 plotted against pre-measure S_I.*

3.4 Discussion

Extending the utility of the methodology presented in Chapter 2 requires a new framework for generating BG predictions. The kernel-density based method for generating S_I PDF matrices [49] performed well for SPRINT data, but cannot cope with irregular or continuous S_I profiles. Carrying out BG predictions with the new fitting method required quantification of observed changes in both S_I and G_x. Thus, the presented methodology was developed with the aim of using a fully non-parametric approach.

A non-parametric approach was deemed important, as the kernel-density methodology was significantly too computationally expensive to update in real-time. The per-patient results of Table 3.2 showed a moderate degree of variation between in predictive performance. Using a non-parametric approach will allow control to be improved for these patients through real-time updating of the PDF matrices.

The major area for concern was the relationship between measurement interval and likelihood of exceeding the 90% interval BG predictions. Figure 3.12 indicates this likelihood is not uniform, as the CDFs show a slightly greater tendency to exceed for shorter than longer intervals. This non-uniformity suggests the unification of the G_x and S_I predictions is not perfect. However, the scope of the problem does not appear to be large enough for a dedicated solution, in particular because longer intervals do not appear dramatically over-conservative. Additionally, the effect is more pronounced for the old method.

Table 3.2 demonstrates the methodology achieves the desired performance over the entire cohort. Further investigation is required to determine whether the per-patient statistics

can be improved, but these results show that implementation could precede as is. Likelihood of exceeding the 90% band was not affected by S_I level, indicating the discretised S_I percentiles were not producing unexpected results.

Finally, the comparative self-validation ability of the original and new method demonstrate the strength of the new method, despite comparative simplicity. The original method has significantly reduced predictive capability for the STAR data set, particularly at the 5^{th} and 95^{th} percentiles. The new methodology improves both predictive capability and consistency, as demonstrated by the band widths in Figures 3.11 to 3.14. As these percentiles are of prime importance for the STAR algorithm, the new method is thus better suited for use as the STAR database expands.

3.5 Summary

Representative prediction of BG despite irregular data is possible using the ICING model, the novel SDE fitting methodology presented in Chapter 2, and a non-parameteric approach to prediction. This combination natively supports different measurement intervals, and is computationally simple enough for real-time updating of whole-cohort PDF matrices. Overall, the results indicate the methodology is sound, and is ready for validation on an independent cohort.

Chapter 4

Updated ICING Model Insulin Kinetic Compartments

4.1 Introduction

The core of any model-based decision support is a model that describes the key kinetics and dynamics of the system. In the case of glycaemic control, these kinetics are the appearance and clearance of glucose and insulin in the circulatory system. A plethora of models have been developed to describe glucose-insulin kinetics and dynamics, diagnose diabetes or pre-diabetes, or control blood glucose concentration (BG). Each model satisfactorily describes the relevant training data, though differs in model structure, parameter values, fitting methods, or any combination thereof.

The sheer complexity of the human body precludes a truly descriptive minimal model. While compartmental models are perhaps the most intuitive of the available descriptions, they suffer from an array of identifiability issues [50], and the assumption of

perfect mixing inherent in compartmental models can introduce further difficulties. Another fundamental difficulty is the current inability to accurately estimate endogenous processes in real time. Both insulin secretion and endogenous glucose production are poorly understood, and yet they are a critical dynamic of glucose homoeostasis. When these processes become deranged in diabetes or critical illness, exogenous insulin is used to promote glucose uptake into insulin-sensitive cells. However, selecting the optimal subject-specific insulin dose is difficult, as the underlying metabolic dynamics are both hard to assess and model, and variable over time and condition.

An additional difficulty with these models is describing different types of subcutaneous insulin. Each has a unique pharmacokinetic profile, with large inter- and even intra-patient variation [51], and are typically used in combination. As no rapid and inexpensive assay exists for assessing plasma insulin in real-time, insulin models are important for estimating glycaemic response. However, models of subcutaneous insulin tend to neglect consistent plasma insulin descriptions, and as a result multi-insulin therapy is difficult to approach from a model-based perspective.

One model that has been successfully used to guide clinical decisions on IV insulin and enteral/parenteral nutrition is the ICING model [40], presented in full in Chapter 2. However, the ICING model was developed and optimised to describe insulin boluses, and when modelling slower insulin kinetics, descriptive capability is limited. This discrepancy is evident with both infusions and subcutaneous insulin boluses. Additionally, insulin clearance route contributions do not closely match literature values [52], and thus may benefit from a refitted model.

Finally, modelling insulin infusions and boluses in a simple compartment model is difficult, as demonstrated by Figure 4.1. Individual kinetic parameters were fitted on a

median patient created from Dynamic Insulin Sensitivity and Secretion Test (DISST, [53]) data then tested on IV Glucose Tolerance Test (IVGTT, [54]) data, and vice versa. Clearly, descriptive capability was extremely poor when the fitted values were taken out of context.

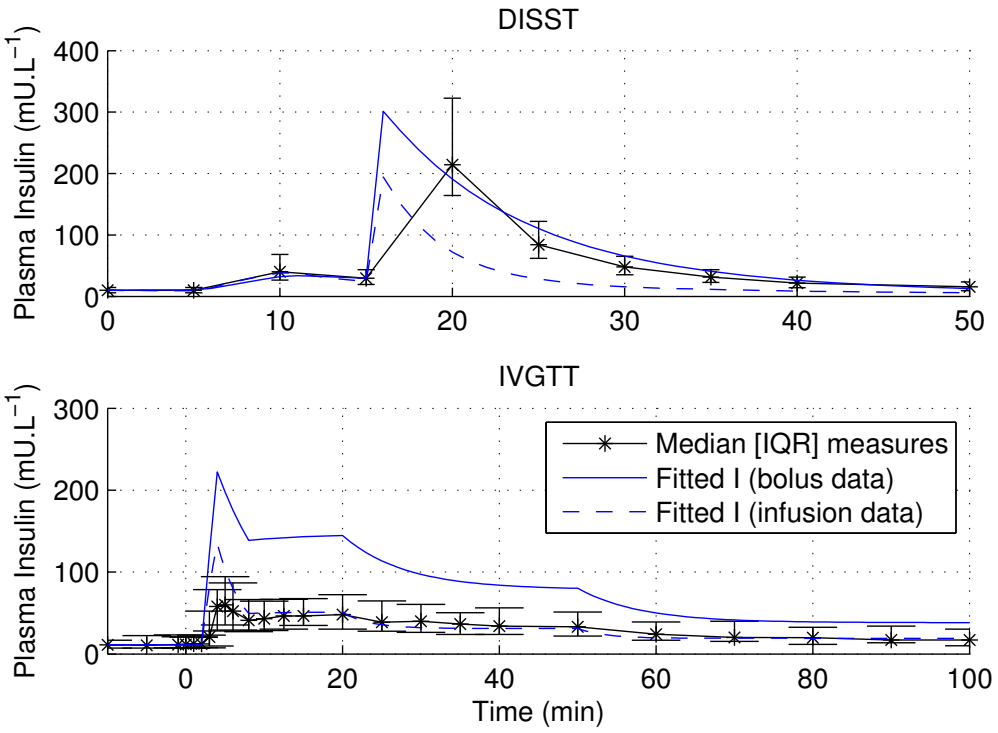

FIGURE 4.1: *Single compartment infusion/bolus comparison, fitted on a median patient created from one data set, and tested on the other. Bars on the measurements show the 25th and 75th percentiles of the measured data. Fitted parameter values were $x_L = 0.213$, $V = 3.50$, and $n_T = 0.127$ (DISST), $x_L = 0.300$, $V = 5.00$, and $n_T = 0.294$ (IVGTT).*

This work aims to re-evaluate the insulin model parameters to improve the descriptive capability of the insulin kinetics in the ICING model, while retaining current IV bolus-specific performance. The new description is intended for use in model-based decision-support both in critical illness and beyond, where subcutaneous insulin is the delivery route of choice.

4.2 Methods

4.2.1 Key insulin dynamics

Insulin generally appears in plasma, but is utilised from the interstitial fluid of skeletal muscle and adipose tissue. Thus, description of insulin effect requires a minimum of two compartments. The liver plays an integral role in insulin disposal, and would thus necessitate an extra compartment for complete description. However, the hepatic glucose balance is primarily influenced by extremely high, pulsatile insulin levels in the hepatic portal vein [55]. Exogenous insulin cannot presently achieve such portal vein profiles, and therefore may have limited effect on hepatic glucose production. Additionally, this effect cannot be separated from interstitial insulin action with the available measurements. Thus, a dedicated hepatic compartment was omitted.

Degradation of insulin occurs in several key locations. The liver provides the major insulin clearance at physiological concentrations, clearing approximately 60% of presented insulin [52], but has been demonstrated to saturate in supra-physiological insulin levels [56]. This clearance has been positively correlated with endogenous insulin secretion, suggesting a fractional extraction. Renal insulin clearance is lower than hepatic at physiological concentrations, but does not saturate, and is estimated at 39% of presented insulin [57], or 80% of peripheral insulin [56]. These two sites, hepatic and renal, are the main clearances from the central, circulating insulin compartment.

Remaining insulin passively diffuses into interstitial fluid, where binding and degradation occur. A third compartment can be justified by non-uniform interstitial fluid dynamics. Insulin-sensitive cells include muscle, adipocytes, gastrointestinal cells, fibroblasts, monocytes, and lymphocytes [52]. The remaining tissues lack insulin receptors, and so

cannot degrade insulin. Interstitial fluid can therefore be separated into two compartments, active interstitium and passive interstitium. Diffusion kinetics will be identical, but the active interstitium includes an additional clearance from the compartment. The volume of each compartment can be estimated by body composition, extracellular water fractions, and total extracellular fluid volumes. Saturation is omitted from the clearance, as although insulin *effect* saturation has been widely reported, micro-dialysis studies of interstitial insulin have not reported consistent reductions in plasma-interstitial insulin concentration ratios with increasing plasma insulin concentrations. Effect saturation is easily incorporated into the glucose model, and is justifiable because the insulin internalisation and GLUT-4 promotion are separate (but related) processes.

Combination of bolus and infusion delivery dynamics necessitate an additional dynamic. After injection, an IV insulin bolus will form a local volume of insulin that is extremely concentrated relative to the average plasma concentration. This area will behave very differently to the well-mixed assumption of a compartment model, creating some of the disparity shown in Figure 4.1. In particular, the subvolumes that travel to peripheral capillary beds will create a locally large plasma-interstitial ratio, so trans-endothelial transport will happen rapidly. Mixing, hepatic clearance, renal clearance, and this rapid transport will disperse the local high concentration quickly, and plasma insulin will then be elevated by re-entry of the transported insulin. To include this dynamic without subdividing the interstitial compartment, this temporarily unavailable insulin is assumed to be non-specifically bound, and released into both interstitial fluid and plasma.

By separately handling IV boluses, the increased clearance rates needed to improve Figure 4.1 are thus possible. Once IV boluses and infusions can be modelled by the same circulating insulin compartment, the infusion-like dynamics of subcutaneously injection

will be more accurately described. As the circulating insulin dynamics are unidentifiable with available subcutaneous insulin experimental data, this improved description may lead to a more representative model of subcutaneous insulin dynamics.

4.2.2 Insulin model structure

The resulting three compartment model is defined:

$$\dot{I} = \frac{k_1 X + U_{x,i} + (1 - x_L)U_n}{V_I} - n_K I - n_I(2I - Q - Q_p) - n_L \frac{I}{1 + \alpha_I I} \tag{4.1}$$

$$\dot{X} = (1 - x_B)U_{x,b} - (k_1 + k_2)X \tag{4.2}$$

$$\dot{Q} = n_I(I - Q)\frac{V_I}{V_q} + \frac{k_2}{V_q + V_p}X - n_C Q \tag{4.3}$$

$$\dot{Q}_p = n_I(I - Q_p)\frac{V_I}{V_p} + \frac{k_2}{V_q + V_p}X \tag{4.4}$$

where I, Q, and Q_p [mU.L^{-1}] are the time-varying plasma insulin, active interstitial insulin, and passive interstitial insulin concentrations, respectively. X [mU] is the total non-specifically bound insulin after bolus insulin administration, and $U_{x,b}$ [mU] is the exogenous insulin delivered as a bolus. This compartment includes both insulin removed from plasma due to binding and insulin that was transported out of plasma due to the local high concentration, but has not diffused about the interstitial fluid. $U_{x,i}$ [mU] denotes exogenous insulin appearance in plasma due to an infusion, either from direct injection or as an appearance profile from a subcutaneous model [58]. U_n [mU] is the time-varying endogenous insulin secretion. All population constants requiring values to be chosen/fitted are described in Table 4.1.

TABLE 4.1: Insulin model constant parameters

Variable	Description	Units
n_I	Insulin transport to interstitium	min^{-1}
n_K	Renal insulin clearance	min^{-1}
n_L	Hepatic insulin clearance	min^{-1}
n_C	Insulin clearance from interstitium	min^{-1}
k_1	Bound insulin dissociation to plasma	min^{-1}
k_2	Bound insulin dissociation to interstitium	min^{-1}
x_L	First-pass hepatic extraction	-
x_B	First-pass clearance of insulin bolus	-
V_I	Insulin volume of distribution, plasma	L
V_q	Insulin volume of distribution, active interstitium	L
V_p	Insulin volume of distribution, passive interstitium	L
α_I	Saturation of hepatic insulin clearance	L.mU^{-1}

4.2.3 Insulin measurement bias

Compartment models suffer from the assumption of instantaneous, uniform mixing throughout each compartment. This assumption drastically reduces computational burden, but may introduce difficulties when insulin is delivered in an inherently transient bolus form, and measured at a site that is significantly different from the mean. If trans-endothelial transport is net positive to plasma, the venous concentration at the post-capillary bed measurement site will be elevated relative to the average plasma value, introducing bias to the insulin measurement. Experimental work has demonstrated arteriovenous insulin gradients of approximately 20% for skeletal muscle at steady state [59, 60]. Given the cephalic vein (a typical measurement site) receives an infinitesimal fraction of total cardiac output, this difference affects insulin measurement without significantly altering the average concentration in the plasma insulin pool. As both endogenous and exogenous insulin are added to the venous system post-measurement

site, and assuming the dominant tissue pre-measurement site is skeletal muscle, the local instantaneous concentration at the venous site is assumed:

$$I_m = I - \alpha_m \left[n_I(I - Q) - \frac{k_1}{V_I} X \right] \tag{4.5}$$

where I is the true plasma concentration, and I_m is the local value at the measurement site after being affected by capillary bed extraction. The averaged equilibrium across the peripheral capillary beds is scaled by α_m to achieve the desired arteriovenous gradient. At steady-state, $Q \to \frac{1}{2}I$ and $X \to 0$, thus:

$$\alpha_m = \frac{2}{n_I} \Delta_{AV} \tag{4.6}$$

where the arteriovenous gradient, Δ_{AV}, is set to 0.2 based on [59, 60]. This transformation allows the model to be identified using venous insulin data for both boluses and infusions.

4.2.4 *A-priori* parameters

One key aim is to identify or physiologically justify every constant parameter value in Table 4.1. With unknown clearances and volumes of distributions for hidden compartments, this model is unidentifiable with any realistic data density and quality [38]. Thus, volumes of distribution were selected for a-priori description using knowledge of human body composition. Although pharmacokinetic volumes of distribution are not strictly fluid volumes, using plasma and extracellular fluid (ECF) volumes is an approximation that may introduce bias, but will be adjusted for by fitting the remaining parameters.

A volume of distribution can be defined as the volume over which a species is homogeneously distributed immediately after direct injection into the relevant compartment. Accordingly, any heterogeneity in concentration or mismodelled clearances will affect the estimated volume. These factors make identification of these volumes difficult with insulin, as clearances are high and endogenous production is present. As an approximation, the central compartment was assumed to be circulating plasma volume, with $V_I = 2.8$L [61].

Interstitial fluid of insulin-sensitive tissues predominantly consists of skeletal muscle and adipose tissue. Skeletal muscle and adipose tissues contain approximately 10% ECF by mass [62, 63]. Estimates of adipose and muscle tissue masses in males (20% and 38% body mass, respectively) and females (28% and 30% body mass, respectively) [64, 65] can therefore be used to estimate the volume of this compartment. With an average human adult weight of 62 kg, $V_q = 3.6$L. The remaining interstitial fluid is from insulin-insensitive tissues, and can be estimated using the remaining ECF. Total ECF was estimated as 12.1L using anthropometric values [66]. Consequently, $V_p = 5.7$L.

The fraction of bolus insulin cleared prior to affecting measured plasma insulin was assumed to be $x_B = 0.20$. Local high concentrations around a bolus are assumed to dissipate after a single pass through the splanchnic, renal, and peripheral capillary beds. The liver and kidneys receive approximately 40% of normal cardiac output [67, 68], and both organs typically extract 50% of presented insulin. Thus, 0.2 is an appropriate value for this disappearance. Finally, hepatic saturation was taken directly from the ICING model [40]. Hepatic insulin clearance has previously been demonstrated to saturate [56, 69]. This saturation occurs at supraphysiological plasma insulin values, giving an estimate of $\alpha_I = 1.7{\times}10^{-3}$. All *a-priori* insulin model parameters are summarised in Table 4.2.

TABLE 4.2: *A-priori* insulin model parameters

Variable	Value	Units
V_I	2.8	L
V_q	3.6	L
V_p	5.7	L
x_B	0.2	-
α_I	1.7×10^{-3}	L.mU^{-1}

4.2.5 Identified parameters

The insulin model parameters that remain to be identified are diffusion rate of insulin between plasma and interstitium, first-pass hepatic extraction of endogenously secreted insulin, hepatic, renal, and interstitial clearances, and bound insulin dissociation to plasma and interstitium. Studies investigating the steady-state insulin ratio in insulin-sensitive tissues suggest a value of 0.5 (range 0.4-0.6) [59, 70, 71]. This value can be used to deparameterise the equation by ensuring net flux of insulin is zero at this ratio. Steady-state forces net flux out of the active interstitium to be zero:

$$n_I(I_{ss} - Q_{ss})V_I = n_C Q_{ss} V_q \tag{4.7}$$

As $I_{ss} = 2Q_{ss}$, the relationship between n_I and n_C can be defined:

$$n_I = \frac{V_q}{V_I} n_C \tag{4.8}$$

The model can be further deparameterised by relating the relative clearances out of the hepatic, renal, and interstitial fluid routes. Insulin clearance studies suggest approximately 60% of insulin is cleared by the liver, and the kidney clears 80% of the remaining

40%, or 32% of the total [52, 56]. The fractional clearances at steady state are therefore 60% hepatic, 32% renal, and 8% tissue. While these values are an approximation, the clearances are not uniquely identifiable with the available data, and thus this approximation was chosen over arbitrarily setting one or more of these clearances. Using the previously mentioned steady-state ratio, Equations (4.9) and (4.10) can be used to describe hepatic and renal insulin clearance in terms of n_C:

$$n_L V_I I_{ss} = \frac{0.6}{0.08} n_C V_q Q_{ss} \rightarrow n_L = 7.5 n_C \frac{V_q}{2V_I} \tag{4.9}$$

$$n_K V_I I_{ss} = \frac{0.32}{0.08} n_C V_q Q_{ss} \rightarrow n_K = 4.0 n_C \frac{V_q}{2V_I} \tag{4.10}$$

C-Peptide measurements and kinetics [72] compared to peak insulin levels after IV glucose injection [53] make first-pass hepatic extraction of endogenously secreted insulin identifiable, assuming equimolar simultaneous secretion of c-peptide and insulin. Nonlinear optimisation techniques can thus be used to fit the optimal values of n_C, k_1, k_2, and x_L, and Equations (4.8) to (4.10) used to calculate the corresponding values of n_I, n_L, and n_K.

4.2.6 Clinical data

4.2.6.1 DISST data

A dense data set including insulin secretion and an insulin bolus was available for use identifying insulin model parameters. A total of 217 DISST tests were undergone by 74 female participants from the Otago region of New Zealand. These individuals were undergoing these tests as part of a 10-week dietary intervention trial described by Te Morenga and colleagues [73]. Inclusion criteria required that participants either had a

body mass index (BMI) greater than 25, or greater than 23 and a family history of type 2 diabetes, or ethnic disposition toward type 2 diabetes. Participants were excluded if they had a major illness, including established diabetes, at the time of testing. Participant characteristics are summarized in Table 4.3. Ethical approval for this study was granted by the University of Otago Ethics Committee. Acronyms in the table are: NGT, normal glucose tolerance; IFG, impaired fasting glucose; T2DM, type 2 diabetes mellitus; and IQR, interquartile range.

TABLE 4.3: DISST cohort details

Status *NGT/IFG/T2DM*	Body mass index *Median [IQR]*	Sex *Male/Female*	Age *Median [IQR]*
63/11/0	32.4 [27.6-36.3]	0/74	42 [34.8-50.3]

A DISST test is a low cost, high sensitivity test for insulin sensitivity [74]. Low cost is achieved by sparse sampling, and the dynamic response to sequential IV glucose (10g, t=5 minutes) and insulin (1U actrapid, t=15 minutes) challenges. During a fully-sampled DISST test, BG, insulin and C-Peptide are sampled at t=0, 5, 10, 15, 20, 25, 30, 35, 40, and 50 minutes. C-Peptide measurements are used in conjunction with van Cauter kinetics [72] to estimate endogenous insulin secretion, and a coupled glucose-insulin system model is used to identify unknown model parameters, including insulin sensitivity. Figure 4.2 gives an overview of the DISST data set.

4.2.6.2 IVGTT data

A second dense data set including insulin infusions was also available. A total of 36 IVGTT tests were undergone by 14 participants from the Wellington region of New

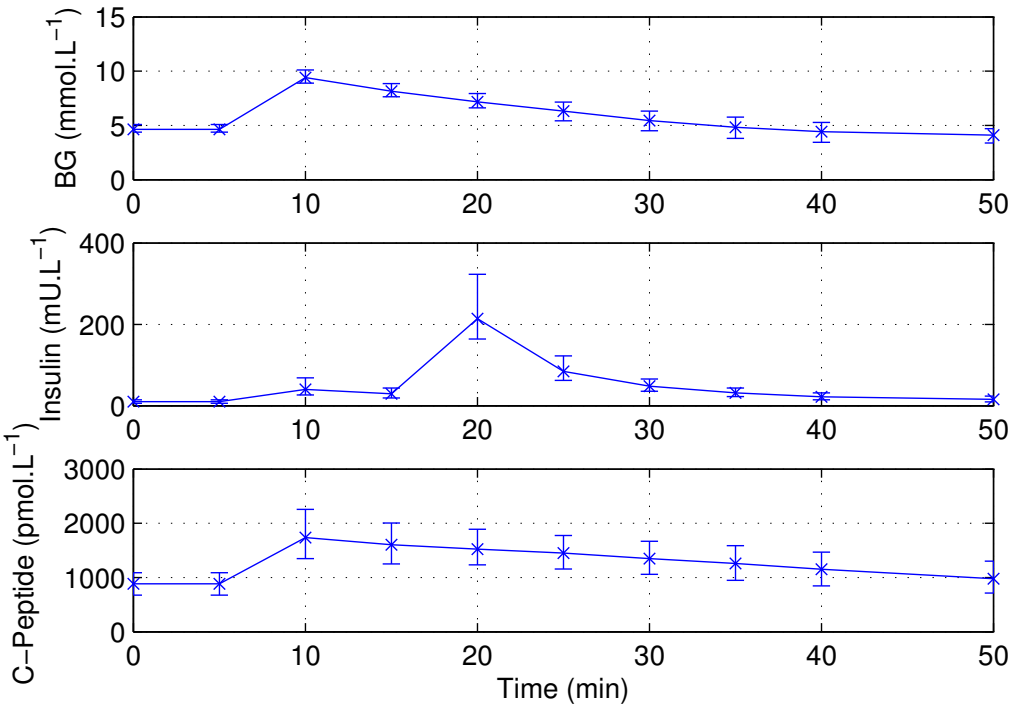

FIGURE 4.2: *Median DISST data for all species at each measurement time. Error bars show the 25th and 75th percentiles for each measurement set.*

Zealand as part of an investigation into the effect of the Atkins diet in a cohort of overweight and insulin resistant individuals with established type 2 diabetes [75]. Inclusion criteria required that subjects had established type 2 diabetes and were aged between 30 and 65 years with a BMI between 27 and 40 kg.m^2. Participants were excluded if they had any major physiological or psychological illness at the time of testing, or were pregnant or lactating. Insulin sensitivity tests were undertaken at weeks 0, 12 and 24, and two subjects withdrew during the study. This research was approved by the New Zealand Ministry of Health, central regional ethics committee. Cohort details are summarised in Table 4.4.

The insulin-modified IVGTT protocol described by Ward et al. [54] was used to assess insulin sensitivity during the study. The experimental protocol was a two-minute glucose infusion of 0.1g.kg.min^{-1} started at t=0 min, and insulin infusions of 3.5 mU.kg.min^{-1}

TABLE 4.4: IVGTT cohort details

Status *NGT/IFG/T2DM*	Body mass index *Median [IQR]*	Sex *Male/Female*	Age *Median [IQR]*
0/0/14	41.2 [37.8-43.8]	8/6	46 [41-54]

(t=2 to t=4 min), 0.5 mU.kg.min^{-1} (t=7 to t=17 min), 0.25 mU.kg.min^{-1} (t=17 to t=50 min), and 0.1 mU.kg.min^{-1} (t=50 to t=300 min). This insulin profile was selected to mimic the first and second insulin production phases of healthy, normo-glucose tolerant individuals. Blood samples were taken at t=-10, -5, -1, 0, 1, 2, 3, 4, 5, 6, 8, 10, 12.5, 15, 20, 25, 30, 35, 40, 50, 60, 70, 80, 90, 100, 120, 140, 160, 180, 210, 240, 270, and 300 minutes, and assayed for both insulin and glucose. Figure 4.3 gives an overview of the IVGTT data set.

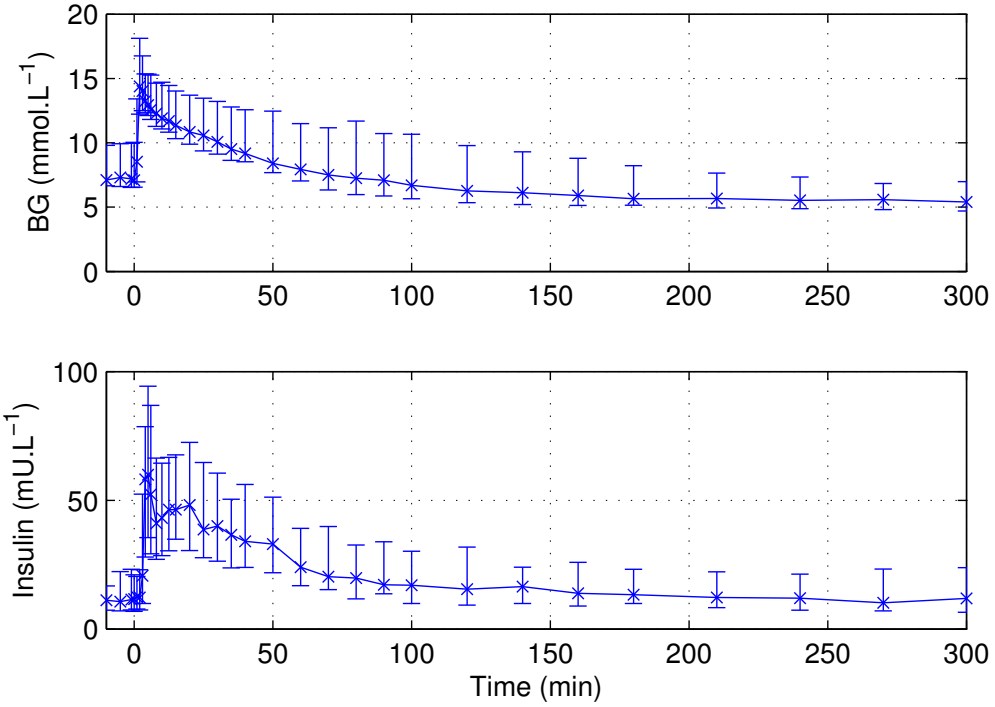

FIGURE 4.3: *Median IVGTT data for all species at each measurement time. Error bars show the 25th and 75th percentiles for each measurement set.*

4.2.7 Analyses

The aim of this research was to create a whole cohort model, matching both infusion and bolus delivery. Thus, a median patient was created from both the DISST and IVGTT data. As C-Peptide data was not available during the IVGTT tests, insulin secretion was calculated from basal plasma insulin, and the data around the first-phase secretion (t < 7 min) was omitted during fitting. Additionally, all points after t=100 min in the IVGTT were discarded to prevent these points dominating the parameter identification procedure. The two median patients were identified concurrently to find n_C, k_1, k_2, and x_L, recovering the parameter values that best describe the two cohorts simultaneously. Descriptive capability was then assessed by simulating this model for all patients in each cohort, and calculating the relative error.

Relative error for the training data was reported as a percentage for each measurement. The error between the whole-cohort model and individual patient data was reported as the integral of the absolute error relative to the integral of the measured data. Low insulin measurements and high variation during the final 20 minutes of the DISST test meant error integrals were more suitable than individual measurements.

4.3 Results

Identified parameter values were $n_C = 0.0448$, $k_1 = 0.224$, $k_2 = 0.0184$, and $x_L = 0.303$. The dependent parameters, and all *a-priori* constants, are summarised in Table 4.5. The influence of the measurement site insulin transformation is shown for IV bolus administration in Figure 4.4, showing the magnitude of the transient insulin peak due to non-uniform mixing.

TABLE 4.5: Summary of model constants

Variable	Value	Units	Origin
n_I	0.0576	min^{-1}	fitted, dependent
n_K	0.115	min^{-1}	fitted, dependent
n_L	0.216	min^{-1}	fitted, dependent
n_C	0.0448	min^{-1}	fitted
k_1	0.224	min^{-1}	fitted
k_2	0.0475	min^{-1}	fitted
x_L	0.303	-	fitted
x_B	0.2	-	*a-priori*
V_I	2.8	L	*a-priori*
V_q	3.6	L	*a-priori*
V_p	5.7	L	*a-priori*
α_I	1.7×10^{-3}	L.mU^{-1}	*a-priori*
α_m	6.94	min	*a-priori*

The resulting relative error between the fitted profile and the training data is shown in Figure 4.5 for both the DISST and IVGTT tests. Relative error is similar between the two tests, despite differing insulin administration and plasma insulin profiles. All error values are within 30%, with the largest relative error occurring during the low infusion rate period after t=50min during the IVGTT. Error across all patients in each cohort is also similar, as seen in Figure 4.6, where median error is approximately 30%, with 75% of values below a relative error of 40%.

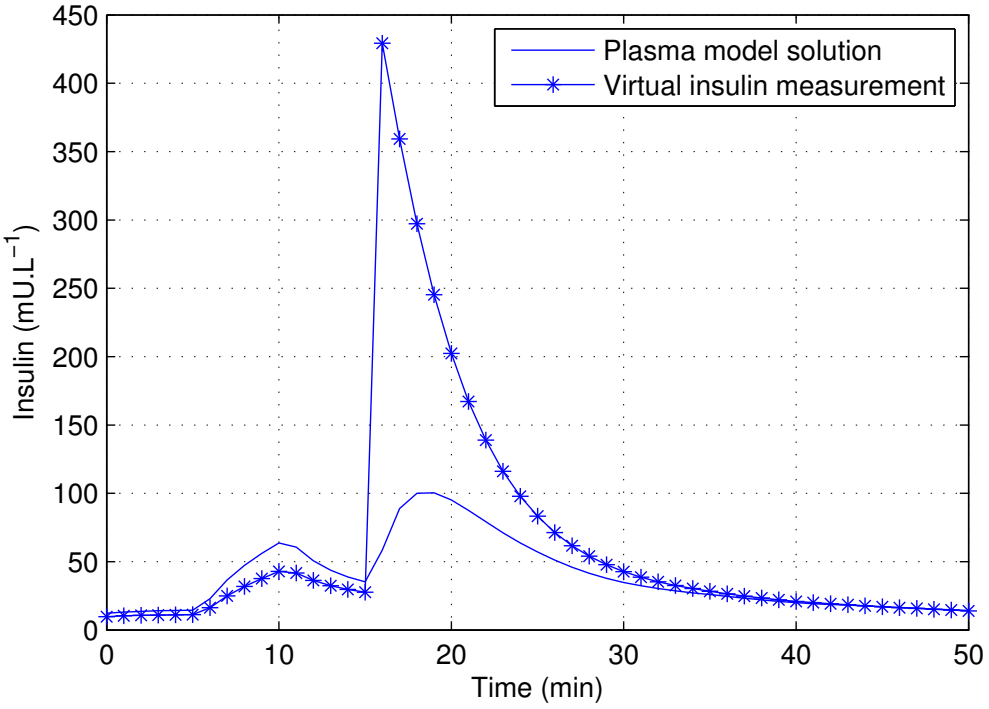

FIGURE 4.4: *Effect of insulin measurement transformation. The model solution for the fitted parameters is shown alongside the transformed insulin measurement for a DISST test. The non-uniform mixing acts to reduce the apparent effect of endogenously secreted insulin, and increase the apparent effect of an IV insulin injection.*

4.4 Discussion

This work is a natural progression of the ICING model insulin kinetics. While the ICING model [40] has proved useful for describing and predicting BG, the insulin model can benefit from a more physiologically relevant description. The new model developed with this focus proved capable of simultaneously describing both bolus and infusion dynamics, while using more physically relevant volumes of distribution and balancing insulin clearance sites to match mean reported data in [52]. Additional complexity was introduced in the form of an intermediate bolus compartment and an adjusted insulin measurement concentration, but was necessary to describe both the bolus and infusion kinetics simultaneously.

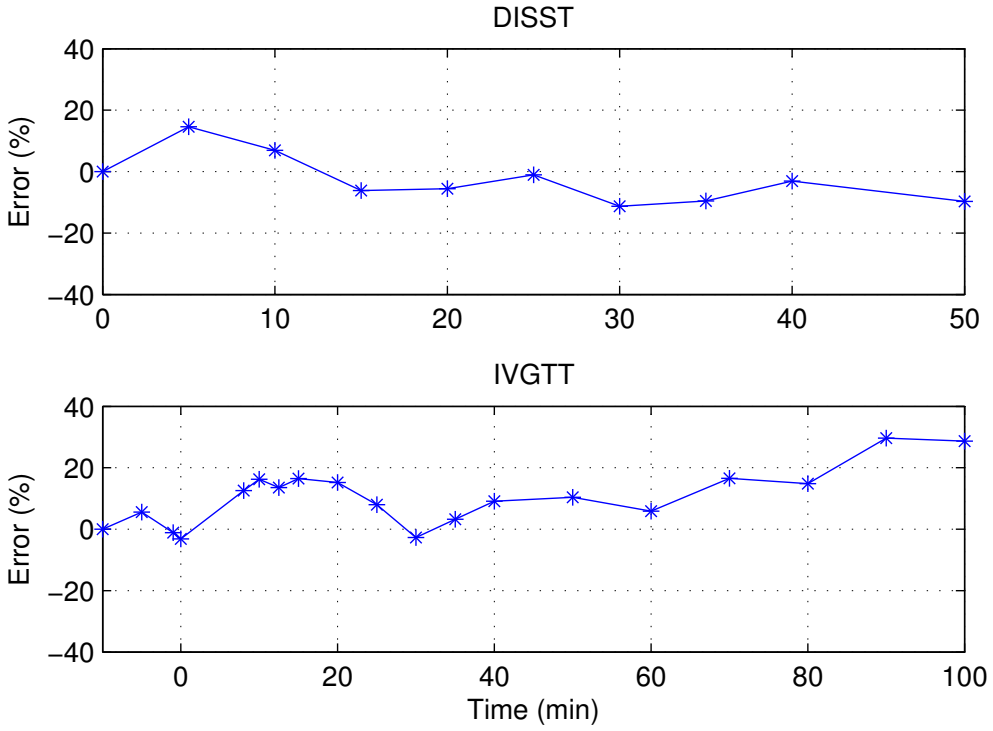

FIGURE 4.5: *Relative error between training data and the model solution generated using the selected parameter set.*

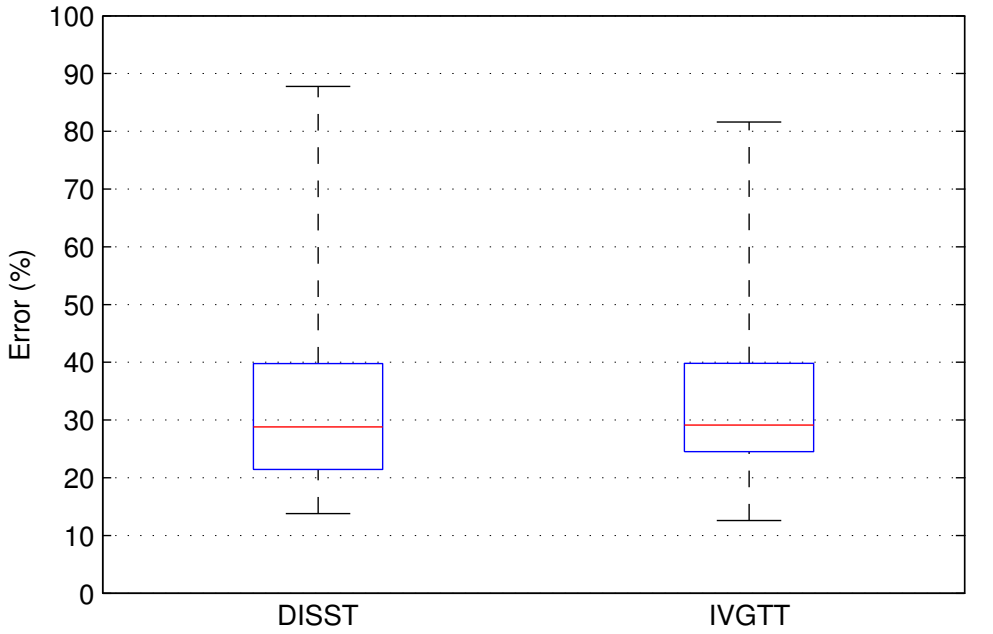

FIGURE 4.6: *Cumulative error relative to integral of measured data across all patients in each cohort, using the selected parameter set. Boxplot whiskers show the 5th and 95th percentiles.*

All models approximate reality and make assumptions. The new model formulation was developed using a range of assumptions, and exhibited strong descriptive capabilities. A-priori associations between anthropometric values and fluid volumes were used to estimate the volumes of distribution, under the assumption that insulin diffuses about a physical volume, and that the main portion of insulin sensitive cells are found in either muscle or adipose tissue, which matches the physiology [52]. Diffusion kinetics were estimated by assuming a steady-state insulin ratio between plasma and the interstitial fluid of insulin sensitive tissues was maintained. Finally, insulin clearances were fitted under the assumption that a physiological levels, 60% of peripherally infused insulin is cleared by the liver, 32% by the kidneys, and 8% by peripheral tissues.

Each of these assumptions may introduce error. However, limitations on available data, particularly when used clinically, and inherent non-uniformities introduce a necessity for these choices to ensure identifiability of critical parameters. Furthermore, as this model is intended for use in control, rather than diagnostic purposes where there is greater data availability, the error introduced can be offset to a significant degree as differences in magnitude simply cause an offset in the fitted insulin sensitivity. An adaptive control algorithm can therefore respond safely. These arguments apply in particular to volumes of distribution, where errors introduce linear offsets in the absence of saturation dynamics. As saturation terms in this model have little effect at physiological dynamics, accuracy in these volumes has few implications. However, non-representative anthropometric relationships and insulin antibody binding are likely to be the main sources of error in the estimated volumes.

As the steady-state ratio between active interstitial fluid and plasma has been well established [59, 70, 71], the major assumption requiring justification is the presumed relative contribution of each clearance route. An assumption here is necessary, as renal insulin

clearance has not been shown to saturate, while hepatic clearance has [56]. At physiological ranges, the similarity between the hepatic and renal clearance dynamics prevents unique identification [38] and thus fitting is not robust in the presence of noise. As a result, the relative contribution of each must be estimated. Identified tissue clearance depends heavily on the volume of distribution of the active interstitium compartment. Thus, the relative contribution of tissue clearance was included to reduce the correlation between this volume error and error in n_C from Equation 4.7. While this assumption is very broad, using relative contributions taken from literature [52] still permitted clinically observed to be well matched in Figure 4.6. Overall, these results show that use of a median patient to derive whole-cohort parameters did not compromise ability to capture fundamental kinetics.

However, the DISST cohort is not heterogeneous, and the IVGTT cohort includes only T2DM individuals and is much smaller. Inclusion criteria for the study using DISST tests in the study prevented any males, individuals with BMI less than 25, or diagnosed diabetes. This dataset was chosen due to a combination of availability, relative density of measurements, size, and complexity of dynamics. In particular, separation of IV glucose (stimulating a first phase secretory response) and IV insulin permitted greater resolution of first-pass hepatic extraction and the other insulin clearances. In addition, relatively expensive C-Peptide measurements permit estimation of insulin secretion. For the IVGTT, T2DM individuals have a limited first-phase secretory response to IV glucose, and thus lack of C-Peptide has a limited affect. The two cohorts are thus suitable for parameter identification. The main area that will require work is an insulin secretion model for T2DM, where impaired beta cell function in T1DM means insulin secretion is negligible beyond early stages.

Overall, parameter identification was carried out in a manner appropriate to the inter-

and intra- patient variation in insulin kinetics. Restricting parameter values by enforcing a-priori relationships ensures the fate of insulin in the body is realistic and matches observations, which may allow inclusion of hepatic glucose balance kinetics in future. Particularly, the transparent nature of the a-priori relationships also permits simple modifications as new knowledge arises.

4.5 Summary

The outcome is a set of parameter estimates derived in a stable manner using a dense dataset. A-priori values and physiological estimates of the fate of circulating insulin were used to circumvent a practically unidentifiable model, and restrict assumptions to easily updated values. The resulting formulation adequately describes circulating insulin dynamics, including both bolus and infusion dynamics. Thus, the ICING model has been extended and improved, and is better suited to describe subcutaneous insulin dynamics after absorption.

Chapter 5

A Unified Model of Subcutaneous Insulin Absorption

5.1 Introduction

One significant modelling problem in model-based glycaemic control is the appearance rate in plasma of slow-release subcutaneous insulin types. A need for unified, simple models exists, as treatment of insulin-dependent outpatient diabetes typically involves multiple daily subcutaneous insulin injections. Optimising insulin therapy through model-based decision support thus requires the action of each insulin form present in the body to be described both independently and in a unified format with other insulin types. Numerous attempts have been made to model and validate these absorption profiles [51, 58, 76–78], but no definitive approach has arisen.

Subcutaneous insulin injections can be administered to the abdomen, upper arm, or thigh, and can range from basal insulin analogues to extremely short acting monomeric

insulins. The complexity of each absorption profile depends on the particular preparation, with the molecular affinity for larger insulin complexes, or association state, the key predictor [79]. Significant degradation occurs at the insulin depot [80, 81], while temperature changes, local massage, exercise, and many other factors can alter the absorption profile [51]. The inherent inter- and intra- patient variability in the appearance rate of insulin in plasma is thus extremely high, creating significant uncertainty in any dosing protocol.

A simple yet powerful approach to modelling subcutaneous insulin is a compartment model. However, as with all mathematical models, even simple models suffer from the problem of non-identifiability [50] when identifying parameters with incomplete data. In the case of subcutaneous insulin, multiple hidden compartments make unique identification of all possible parameters implausible. This factor has been consistently overlooked in publications on the subject to date, and as a result, even models with the same structure can vary significantly in internal model parameter values.

In short, the use of model-based methods in glycaemic control requires an inclusive model that permits superimposed insulin profiles with different insulin analogues. However, very few efforts have been made to unify an independently derived model of circulating insulin kinetics with a subcutaneous insulin model. The level of uncertainty precludes a standard parameter identification approach. The slow changes in appearance of a subcutaneous insulin dose further prevent unique identification of volumes of distribution, clearances, and transport rates, while also identifying the pharmacokinetic parameters associated with subcutaneous insulin appearance in plasma.

This research proposes a model that incorporates four of the major insulin analogues, and interfaces with an independently derived model of circulating insulin. The resulting

model is intended to recreate the plasma insulin profiles observed in clinical trials on a descriptive, rather than diagnostic, level, enabling its use in decision-support algorithms. Prior work by the wider research group led to a unified description of the major insulin types [58, 82], but a non-physiological plasma insulin compartment was used. This work is thus unique in independently fitting a circulating insulin model, and using common compartments to simultaneously fit parameters describing all insulin types, thus circumventing non-identifiability for long-acting insulins such as glargine.

5.1.1 Literature review

The variation between researchers can be simply outlined by comparing the circulating insulin compartments in four published models when forced by an IV bolus. Comparing the appearance profile of subcutaneous insulin shows little difference, as each full parameter set has been fitted to match clinical data, while IV insulin directly enters the main compartment and allows for direct comparison. Figure 5.1 and 5.2 show the simulated responses to an IV insulin bolus, with endogenous insulin secretion calculated using median C-Peptide measurements and a widely accepted model [72].

Kobayashi et al. [83] presented two models in the same paper (Figure 5.1). While the single compartment formulation is extremely poor, the two-compartment formulation is perhaps the most descriptive of those published to date. The accuracy of this formulation can be attributed to the use of IV insulin responses to fit this portion of the model. Unfortunately, the authors then proceeded to conclude that a "one-compartment open model with first-order absorption and elimination was appropriate for estimating the kinetics of subcutaneously administered insulin", thus somewhat negating one of the more diligent approaches to modelling subcutaneous insulin. On the other hand, Mosekilde

et al. [76] opted for extremely high clearance rates, and transport rates between plasma and interstitium were fast enough to render the second compartment irrelevant.

Tarin et al. modelled both NPH and glargine [84] using a three compartment description of circulating insulin shown in Figure 5.2. In contrast, Wong et al. used a single compartment, and more closely resembles the DISST data. The subcutaneous models themselves differ significantly also, with Kobayashi and Wong both using simple compartmental models, and Mosekilde and Tarin discretising the spherical depot itself and utilizing a series of partial differential equations.

Although Figures 5.1 and 5.2 cannot be called representative or quantitative, the comparisons highlight how inconsistent the description of circulating insulin is in literature. Such inconsistency means that each model is not useful practically. In particular, even though the underlying justifications may be acceptable, the varied descriptions of plasma insulin mean the fitted parameters of the presented models are not relevant, because the absorption parameters will have adjusted to ensure the model fits, and cannot be used in isolation. Thus, there is the problem of effective over-parameterisation, and a new description is required to adequately fit a validated model of circulating insulin dynamics.

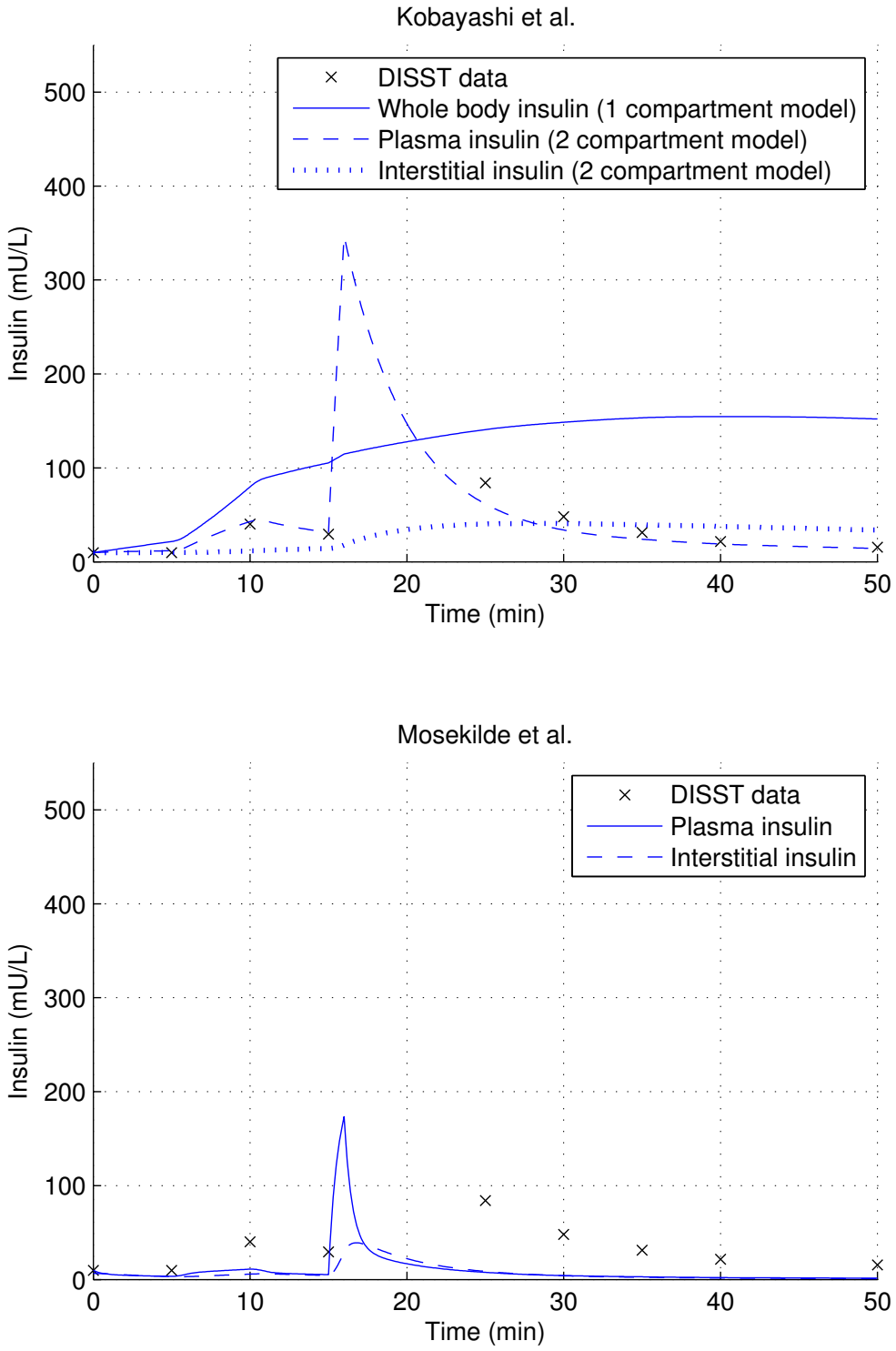

FIGURE 5.1: *Simulation of a DISST test using the models fitted by Kobayashi et al. [83] and Mosekilde et al. [76] plotted against median data from the DISST cohort [53]*

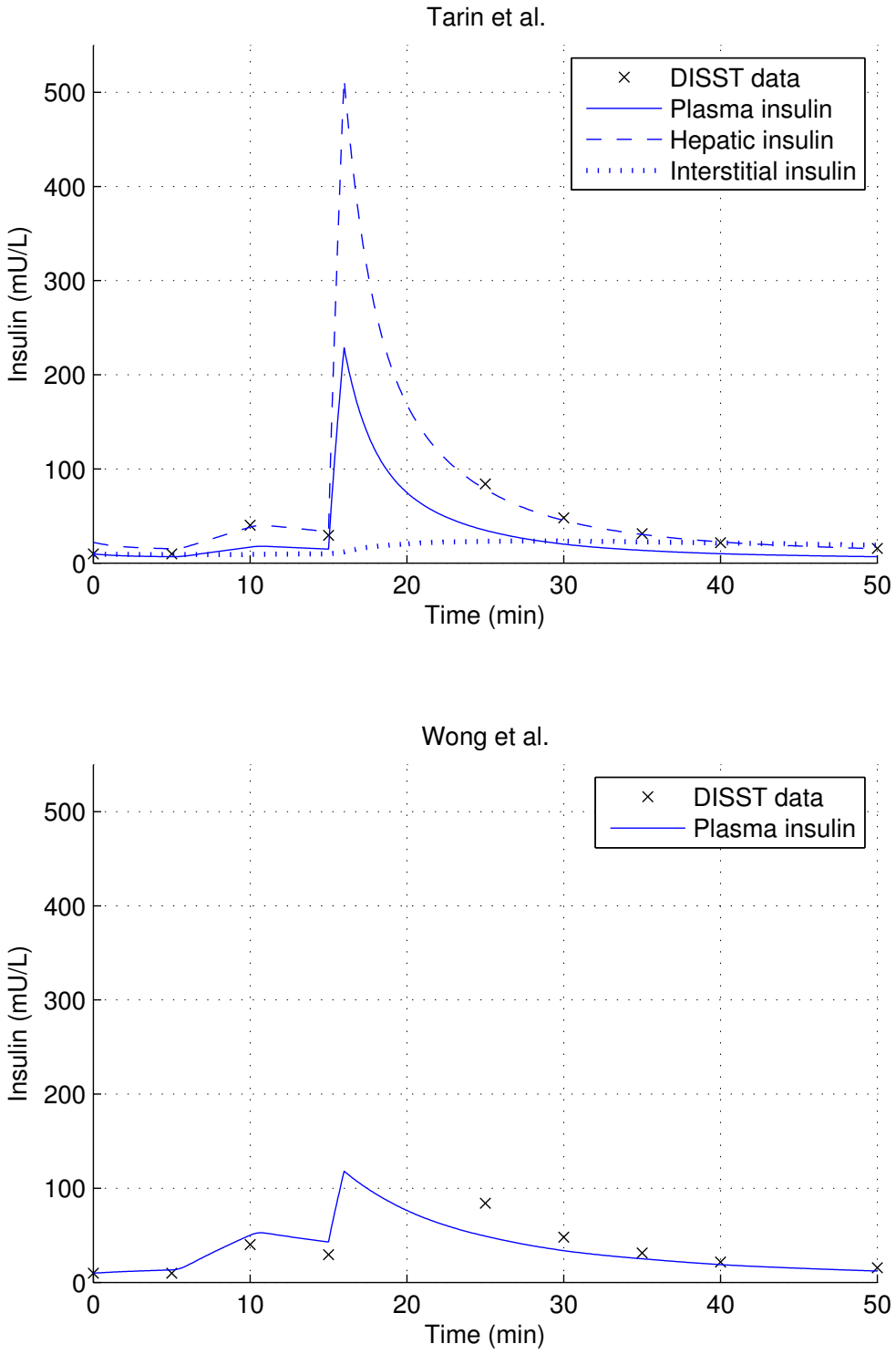

FIGURE 5.2: *Simulation of a DISST test using the model fitted by Tarin et al. [84] and Wong et al. [58] plotted against median data from the DISST cohort [53]*

5.2 Methods

5.2.1 Model

Insulin and its analogues have a number of molecular states, including monomeric, to dimeric, hexameric, crystalline, or precipitate forms. The fastest absorbing insulins have little tendency to self-associate into larger molecules, thus remaining largely in the monomeric state and rapidly traversing the capillary membrane [85]. The absorption of dimeric and monomeric insulin has been demonstrated to be different [79], but, as the magnitude of the difference is much smaller than the difference between other forms, these two states have been lumped into a single shared local delivery site compartment.

The mono-exponential absorption of low molecular weight insulin to the plasma [79] justifies a linear clearance from this shared compartment. However, while absorption is mono-exponential, a dual exponential clearance is observed in circulating plasma insulin levels. As the half-life of insulin in plasma is much faster than the timescale of subcutaneous insulin absorption, this dual exponential justifies a local interstitial insulin compartment that linearly clears into plasma. Depot spreading due to diffusion is ignored, as the larger molecules diffuse slowly (or are stationary), and diffusion of the smaller molecules is assumed to be clearance into the local interstitium.

More complex, longer acting insulin preparations include a hexameric form, in equilibrium with the dimeric concentration:

$$C_h = Q{C_{dm}}^3 \tag{5.1}$$

where C_h and C_{dm} are the concentrations of hexameric and dimeric/monomeric insulin [mU/mL], respectively, and Q is the equilibrium constant [ml^2 mU^{-2}].

Insulin glargine and neutral protamine Hagedorn (NPH) both have insoluble forms, the slow clearance of which gives their protracted action profile. NPH is assumed to have a linear clearance out of a crystalline compartment, while glargine achieves a uniquely flat basal profile through a saturating clearance out of a micro-precipitate compartment. As glargine doses do not saturate at the same level, this saturation is based on concentration instead of absolute quantity. These interactions, and the model structure, are summarised in Figure 5.3.

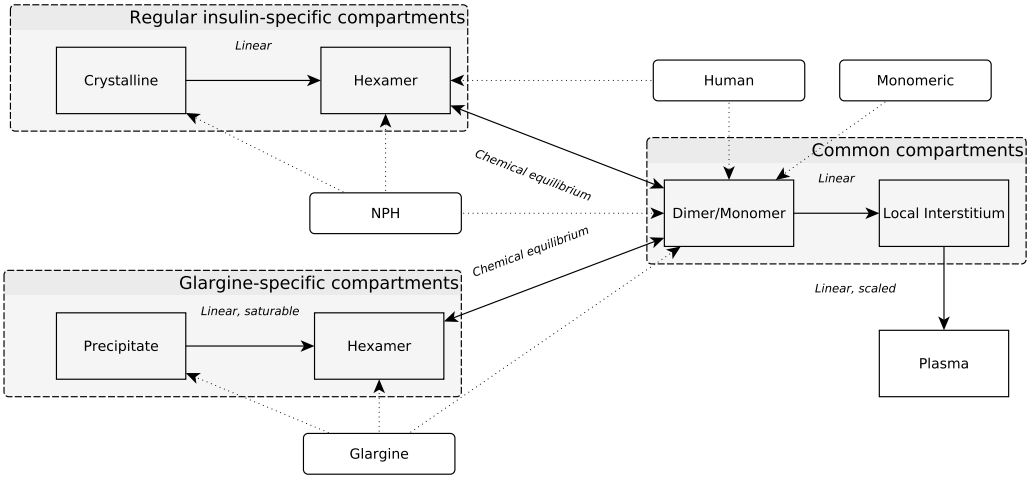

FIGURE 5.3: *Schematic of subcutaneous model compartments and relationships. The clearances are labelled with a brief description.*

The corresponding equations describing the model dynamics are defined for each compartment, as follows:. Local interstitium:

$$\dot{x}_i = k_{dm} x_{dm} - k_i x_i \tag{5.2}$$

Dimeric/Monomeric compartment:

$$\dot{x}_{dm} = \begin{cases} U_{dm} - k_{dm} x_{dm}, & \text{monomeric} \\ U_{dm} + p_d \left(\frac{1}{3} x_h - Q \frac{x_{dm}^3}{V^2} \right) - k_{dm} x_{dm}, & \text{regular/NPH} \\ U_{dm} + p_d \left(\frac{1}{3} x_{h,gla} - Q_{gla} \frac{x_{dm}^3}{V^2} \right) - k_{dm} x_{dm}, & \text{glargine} \end{cases} \tag{5.3}$$

Hexameric compartment:

$$\dot{x}_h = U_h + k_c x_c - p_d \left(\frac{1}{3} x_h - Q \frac{x_{dm}^3}{V^2} \right) \tag{5.4}$$

Hexameric glargine compartment:

$$\dot{x}_{h,gla} = U_{h,gla} + \frac{k_p x_p}{V + \alpha_{gla} x_p} V - p_d \left(\frac{1}{3} x_{h,gla} - Q_{gla} \frac{x_{dm}^3}{V^2} \right) \tag{5.5}$$

Crystalline compartment:

$$\dot{x}_c = U_c - k_c x_c \tag{5.6}$$

Micro-precipitate compartment:

$$\dot{x}_p = U_p - \frac{k_p x_p}{V + \alpha_{gla} x_p} V \tag{5.7}$$

where x_i, x_{dm}, x_h, $x_{h,gla}$, x_c, and x_p are the total insulin in local interstitium, dimeric or monomeric, hexameric, hexameric glargine, crystalline, and precipitate compartments [mU], respectively. k denotes a clearance [min^{-1}] and U an exogenous appearance [mU min^{-1}], with the subscript corresponding to the compartment listed previously. Q_{gla} is the equilibrium constant of the more stable glargine hexamer [ml^2 mU^{-2}], V is the

volume of the subcutaneous depot [ml], α_{gla} is the saturation constant for precipitate dissolution [ml mU^{-1}], and p_d is the hexameric dissociation rate [min^{-1}].

When monomeric insulins are used, total insulin dose $U_T = U_{dm}$. However, more complex insulins exist in multiple forms simultaneously (e.g. U_{dm}, U_h, and U_c, Figure 5.3), and equilibrium conditions must be used to calculate initial conditions for each compartment. In particular, human insulins exist in an equilibrium state between hexameric (h) and dimeric/monomeric (dm) forms in the subcutaneous depot. As a result, the total insulin dose is defined:

$$U_T = U_h + U_{dm} \tag{5.8}$$

where equilibrium conditions dictate that the rates of forward and reverse chemical association/dissociation reactions are identical:

$$\frac{1}{3}U_h = Q\frac{U_{dm}^3}{V^2} \tag{5.9}$$

Substitution of Equation (5.9) into Equation (5.8) gives:

$$U_T = 3Q\frac{U_{dm}^3}{V^2} + U_{dm} \tag{5.10}$$

which can be solved for given U_{dm}, and subsequently U_h. Equation (5.10) is of the form $\alpha x^3 + x + \beta = 0$, where $\alpha = 3Q/V^2$ and $\beta = -U_T$. A closed form solution is available for rapid evaluation:

$$U_{dm} = \frac{\sqrt[3]{\sqrt{81\alpha^4\beta^2 + 12\alpha^3} - 9\alpha^2\beta}}{\sqrt[3]{18}\alpha} - \frac{\sqrt[3]{\frac{2}{3}}}{\sqrt[3]{\sqrt{81\alpha^4\beta^2 + 12\alpha^3} - 9\alpha^2\beta}} \tag{5.11}$$

Long-acting insulins precipitate or crystallise when introduced to interstitial fluid. A

fraction of NPH, β_{NPH}, is assumed to form a crystalline structure upon injection. Exogenous insulin appearance in the crystalline compartment is therefore $U_c = \beta_{NPH} U_T$. The remaining insulin, $(1 - \beta_{NPH})U_T$, is distributed between the remaining compartments, as described by Equation (5.10). Glargine behaves similarly, with $U_p = \beta_{gla} U_T$, and substituting $(1 - \beta_{gla})U_T$ for U_T in Equation (5.10).

Finally, appearance of dimeric/monomeric insulin in plasma is described:

$$U_x = f_{type} k_i x_i \tag{5.12}$$

Each different formulation has a unique scaling factor, f_{type}. This parameter is analogous to a unique clearance in the local interstitium, and highlights the many currently unquantified processes at work during the absorption process. In essence, f_{type} lumps together such dynamics as clearance from the subcutaneous depot, affinity to antibodies (appearing as different volumes of distribution), and altered clearance routes that affect the deconvolved integrals in parameter identification with sparse data.

$$f_{type} = \begin{cases} f_{dm}, & \text{monomeric insulin} \\ f_{RI}, & \text{regular (human) insulin} \\ f_{NPH}, & \text{NPH insulin} \\ f_{gla}, & \text{insulin glargine} \end{cases} \tag{5.13}$$

This mixed chemical and kinetic modelling approach allows a consistent model formulation to be used while retaining drug-specific behaviour.

5.2.2 Parameter identification

Equations (4.3) and (4.4) can be directly solved for Q and Q_p, given a known I. Endogenous insulin secretion is minimal at basal levels, and is adjusted for by subtracting the basal insulin concentration from the I solution. Thus, a known I can permit deconvolution of U_x from Equation (4.1), using:

$$I(t) = I(t_0) + \frac{1}{V_I}\int_{t_0}^{t} U_x \mathrm{d}x - n_K \int_{t_0}^{t} I \mathrm{d}x \\ - n_I \int_{t_0}^{t} (2I - Q - Q_p)\mathrm{d}x - n_L \int_{t_0}^{t} \frac{I}{1+\alpha_G I}\mathrm{d}x \quad (5.14)$$

$$\frac{1}{V_I}\int_{t_0}^{t} U_x \mathrm{d}x = I(t) - I(t_0) - n_K \int_{t_0}^{t} I \mathrm{d}x \\ - n_I \int_{t_0}^{t} (2I - Q - Q_p)\mathrm{d}x - n_L \int_{t_0}^{t} \frac{I}{1+\alpha_G I}\mathrm{d}x \quad (5.15)$$

Equation (5.15) gives a value for total exogenous insulin appearing in plasma at each plasma insulin measurement. The error between the subcutaneous insulin model and this estimated appearance at each measurement is defined:

$$\epsilon_{t_m} = \int_{t_0}^{t_m} U_x \mathrm{d}x - f_{type} k_i \int_{t_0}^{t_m} x_i \mathrm{d}x \;\forall\; t_m \quad (5.16)$$

Furthermore, f_{type} is a scaling factor, and thus depends on the total error. This dependence is defined by:

$$f_{type} \begin{bmatrix} k_i \int_{t_0}^{t_0} x_i \mathrm{d}x \\ \vdots \\ k_i \int_{t_0}^{t_m} x_i \mathrm{d}x \end{bmatrix} = \begin{bmatrix} \int_{t_0}^{t_0} U_x \mathrm{d}x \\ \vdots \\ \int_{t_0}^{t_m} U_x \mathrm{d}x \end{bmatrix} \quad (5.17)$$

where f_{type} can be calculated by solving the linear system. By deconvolving the exogenous appearance profile and using Equation (5.17) to solve for f_{type}, rather than simulating the full system and using error in the plasma insulin compartment, one parameter is removed from the gradient descent algorithm. Additionally, Equation (5.17) ensures the error vector of the objective function ideally has a centroid of zero, allowing a gradient descent algorithm to identify the parameters corresponding to the optimal shape. Removing a single parameter when fitting each insulin type means 4 parameters are removed from the overall system, which significantly reduces the dimensionality of the error surface when multiple insulin types are used in the same optimisation routine. Use of multiple insulin types allows "averaged" parameters to be estimated that work for all insulin types.

5.2.3 Clinical data

Published data was gathered to describe typical plasma insulin profiles for monomeric insulin [86], regular insulin [86], NPH insulin [87], and insulin glargine [88]. The baseline-corrected plasma insulin profiles for each insulin formulation are shown in Figure 5.4. These profiles were electronically extracted to minimise error, and used in the following fitting procedure. Available cohort details are recorded in Table 5.1. All doses had a concentration of 100 U.ml^{-1}, and where weight was not explicitly published, BMI was used to estimate the dose size.

TABLE 5.1: Average cohort details

Cohort	N	Age	BMI	Weight	Insulin dose	Gender	Diagnosis
Novorapid	18	31	23.6	-	0.2 U/kg	Male	Healthy
Actrapid	18	31	23.6	-	0.2 U/kg	Male	Healthy
NPH	11	22.8	23.4	76.5	0.5 U/kg	Male	T1DM
Glargine	15	27.4	22.2	-	0.4 U/kg	Male	Healthy

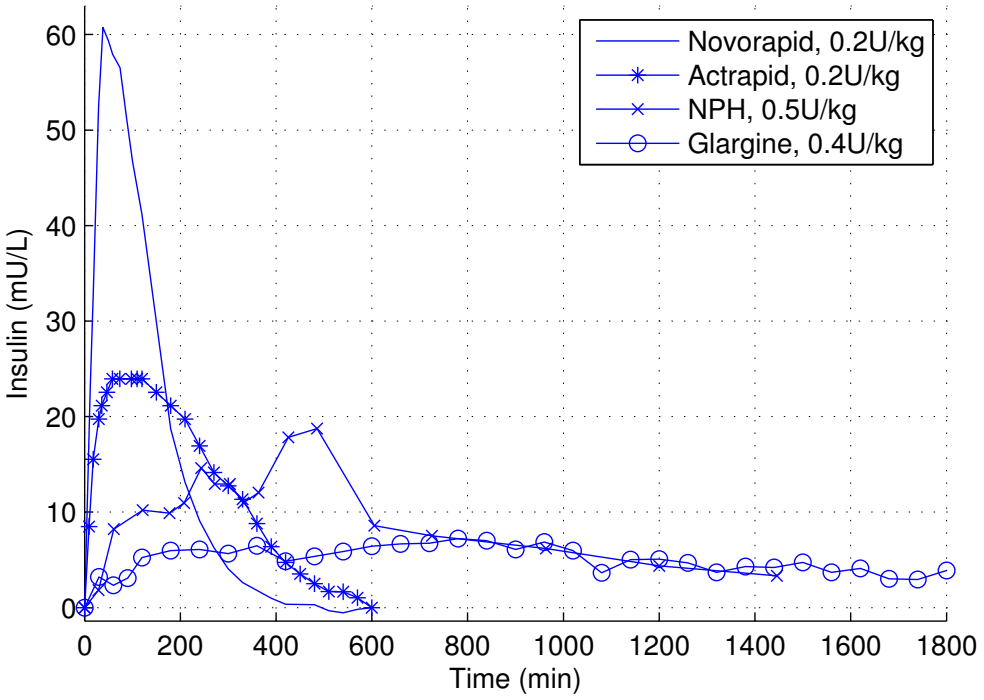

FIGURE 5.4: *Raw baseline-corrected plasma insulin profiles for monomeric insulin [86], regular insulin [86], NPH insulin [87], and insulin glargine [88].*

5.3 Results

The exogenous insulin appearance profiles shown in Figure 5.5 were derived from the fundamental plasma insulin profiles presented in Figure 5.4. The parameters in Table 5.2 were identified from these profiles. Note that p_d was selected (not identified), as the parameter has been previously demonstrated to be poorly correlated with error in the appearance profile [76].

Figure 5.6 shows the identified and raw cumulative appearance profiles, while Figure 5.7 indicates the quality of the fit by showing the residuals for each profile. For the longer acting insulins, NPH and glargine, the fitted parameter set indicates absorption is incomplete at the end of the measurement period.

Finally, Figure 5.8 gives a qualitative comparison of the different appearance profiles

modelled. The simulated response to 10U of 100U/ml insulin through each of the routes shows the major features captured by the model. These features are the rapid appearance and decay of monomeric insulins, the reduced peak and protracted action of self-associating regular insulins, the irregular protracted action of NPH, and the uniquely flat action profile of glargine.

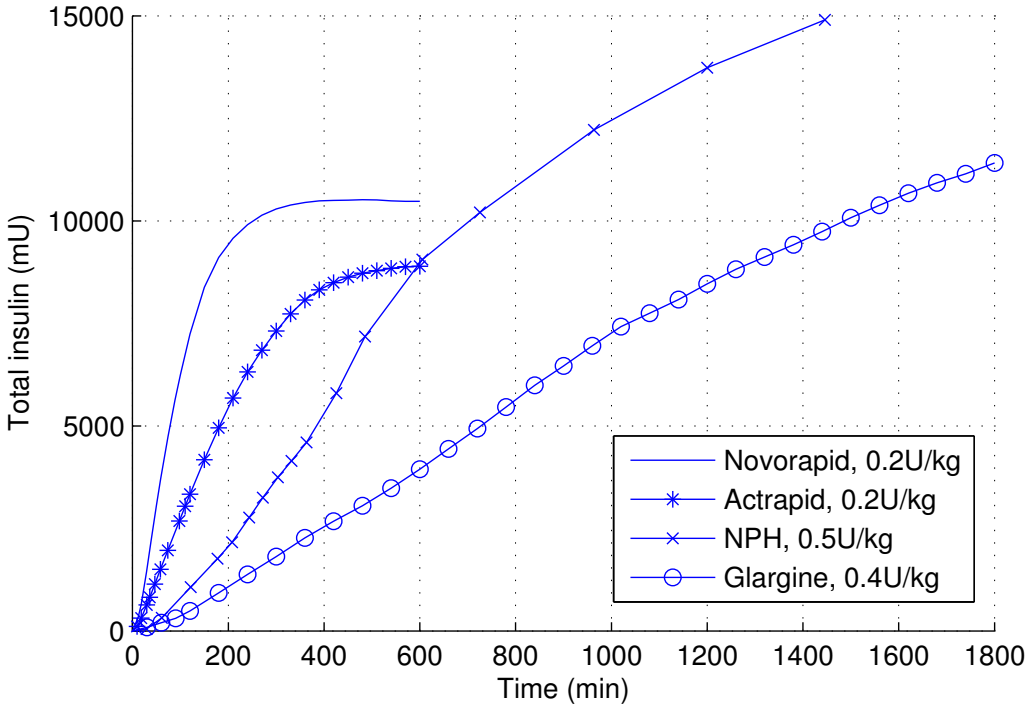

FIGURE 5.5: *Deconvolved cumulative appearance profiles for 4 distinct insulin formulations.*

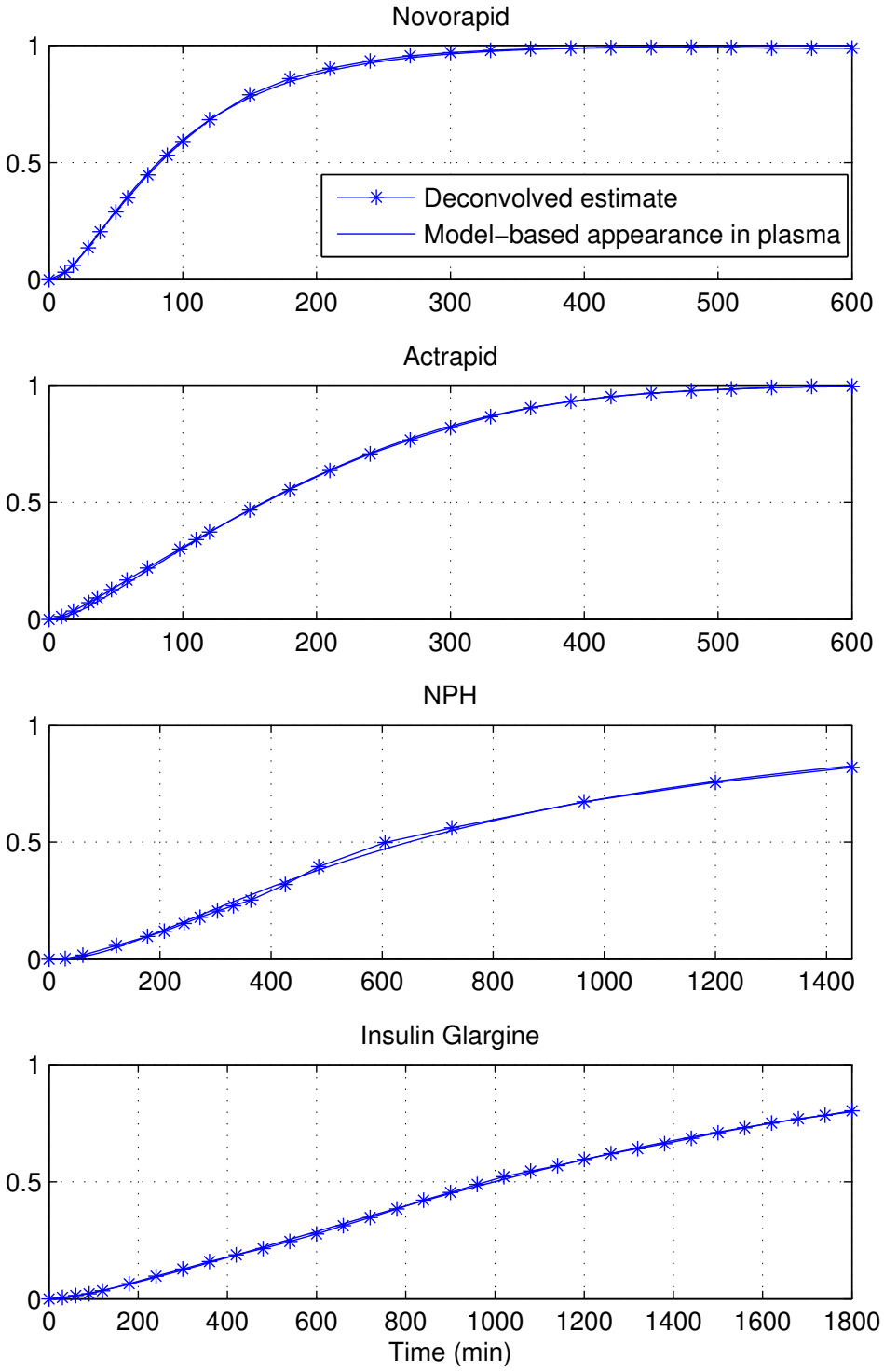

FIGURE 5.6: *Fractional appearance profiles for 4 distinct insulin formulations. Absorption is thus incomplete for the longer acting NPH and glargine insulins.*

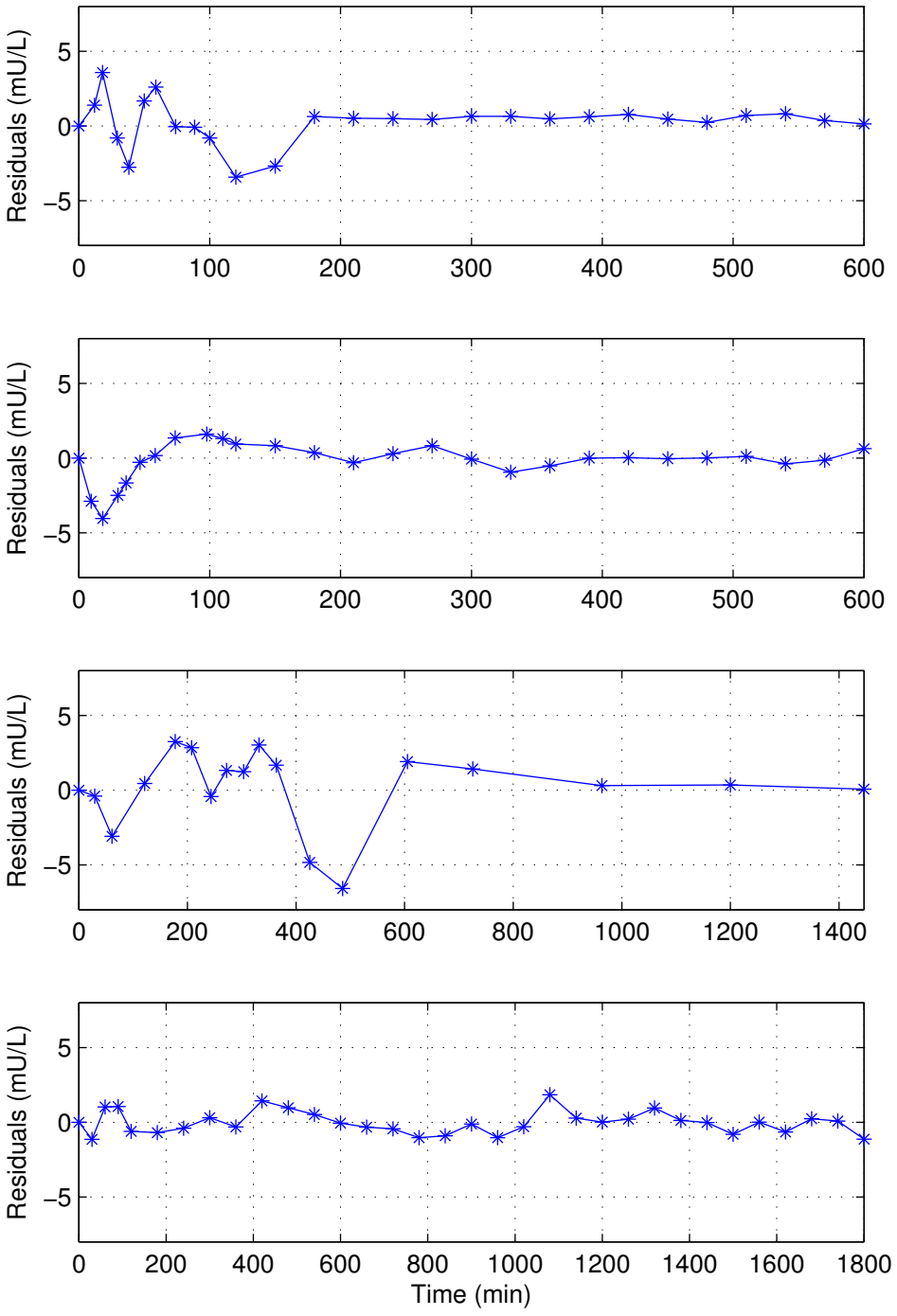

FIGURE 5.7: *Residual profiles for 4 distinct insulin formulations.*

TABLE 5.2: Fitted values of subcutaneous insulin model constants

Parameter	Value
k_i	4.60×10^{-2}
k_{dm}	1.20×10^{-2}
k_c	1.31×10^{-3}
k_p	1.21×10^{-3}
Q	5.02×10^{-10}
Q_p	2.38×10^{-8}
p_d	1[a]
α_{gla}	5.72×10^{-6}
β_{NPH}	1
β_{gla}	0.968
f_{dm}	0.709
f_{RI}	0.597
f_{NPH}	0.480
f_{gla}	0.509

[a] p_d was selected (not fitted) as the parameter has been previously demonstrated to be poorly correlated with error in the appearance profile [76].

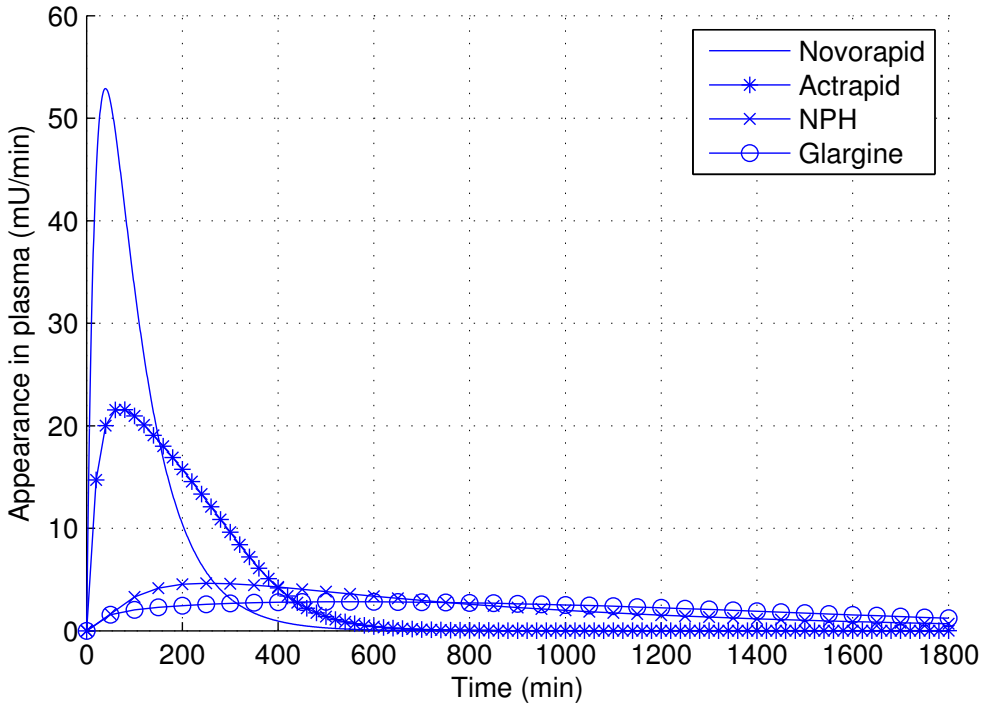

FIGURE 5.8: *Model-based appearance profiles for 10U (100U/ml) of 4 distinct insulin formulations.*

5.4 Discussion

A novel compartment model approach combining linear clearances and kinetics, saturable clearances, and chemical equilibriums was able to capture the dynamics of 4 major insulin types with minimal parameterisation. By assuming a set of circulating insulin dynamics shared by all insulin types, the potential for parameter variance was reduced (likely at the cost of bias between insulin types). Approximately half of the total possible parameters were removed from the fitting procedure as a result, deparameterising the model and increasing practical identifiability [18].

Model consistency was supported by the identified equilibrium constants Q and Q_p in Table 5.2. While glargine shares the hexamer form with other self-associating insulins, glargine hexamers dissociate more slowly than typical insulin hexamers. This effect was reflected in the parameter values, with $Q_p >> Q$ without imposing any constraints on the fitting process. Greater Q_p values mean the glargine hexamer has a greater affinity, reducing the available quantity of dimeric/monomeric insulin. While the significance of this observation may be limited, Q and Q_p represent the only kinetic parameters that can be directly compared, and so this consistency retains some importance.

The bias between different insulin types was partly accounted for by the scaling factor, f_{type}. Interestingly, the value of f_{type} was clearly correlated with the length of the action period of the insulin type. The monomeric scaling factor, f_{dm}, had the highest value of 0.709. The increased self-association of regular insulin resulted in a comparatively longer action profile, with a smaller scaling factor $f_{RI} = 0.597$. Finally, the scaling factors of extremely prolonged NPH and Glargine insulins were similar, at 0.480 and 0.509, respectively. These values are in line with reported bioavailability of subcutaneous insulin. The largest reported fraction of subcutaneously injected insulin degraded at the

depot site is approximately 50% [81] at steady state. Other studies put this figure at approximately 20% [80]. If the correlation with action period is physiological, instead of an artefact of fitting a limited dataset, possible implications include:

- Greater time at conditions close to equilibrium increases the respective volumes of distribution relative to an IV insulin bolus, where less well perfused tissues do not have sufficient time to accumulate insulin. This effect would suggest that in prior studies plasma insulin clearances have been underestimated by fitting clearances while overestimating the volume of distribution around an IV bolus.
- Subcutaneous insulin degradation at the depot site saturates, thereby having a greater effect on longer acting insulins and appearing as a reduced f_{type}.
- Prolonged action periods result in increased bias due to assumptions on endogenous insulin secretion.

A limitation of this section of the work is the data itself. Individual profiles were not available, and the information on the cohort itself was limited. In each study, insulin dose was selected based on body weight. However, 3 out of 4 studies failed to report the average weight, and thus the absolute size of the insulin dose had to be estimated. The advantage of using f_{type} to scale the appearance profile is that error in this absolute size will be absorbed by this parameter, and have limited effect on the remaining parameter set. Also of note is the incomplete absorption of the longer acting insulins, as seen in Figure 5.5. This may introduce error in the fitting procedure, but extending the experimental protocol is impractical due to the prolonged action period of these insulins.

Due to the relative expense, C-peptide measurements were not reported in equivalent density. This lack of data meant endogenous insulin secretion could not be fully adjusted

for, and basal insulin levels were used as a surrogate. While this effect is unlikely to have any significance for a T1DM participant, three of the studies used healthy volunteers, and a bias may be introduced here. To correct each of these factors greater access to data, or a dedicated trial, is required. However, equally, the body of literature has frequently suggested large variation in appearance profiles even for the same patient. As a result, these effects may not be large enough to warrant such attention given the inter- and intra- patient variation reported [89].

These results provide a unified and physiologically justifiable model description of slow-acting, subcutaneous insulin appearance profiles that will allow multiple insulin types to be considered simultaneously. Such a model has wide-ranging applications in model-based therapeutics for diabetes management, and bridges the gap left by existing models of particular insulin analogue kinetics. Slow acting insulins are typically used in non-acute cases, and thus, the rate of attendance is limited. These results provide a more robust approach to estimating the appearance, and action, of insulin analogues. Hence, the proposed model has the potential to enable model-based algorithms that have proven effective in critical care [22, 34] to be used in non-acute cases.

5.5 Summary

A novel mixed chemical and kinetic model is presented that describes subcutaneous insulin absorption kinetics. The combined model provides a unified framework for multiple insulin types. Circulating insulin dynamics were described by an independently derived model where a-priori values and physiological estimates of the fate of circulating insulin were used to circumvent a practically unidentifiable model. When combined with the subcutaneous insulin absorption model, parameter estimates in the subsequent model showed consistency, and captured each of the required dynamics.

Chapter 6

Characterisation of Diurnal Insulin Sensitivity Parameter Identification under High Internal Noise

6.1 Introduction

Chapter 2 introduces a novel parameter fitting technique that uses a non-linear model, basis functions, and stochastic elements to robustly identify an underlying insulin sensitivity profile. The applicability of this method was demonstrated on ICU data, with Chapter 3 showing how prediction was possible. Chapters 4 and 5 provide an insulin model capable of describing both IV and subcutaneous insulin administration in a single unified framework. The requisite models and methods have thus been prepared for characterising insulin sensitivity beyond the critical care setting.

Due to high measurement frequency, nutrition regulation, and intensive supervision, data obtained in the ICU represents an upper limit in quality for glycaemic control. When extending model-based glycaemic control from critical illness to chronic care, either in a hospital ward or outpatient setting, BG measurement frequency and quality decreases, and uncertainty about nutrition intake increases. Additionally, insulin administration is subcutaneous, rather than intravenous, increasing the action period and uncertainty in appearance, and thus the hypoglycaemic potential of overaggressive dosing. A schematic summarising these factors in shown in Figure 6.1.

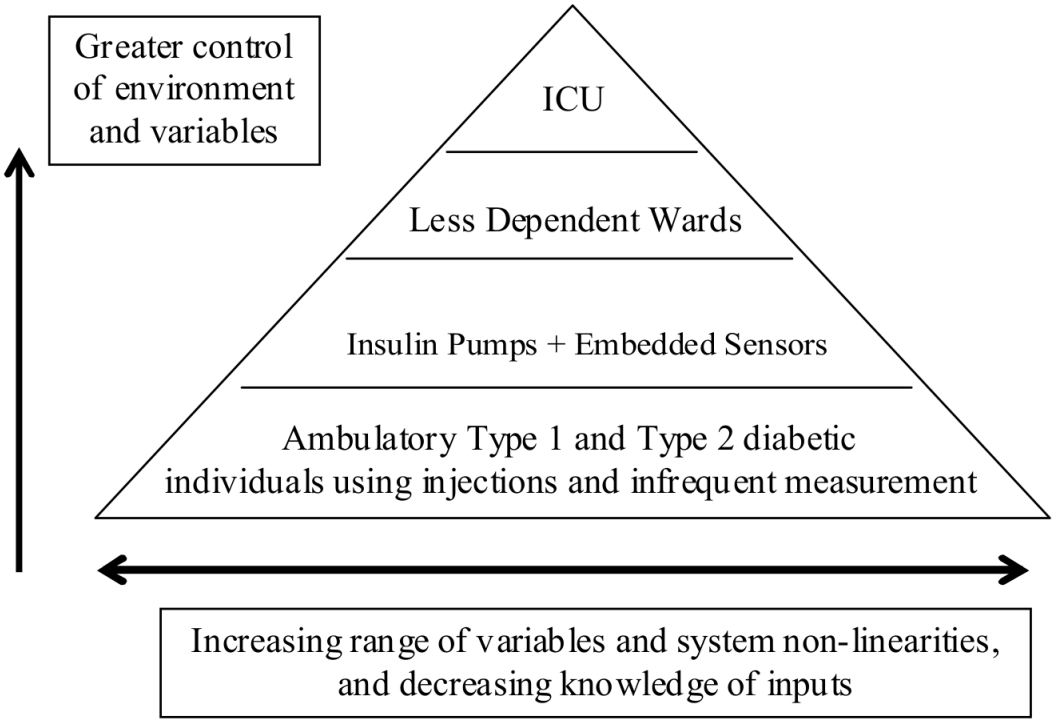

FIGURE 6.1: *Pyramid description of glycaemic control problems in terms of ability to control variables based on knowledge of their value or input (vertical axis), and the range of variables to be considered and resulting level of uncertainty (horizontal axis).*

Furthermore, hypoglycaemia is a greater concern in everyday life, where the consequences of a hypoglycaemic event while carrying out some routine activities, such as driving, can be severe. A robust, safe decision support protocol thus could be of significant benefit. The foundation of such a decision support protocol is the parameter

identification method. Due to high noise and long delays between measurements, the STAR approach of identifying the "current" S_I and predicting forward is no longer applicable.

An example is the morning insulin dose. In this case, individuals only have access to the current BG, and no dynamic response, since the prior measurement was the night before or longer. However, they still must decide on an appropriate long-acting (basal) and short-acting (prandial) insulin dose at that time with a single measurement and no prior information. For model-based predictions, categorising a current diurnal S_I profile using multiple days of data is a method of circumventing this problem. Using multiple days of data makes parameter identification more stable in the face of high noise and uncertainty, as will be demonstrated in Chapter 7.

This work presents an adaptation of the parameter identification method presented in Chapter 2, and characterises the method using clinical T1DM "diary" data.

6.2 Methods

6.2.1 Models

The insulin model from Chapter 4 was used to simulate circulating insulin dynamics. Subcutaneous appearance profiles were simulated using the model presented in Chapter 5. In long-term management of diabetes, a basal state is a much more valid assumption than in critical illness. However, basal glucose, G_b, and model-based basal interstitial insulin, Q_b, must be estimated from patient data. The glucose compartment is identical to the DISST [90] formulation:

$$\dot{G}(t) = G_x - p_G(G(t) - G_b) - S_I \frac{G(t)Q(t) - G_bQ_b}{1 - \alpha_G Q(t)} + \frac{P(t)}{V_g} \tag{6.1}$$

$$P(t) = P_{parenteral} + \max(P_{max}, d_2P_2) \tag{6.2}$$

$$P_2 = d_1P_1 - \max(P_{max}, d_2P_2) \tag{6.3}$$

$$P_1 = P_{enteral} - d_1P_1 \tag{6.4}$$

where G, P_1, and P_2 are the plasma glucose concentration, and the glucose content of the stomach and gut, respectively. $P(t)$ is the exogenous glucose appearance in plasma, while $P_{enteral}$ and $P_{parenteral}$ are the enteral and parenteral nutrition administered. The generic absorption model was also left unchanged, with $d_1 = -\log 0.5/20\text{min}^{-1}$ (transfer to gut), $d_2 = -\log 0.5/100\text{min}^{-1}$ (transfer to plasma), and $P_{max} = 6.11\text{mmol.min}^{-1}$ (maximal absorption rate).

The main sites of non-insulin mediated glucose uptake (NIMGU) are the central nervous system and muscles [91]. The central nervous system has a relatively stable energy requirement, but can shift metabolic pathways away from glucose if required. As this

process is gradual, and conditional on extreme situations such as starvation [92, 93], this effect can be negated and the central nervous system's glucose uptake is simply included in G_b. In contrast, NIMGU in muscle cells changes with BG. The relative magnitude of this change [91] gives an estimate of $p_G = 0.006$ min^{-1}, which agrees with the ICING model [40], and is thus left unchanged.

The glucose volume of distribution is assumed to be extracellular fluid volume, giving $V_g = 12.1$L [66]. Finally, α_G is determined by the half-maximal effect of insulin on glucose utilization. Approximate half-maximal effect of insulin on whole-body glucose metabolism occurs at plasma insulin concentrations of approximately 58 mU.L^{-1} (maximal at 200-700 mU.L^{-1}) [94]. As steady-state $Q_{ss} = \frac{I_{ss}}{2}$, α_G is thus set to 29 L.mU^{-1}.

6.2.2 Insulin sensitivity profile

A *b-spline* basis similar to Chapter 2 was generated by choosing identical knot times each day. However, instead of a series of functions, three composite basis functions were generated by combining the functions that occur at the same time of day. An example of these three functions is shown in Figure 6.2. The resulting representation of S_I is a repeating signal with a period of 24 hours.

6.2.3 Parameter identification

To identify this repeating S_I, an iterative procedure identical to Chapter 2 was carried out with the three basis functions. Similar to Equation (2.20), for n BG measurements

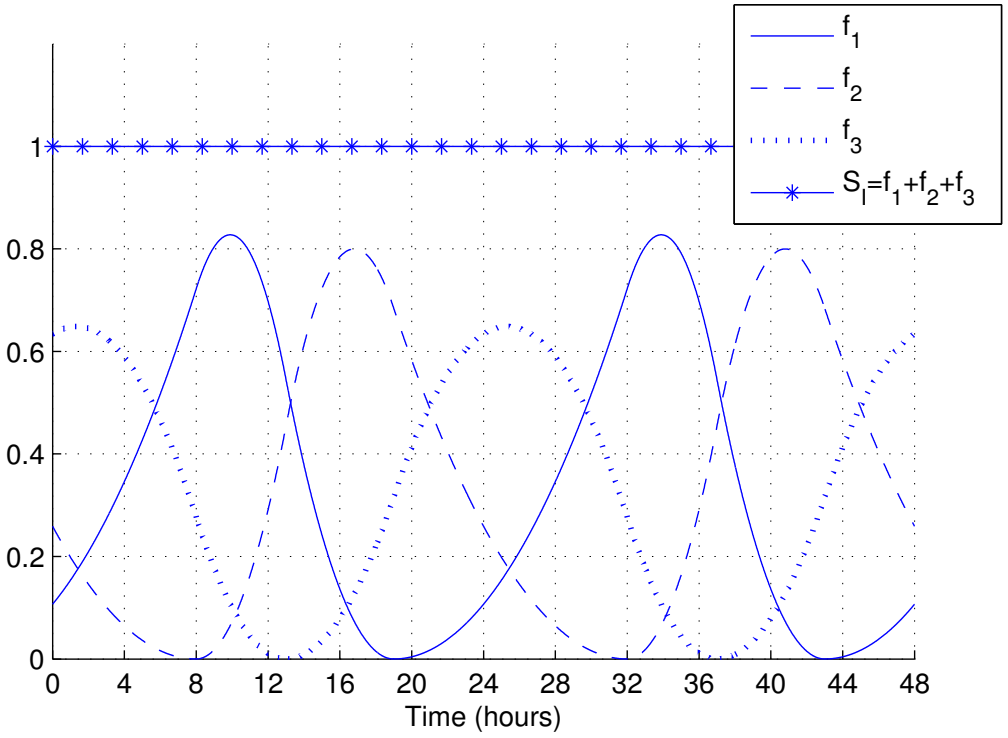

FIGURE 6.2: *Three composite basis functions generated by a 2nd order* b-spline *basis with identical knot times each day. The functions sum to unity to produce the S_I profile.*

and three 2nd order *b-spline* basis functions f_1, f_2, and f_3, as shown in Figure 6.2:

$$\begin{bmatrix} \hat{A}_{1,(n,3)} & \hat{A}_{2,(n,n)} \\ \hat{0}_{(3,3)} & \hat{A}_{3,(3,n)} \end{bmatrix} \begin{bmatrix} \hat{S}_{I,(3,1)} \\ \hat{G}_{x,(n,1)} \end{bmatrix} = \begin{bmatrix} \hat{b}_{1,(n,1)} \\ \hat{0}_{(3,1)} \end{bmatrix} \tag{6.5}$$

where $\hat{S}_{I,(3,1)} = [S_{I,1}, S_{I,2}, S_{I,3}]^\top$ is the vector of scalar multipliers corresponding to f_1, f_2, and f_3, $\hat{G}_{x,(n,1)} = [G_{x,1}, \ldots, G_{x,n}]^\top$ is the vector of noise values between measurements, and:

$$\hat{A}_{1,(n,m)} = \begin{bmatrix} \int_{t_0}^{t_1} f_1 \dfrac{GQ - G_b Q_b}{1 + \alpha_G Q} \mathrm{d}t & \int_{t_0}^{t_1} f_2 \dfrac{GQ - G_b Q_b}{1 + \alpha_G Q} \mathrm{d}t & \int_{t_0}^{t_1} f_3 \dfrac{GQ - G_b Q_b}{1 + \alpha_G Q} \mathrm{d}t \\ \vdots & \vdots & \vdots \\ \int_{t_0}^{t_n} f_1 \dfrac{GQ - G_b Q_b}{1 + \alpha_G Q} \mathrm{d}t & \int_{t_0}^{t_n} f_2 \dfrac{GQ - G_b Q_b}{1 + \alpha_G Q} \mathrm{d}t & \int_{t_0}^{t_n} f_3 \dfrac{GQ - G_b Q_b}{1 + \alpha_G Q} \mathrm{d}t \end{bmatrix} \tag{6.6}$$

$$\hat{A}_{2,(n,n)} = \begin{bmatrix} -(t_1 - t_0) & 0 & \dots & 0 \\ -(t_1 - t_0) & -(t_2 - t_1) & \dots & 0 \\ \vdots & \vdots & \ddots & \vdots \\ -(t_1 - t_0) & -(t_2 - t_1) & \dots & -(t_n - t_{n-1}) \end{bmatrix} \tag{6.7}$$

$$\hat{A}_{3,(m,n)} = \begin{bmatrix} \int_{t_0}^{t_1} f_1(t)\mathrm{d}t & \dots & \int_{t_{n-1}}^{t_n} f_1(t)\mathrm{d}t \\ \int_{t_0}^{t_1} f_2(t)\mathrm{d}t & \dots & \int_{t_{n-1}}^{t_n} f_2(t)\mathrm{d}t \\ \int_{t_0}^{t_1} f_3(t)\mathrm{d}t & \dots & \int_{t_{n-1}}^{t_n} f_3(t)\mathrm{d}t \end{bmatrix} \tag{6.8}$$

$$\hat{b}_{1,(n,1)} = \begin{bmatrix} G(t_1) - G_0 - \int_{t_0}^{t_1} \frac{P(t)}{V_g} - p_G(G(t) - G_b)\mathrm{d}t \\ \vdots \\ G(t_n) - G_0 - \int_{t_0}^{t_n} \frac{P(t)}{V_g} - p_G(G(t) - G_b)\mathrm{d}t \end{bmatrix} \tag{6.9}$$

Parameters were considered converged when the maximum error between the model solution and measured BG was within 0.1 mmol.L^{-1}, and the maximum ΔS_I value was within 1x10^{-6}. To speed convergence, between major iterations each G_x value was updated to bring the model solution within 0.05 mmol.L^{-1} of the measured BG:

$$G_x(t_i) = \frac{1}{t_{i+1} - t_i}\Big(G(t_{i+1}) - G(t_i) + \int_{t_i}^{t_{i+1}} p_G(G(t) - G_b) + S_I \frac{G(t)Q(t) - G_b Q_b}{1 - \alpha_G Q(t)} - \frac{P(t)}{V_g}\mathrm{d}t\Big) \tag{6.10}$$

where i is the i^{th} measurement, and S_I is the current diurnal 24 hour repeating profile.

6.2.4 Clinical data

Data was collected over a 4 day period for N=8 individuals with T1DM as part of a DAFNE educational course [95]. Glucometer BG measurements were taken 4-8 times

daily, insulin doses were recorded, and carbohydrates were estimated by the participants. Some individuals included details of exercise, but this data was difficult to quantify and inconsistent, and was not used for this reason. The dataset is summarised in Table 6.1. Acronyms used in the table are TDI, total daily insulin; TDC, total daily carbohydrates.

6.2.5 Analyses

Initially, the model-based basal state was approximated. The best surrogate for a basal state was assumed to be the first measurement of each day. Thus, G_b was calculated by taking the mean of these values. Model-based Q_b was approximated by solving the insulin kinetic model over the full episode, pairing interstitial compartment solutions with the chosen basal glucose times, and taking the mean.

Second, knots for the basis function were calculated by identifying the median meal times for each episode. *K-means* cluster analyses were carried out on insulin dose and nutrition intake times, providing an optimal classification of data into "morning", "afternoon", and "evening" meal events. The influence of small inter-meal snacks on the chosen knot times was then eliminated by finding the median time within the three classifications. These medians were used as the knot times for basis function generation, as per Chapter 2.

Finally, using the chosen basal state and knot timings, each episode was fit using the methodology presented in Chapter 2. The number of major iterations and total time until convergence on an i7 CPU @ 3.8GHz was recorded. Fitted diurnal S_I profiles were presented alongside fitted G_x profiles for each individual episode to give an overview of the expected results of the fitting methodology.

Table 6.1: T1DM cohort details

	DM001	DM002	DM003	DM004	DM005	DM006	DM007	DM008
Gender	F	F	M	F	M	F	F	F
Age	50	39	49	33	52	70	60	30
Weight	76.0	62.0	92.0	109.0	80.3	97.5	57.8	79.4
Height	1.79	1.62	1.93	1.55	1.78	1.64	1.60	1.65
Num BG samples	33	29	22	30	22	25	22	24
Median [IQR] BG	7.7 [4.8-12.5]	6.3 [5.9-7.3]	7.9 [6.4-10.1]	6.3 [4.4-8.5]	5.7 [5.2-6.2]	10.0 [8.0-12.5]	9.2 [7.4-10.7]	6.9 [4.8-10.0]
Max BG	15.7	9.9	12.5	12.7	8.7	16.7	16.5	15.5
Min BG	2.1	4.2	4.9	2.4	3.6	6.4	5.3	33.0
Median TDI	31.8	20.8	38.0	64.5	13.5	37.5	38.5	41
Median TDC	180.0	122.5	175.0	165.0	97.5	140.0	100.0	147.5
Fast-acting	Humalog	Novorapid	Novorapid	Humalog	Novorapid	Novorapid	Humalog	Humalog
Long-acting	Lantus	Protaphane	Protaphane	Humulin/N	Protaphane	Protaphane	Lantus	Lantus

6.3 Results

Table 6.2 shows the basal states for each of the episodes. Basal glucose, G_b, varied significantly between patients, as might be expected for a T1DM cohort. This median (calculated) G_b of 7.0 is lower than the 8.0 mmol.L^{-1} often found based on median HbA1c in many studies. Equally, model-based basal interstitial insulin was low for all but one patient. This individual, DM004, had the highest TDI in this cohort.

TABLE 6.2: Basal glucose and interstitial insulin values.

	G_b [mmol.L^{-1}]	Q_b [mU.L^{-1}]
DM001	5.5	3.28
DM002	6.1	0.88
DM003	7.7	1.77
DM004	6.2	6.05
DM005	5.9	0.38
DM006	10.5	1.63
DM007	11.0	1.48
DM008	8.4	2.79

Figure 6.3 shows the results of the cluster analysis, and thus the knot times used for each episode. The majority of episodes featured consistent meal times, indicating a regular daily routine. Again, this result reflects a typical, well-motivated cohort.

Figure 6.4 shows the results of the fitting methodology for each episode. Glucose level, noise level, and S_I rhythms all showed large variation between episodes. Noise level, as indicated by the amplitude of the G_x profile, appeared to increase with BG, while diurnal S_I variation had no such apparent correlation. S_I values are plotted on the same axis and comparison across patients shows significant inter-patient variability.

Finally, convergence details are presented in Figure 6.5. While the total number of iterations was both low and consistent, the total time was relatively high, and showed greater variation. The long time to convergence reflects the computational complexity of this fitting methodology, as a data set with n measures will require $n+3$ parameters to converge. The intermediate step of updating G_x dramatically decreases the number of iterations, but has a less marked effect on total time required (results not shown).

6.4 Discussion

These results demonstrate the fitting methodology presented on clinical, "diary-style" data from individuals with T1DM. This data represents typically available data in an outpatient setting, and is thus an important test of this new methodology. Despite high uncertainty in nutritional intake, and high sensor error noise on capillary BG measurements, convergence occurred in a relatively small number of iterations. Computational complexity was reflected by the time taken to reach this converged state.

The individual episodes featured large variation in basal BG levels, suggesting parameter identification is possible across a wide range of typical patients. The importance of a time-varying S_I profile is demonstrated by the difference in S_I profiles between these episodes. DM002, DM003, DM006, and DM007 each showed relatively minor S_I fluctuations, while fluctuations in the remaining 4 episodes were much greater. This significant inter-patient variability clearly reflects the typical range and corresponding variability in hypoglycaemic risk between patients who might otherwise be dosed similarly. While predictive capability remains to be investigated, the size of these fluctuations suggests model-based decision support has scope to improve glycaemic control in this setting.

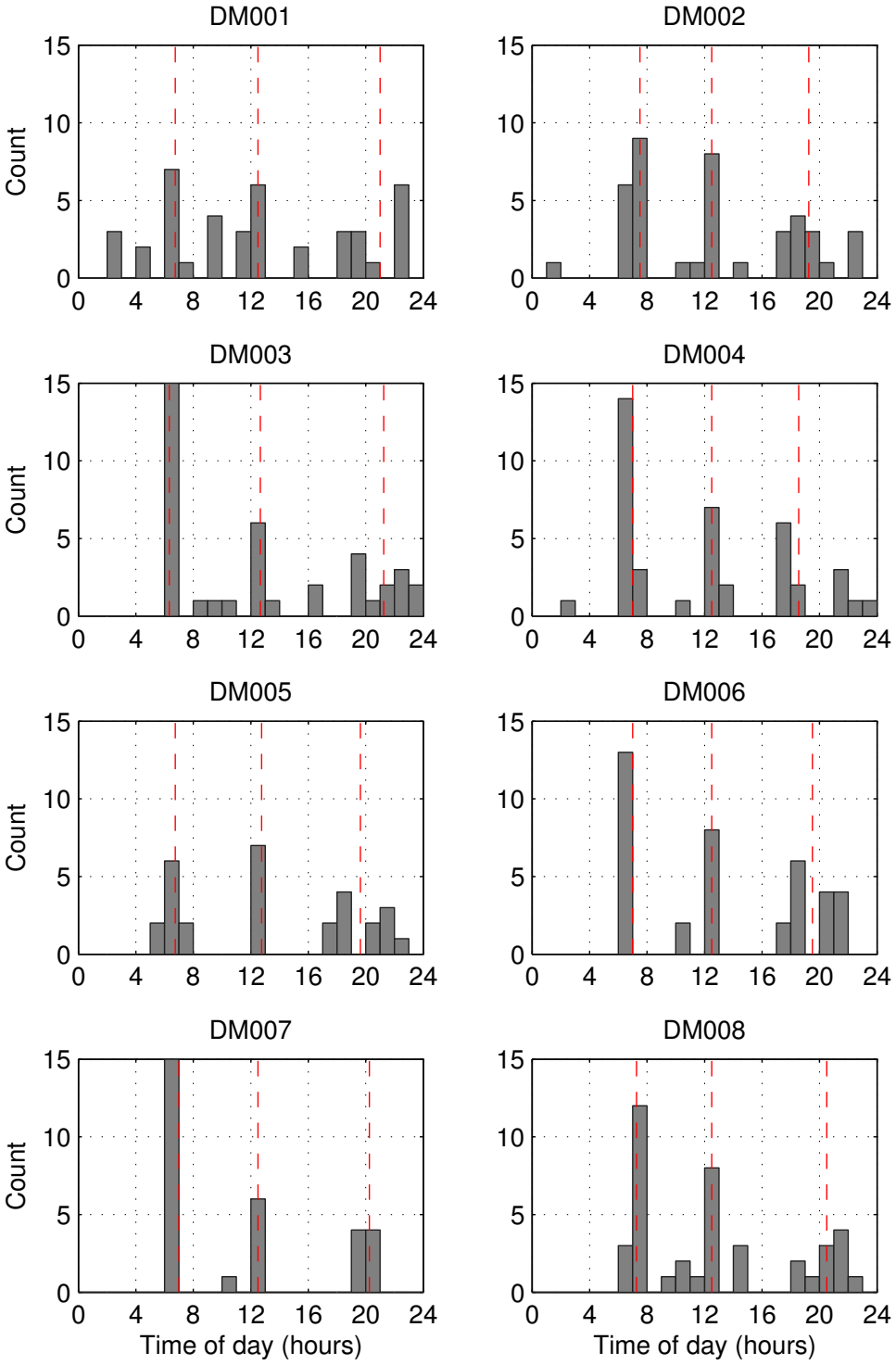

FIGURE 6.3: *Knot times identified using a cluster analysis of nutrition and insulin data. Histogram data shown was used to find the knots (dashed lines).*

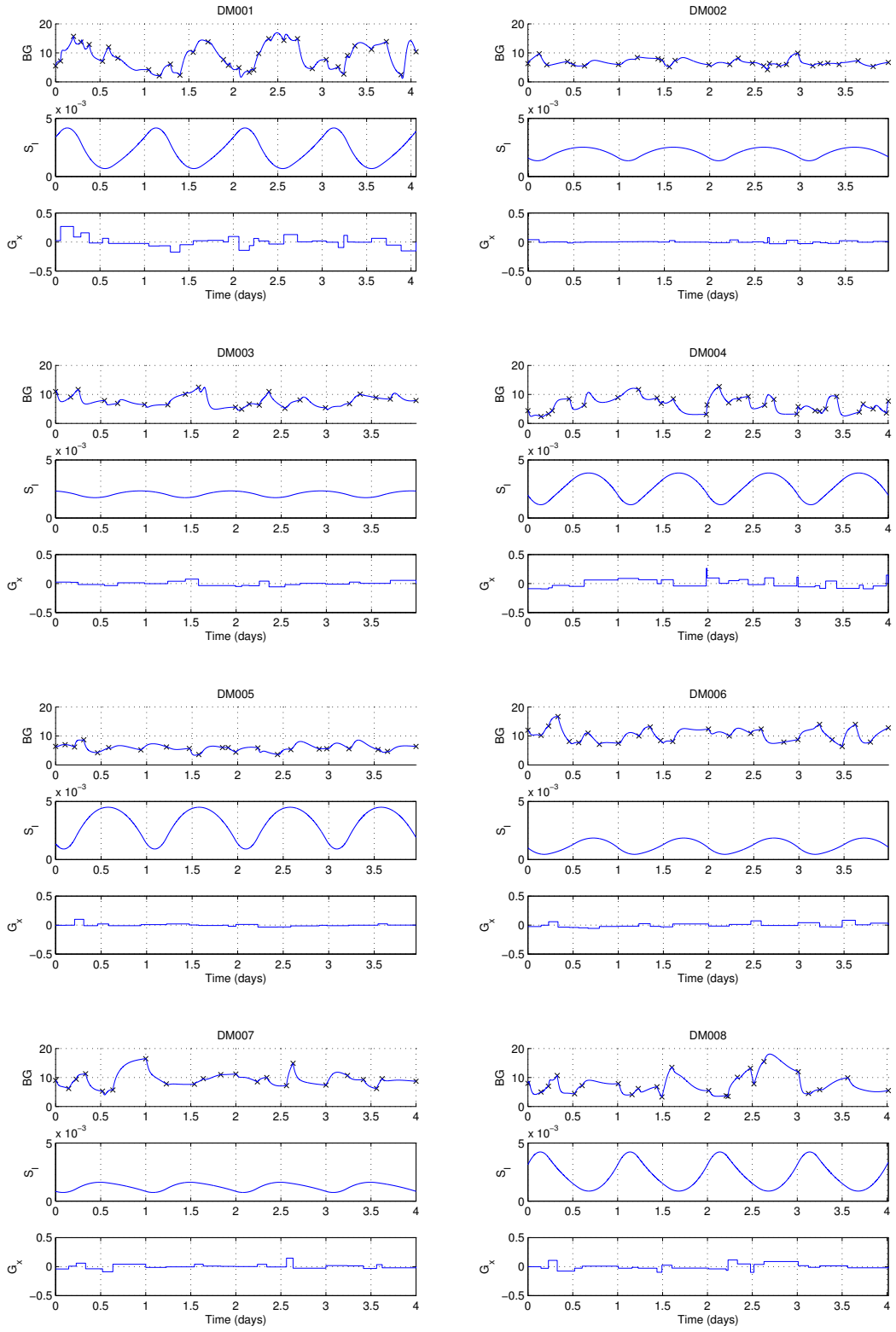

FIGURE 6.4: *Fitted profiles, including S_I and G_x.*

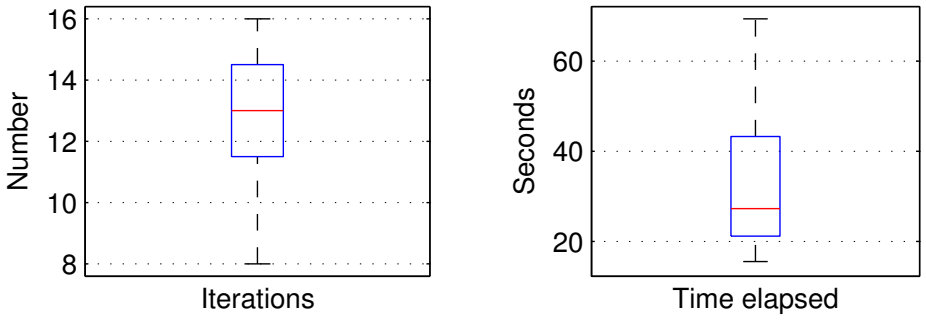

FIGURE 6.5: *Number of iterations and total elapsed time when fitting each episode. Boxplot whiskers show the maximum and minimum values.*

Due to the short length of each episode, an investigation into predictive capability similar to Chapter 3 was not carried out. Longer episodes would allow for quantification of the expected G_x distribution, as well as the likely upper/lower limits of S_I. Thus, these results simply serve to demonstrate the applicability of the new fitting methodology.

An additional future analysis is required on the concept of a basal state in this setting. Intuitively, the concept of a basal state makes sense outside of a critical care setting, yet the "basal" state observed in this data is influenced by prior long-acting insulin doses. This influence is offset by calculating a model-based Q_b rather than the expected value of $Q_b = 0$ for an individual with T1DM. However, use of a model-based Q_b means model-based optimisation of longer acting insulin formulations is difficult, and should be limited to incremental changes based on TDI rather than predicting optimal outcomes. Furthermore, the influence of a changing basal Q on predictive capability should be investigated to understand expected behaviour around changes to the basal insulin regime. Both these issues would be ameliorated by a much larger study with more subjects and days, based on these initial positive results.

What these results do demonstrate is that convergence of an identified diurnal S_I profile is possible using the novel parameter identification methodology. This represents an

entirely new capability to decompose "diary-style" data into quantified insulin sensitivity fluctuations throughout the day, thus enabling model-based decision support to be applied in an area where the inherent challenges have prevented significant advances to date. Future work should focus on demonstrating the validity of the fitted S_I profile on *in-silico* data, then validating prediction capability on longer clinical data sets in a manner similar to Chapter 3.

6.5 Conclusion

The output of a novel diurnal S_I parameter identification methodology was used to characterise the expected results when fitting clinical "diary-style" data. Convergence occurred in all episodes, and showed significant and expected differences in intra-day S_I fluctuations across subjects. Future work should focus on demonstrating the validity of the fitted S_I profile on *in-silico* data and larger cohorts.

Chapter 7

Monte-Carlo Identification of Diurnal Insulin Sensitivity Profiles

7.1 Introduction

Chapter 6 utilises a modified version of the parameter identification methodology presented in Chapter 2 to fit a diurnal S_I to 8 episodes of patient data. Convergence of each episode showed the applicability of the method to this style of data. However, validity of the fitted S_I profile cannot be proven on real data, as the "true" S_I profile is not known. Furthermore, the influence of data density and quality on the validity of this profile must be also understood.

As mentioned in Chapter 6, when extending model-based glycaemic control from critical illness to chronic care, either in a hospital ward or outpatient setting, BG measurement

frequency and quality decreases, and uncertainty about nutrition intake increases. Additionally, insulin administration is subcutaneous rather than intravenous, increasing the action period and thus the hypoglycaemic potential of overaggressive dosing. These factors represent the major challenges outside of an ICU setting. The effect of these factors must be investigated *in-silico* to determine the applicability of the fitting methodology. If a S_I profile cannot be recovered robustly in the presence of noise, model-based treatment recommendations will be too unreliable for use. Such an *in-silico* investigation would also provide insight into an ideal measurement regime.

This study aims to investigate both convergence properties and the quality of the fitted result using this fitting procedure with a single virtual patient. This virtual case study has a known insulin sensitivity profile, allowing assessment of the accuracy of fitted parameters. The effect of post-meal BG timing was assessed, along with the effect of noise, and finally how multiple days of data could be combined to reduce the effect of noise on the fitted insulin sensitivity. In all cases, sufficient simulations were run to ensure outliers did not influence the interpretation of results.

7.2 Methods

7.2.1 Models

The insulin model from Chapter 4 was used to simulate circulating insulin dynamics. Subcutaneous appearance profiles were simulated using the model presented in Chapter 5. No variations in peak time or concentration were simulated during this study.

Nutrition appearance profiles were simulated as described in Equations (6.4) and (6.3). While no noise was added to the dynamics prior to fitting, the inaccuracy of carbohydrate

counting was simulated by adding noise to the size of each meal. Fitting was carried out using the stochastic differential equation fitting procedure detailed in Chapter 6. Glucose dynamics were simulated using Equation (6.1).

7.2.2 Virtual patient details

Monte-Carlo simulations were based on a single, well controlled, virtual T1DM patient. T1DM was chosen over T2DM as T1DM can be assumed to have negligible beta cell function, and thus secretion can be ignored. However, this restriction is artificial, and the models and methods are as applicable in T2DM as they are in T1DM.

Basal BG was set as 8mmol/L, with a basal interstitial insulin concentration of zero. The insulin dosing regime was separated into basal (50U of insulin glargine before the morning meal), and prospective (1U novorapid per 10g of carbohydrate) dosing. Meals were identical day-to-day, with 140g of carbohydrate for breakfast (8:00am), 50g for lunch (1:00pm), and 80g for dinner (7:00pm). Four days of this data are shown in Figure 7.1.

BG measurements were determined by the simulation protocol, and the underlying insulin sensitivity profile was set as a moderately sensitive value that changed during the course of the day. The basis for S_I was changed from serial *b-spline* functions to three repeating 2^{nd} order functions. Figure 7.2 contains an example showing the resulting wrap-around effect. Knot times were set as the start of each meal.

7.2.3 Simulation protocol

Multiple stages were used to investigate different aspects of the fitting methodology. Initial investigation was based around the ability of the methodology to recover a specific

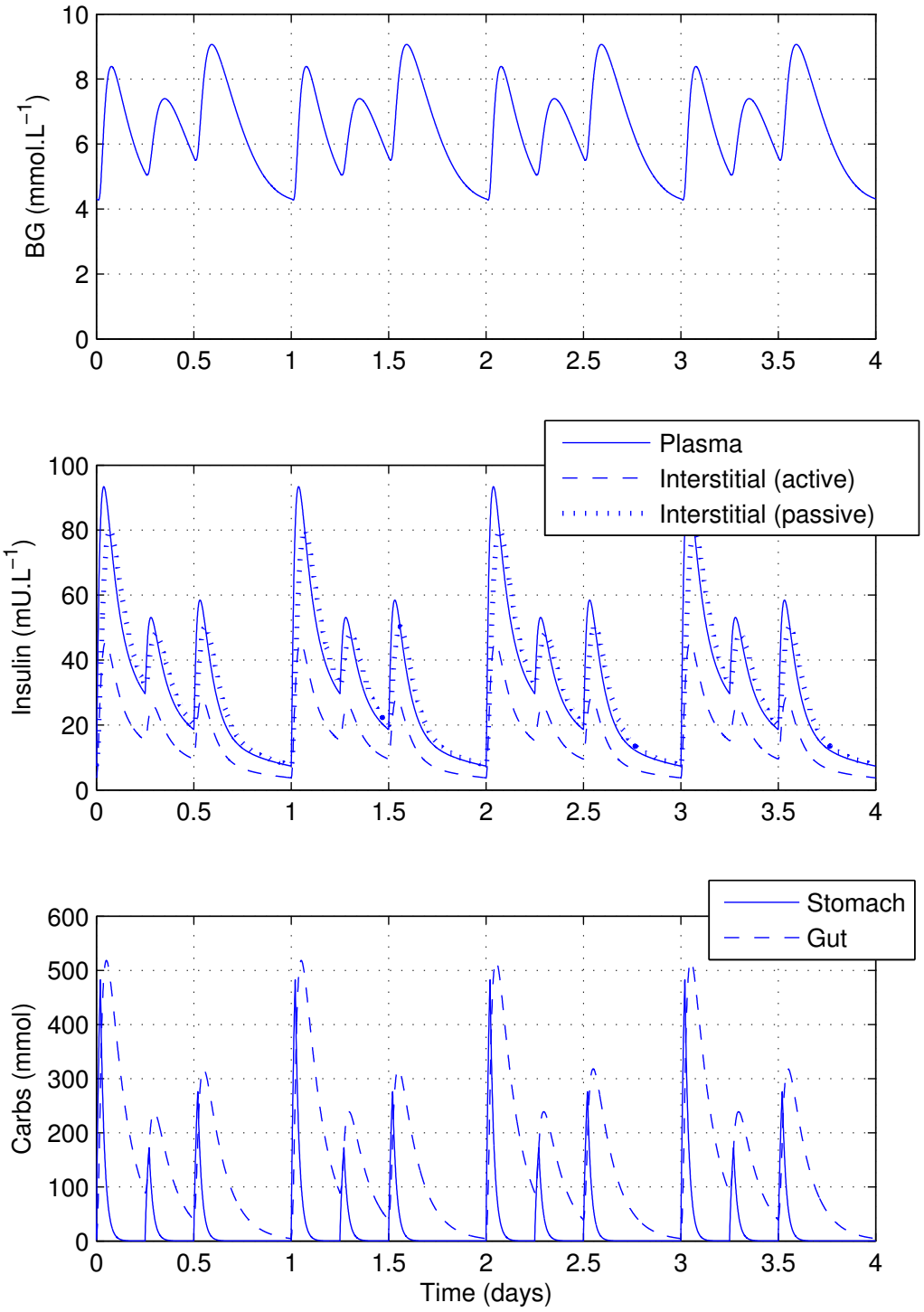

FIGURE 7.1: *Compartment solutions for the virtual patient used in Monte-Carlo simulation. Prior to sampling, the patient was simulated for 3 days to remove any transients.*

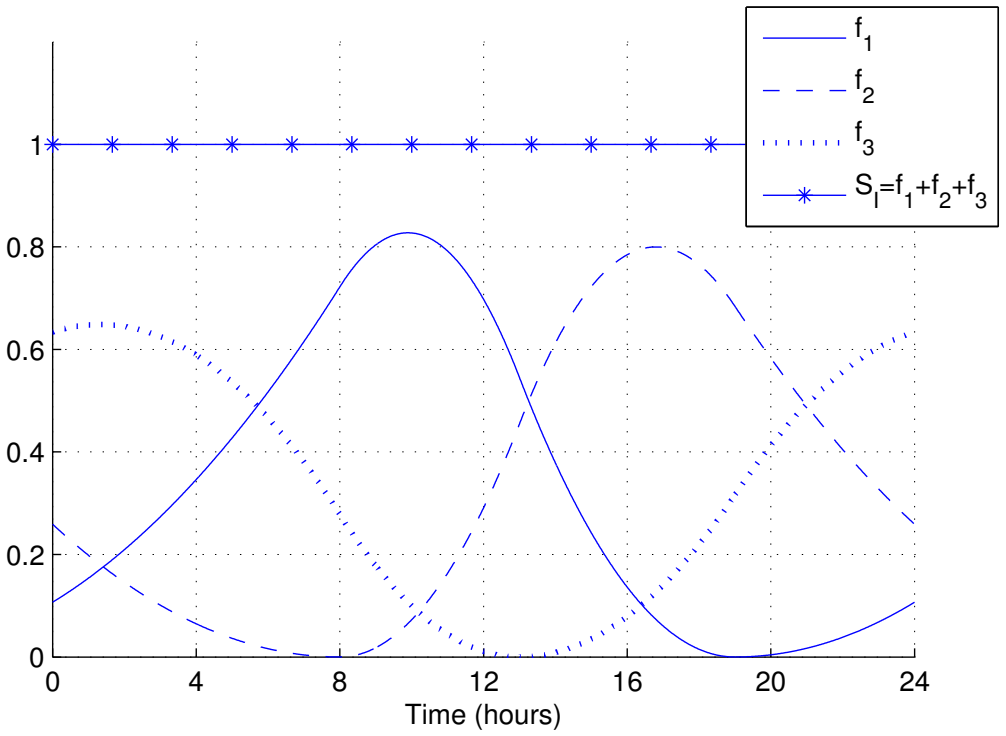

FIGURE 7.2: *Constituent basis functions with knots at meal times, showing wrap-around effect and sum to unity to produce the S_I profile.*

insulin sensitivity profile in the absence of noise, and subsequent investigations aimed to understand properties of, and/or optimise, the required measurements when presented with noisy data. All noise was normally distributed, clamped to $\pm$ 3 standard deviations, and is presented as % CV. The investigations can be broadly categorised as follows:

- Convergence criteria (noise-free data).
- Post-meal measurement timing (10% noise on BG and nutrition).
- Influence of post-meal measurement (10% noise on BG and nutrition).
- Data quantity (10% noise on BG and nutrition).
- Data quality (0% $\rightarrow$ 20% noise on BG, 20% noise on nutrition).

Convergence criteria for the fitting procedure included two separate tolerances, on both insulin sensitivity and error in the plasma glucose compartment. The absolute tolerance for error in plasma glucose was set to ± 0.05 mmol.L^{-1}, within the standard limit of a glucometer scale of 0.1mmol/L. However, the stochastic differential equation approach combined with sparse data meant plasma glucose solutions could converge to within the desired error before the shape of the solution converged. As the shape of the solution corresponds to the shape of the integrals, and therefore the fitted values of insulin sensitivity, a relative tolerance on S_I was required to supplement the standard tolerance on error.

The first stage investigated the convergence over the full range of likely insulin sensitivity profiles. As the n=3, 2$^{\text{nd}}$ order *b-spline* basis consists of 3 individual multiplicative parameters, each of these parameters was varied between 0 (completely unresponsive to insulin) and 2×10^{-3} (moderately high insulin sensitivity) in increments of 4×10^{-4}, and all permutations simulated. The virtual patient details were then used to generate pre- and post- meal BG measurements, which were then used in the fitting procedure. For each simulation, the relative tolerance on S_I was set to each of $\pm\infty$, $\pm1\times10^{-4}$, $\pm1\times10^{-5}$, $\pm1\times10^{-6}$, and $\pm1\times10^{-7}$. The rate of convergence and final error in the recovered S_I profile was then compared.

In the second stage, the post-meal BG measurement timing was varied to investigate the optimal range of times to record BG for fitting purposes in practice. The delay was varied from from 1-4 hours post-meal in 30 minute intervals. Noise was added to both BG measures and carbohydrate dose, reflecting the main sources of error in the intended application. Initially, a moderate value of 10% was used for each simulations, and for all simulations involving noise N=1000 iterations were run. In the third stage,

the importance of this post-meal BG measurement was investigated by comparing the recovered S_I profiles with and without this measurement.

For the fourth stage, 1 to 4 days of data were used in the fitting procedure, and the error between the recovered and original profiles were compared across all simulations. As the fitting methodology aims to recover the diurnal insulin sensitivity profile, multiple days of data can be combined to improve the accuracy of the result. Finally, 4 days of data were used to investigate the effect of increasing noise. In this stage, noise on nutrition was clamped to an appropriate level of 20% [96], while noise on BG was increased from 0% to 20%.

7.2.4 Analyses

As this body of work aims to investigate both the methodology and the quality of results, both accuracy and convergence were considered. Accuracy was defined as the ability to recover the underlying insulin sensitivity profile, while convergence was described by both the total number of iterations and the time taken to reach a solution. Due to the nature of the fitting procedure, all solutions converged, and thus divergence was not considered.

Accuracy was calculated by sampling the S_I profile every minute of the 24 hour period, and subtracting the original profile. For the initial simulations, where no noise was added, the RMS error was calculated from the error array of each simulation, and these RMS values were presented for each convergence criterion in boxplot form. For subsequent Monte-Carlo simulations, if the result was to be considered in isolation, the 5^{th}, 25^{th}, 75^{th}, and 95^{th} percentiles of the raw error array were calculated on a minute-wise basis, and the enclosed areas plotted against the original profile. However,

if multiple related simulations were compared, the error arrays were combined for each category, and a boxplot generated from the entire set. As the purpose of this work was to understand, rather than describe, further quantification of the effect of this error on predictive capability was not carried out.

7.3 Results

7.3.1 Baseline profile recovery

Figure 7.3 details the convergence of the fitting procedure when the full range of likely S_I profiles were used without adding noise. Both error in the final profile and the convergence rate are shown for each tolerance value. During this stage, post-meal BG measures were taken 3 hours after each of the three main meals, and a single day of data used for all simulations.

Error in the recovered insulin sensitivity profiles indicate that the fitting method converges across the full range of S_I values. In these noise-free simulations, a relative tolerance on S_I was not necessary for the recovered profile to converge to approximately 1% of the average S_I profile value. Inclusion of a tolerance improved accuracy at the cost of convergence rate. Due to the sparsity of the available data, the shape of the solution changes significantly from the initial linear interpolation to the final result. This change limits how rapidly S_I can converge, and thus convergence criteria for S_I becomes important. The improvement from a relative tolerance of $1e^{-5}$ to $1e^{-6}$ compared to $1e^{-6}$ to $1e^{-7}$ suggests $1e^{-6}$ is a satisfactory limit, due to the balance between numerical accuracy and convergence speed.

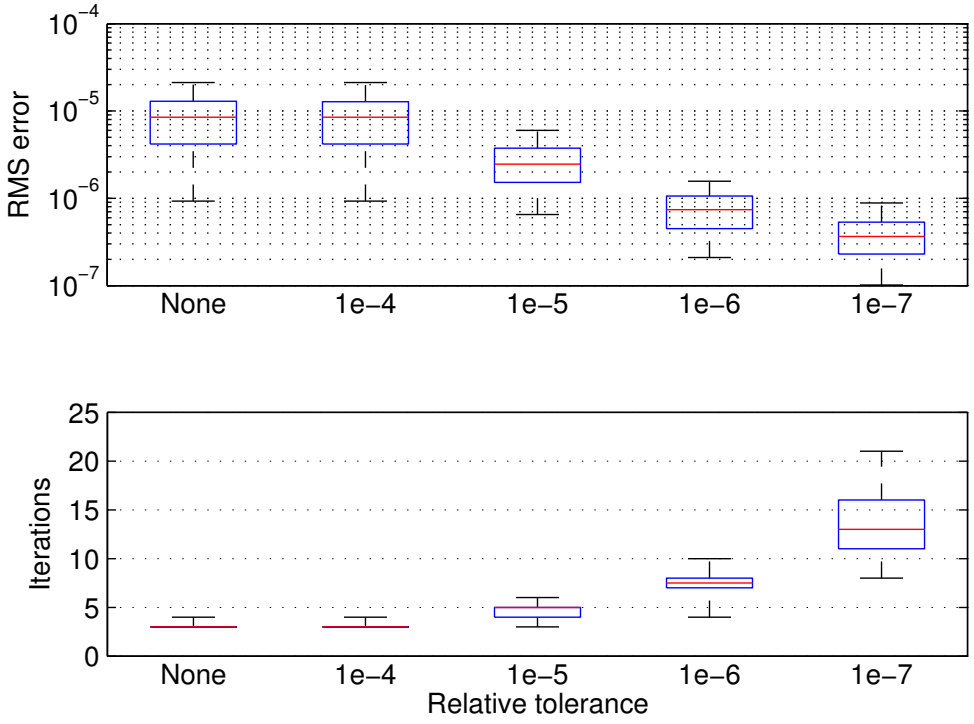

FIGURE 7.3: *Convergence details for the no-noise case, where the virtual patient was generated using the range of likely S_I profiles, and the influence of convergence criteria was assessed.*

7.3.2 Effect of measurement timing

Figure 7.4 shows the results of varying the time of the post-meal BG measurement from 60 to 240 minutes. N=1000 simulations were run for each case, with 10% noise added to both BG measurements and meal size prior to fitting. As accuracy was similar for each measurement time, average band width is shown for the 50^{th} and 90^{th} percentiles to indicate relative uncertainty. A larger number for either suggests reduced ability to recover the underlying insulin sensitivity profile when a second measurement is taken at the relevant time. These results, taken with the average number of iterations to convergence, suggest the best combination of speed and accuracy occurs if BG is measured >2 hours after a meal.

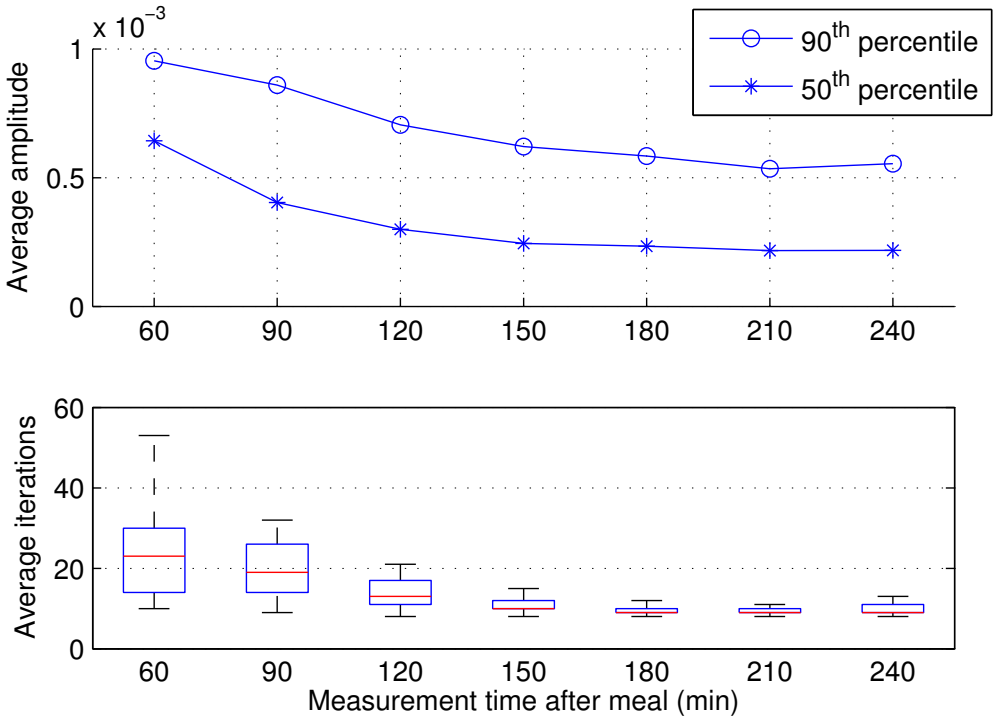

FIGURE 7.4: *Effect of measurement time on identification of insulin sensitivity profiles. N=1000 simulations were run with 10% noise on both BG measurements and nutrition for each measurement time.*

7.3.3 Effect of measurement density

Figure 7.5 compares the convergence rates of dual (pre- and post- meal) and single (pre-meal only) BG measurements in the presence of 10% noise on BG and nutrition. The quality of the identified profiles are contrasted in Figure 7.6 and Figure 7.7. While single measurements are possible to use in the fitting procedure, the process takes significantly longer, and accuracy is reduced.

7.3.4 Effect of data set length

Under the assumption that the underlying insulin sensitivity profile is static, multiple days of data can be used to increase the accuracy of the recovered profile. This approach is valid provided the day-to-day variability of the S_I profile is less significant than the

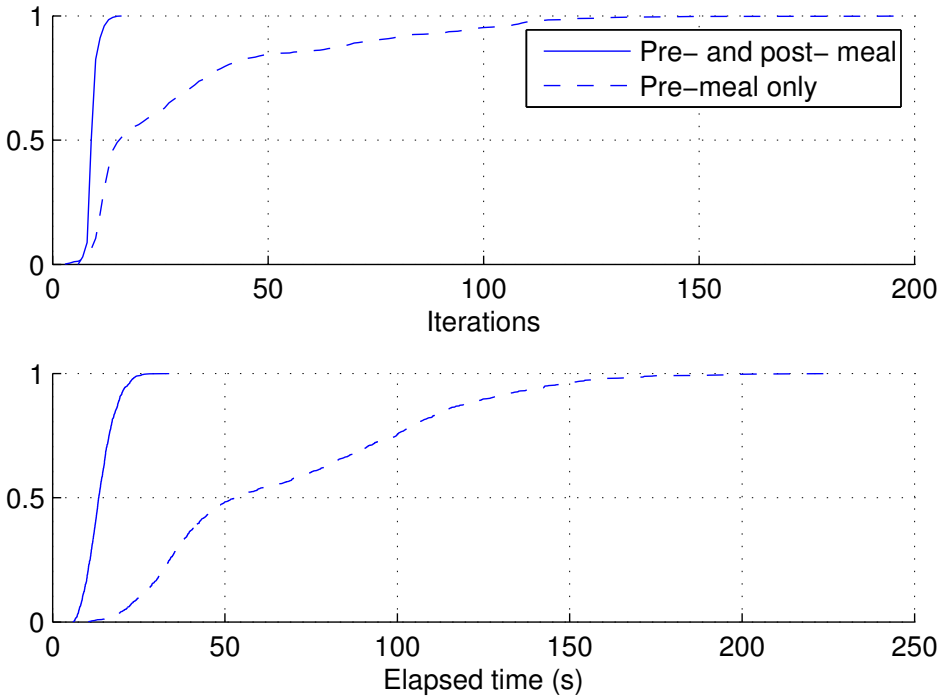

FIGURE 7.5: *Convergence of dual and single measures. N=1000 iterations were run for each with 10% noise on both BG and meal size.*

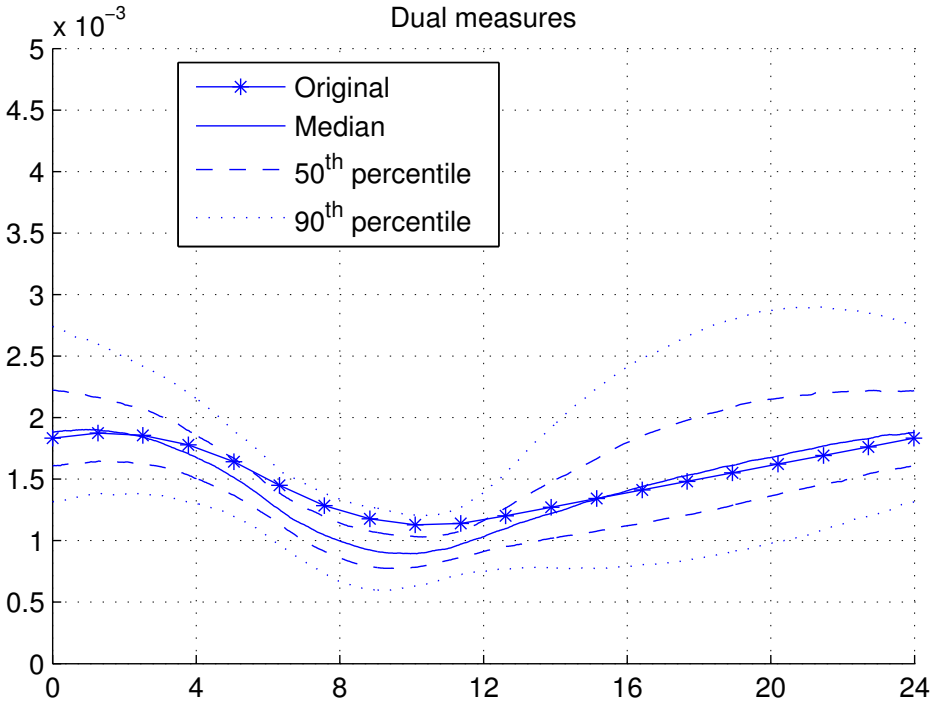

FIGURE 7.6: *50^{th} and 90^{th} percentiles for recovered insulin sensitivity profiles using dual measures. The black line shows the true insulin sensitivity profile.*

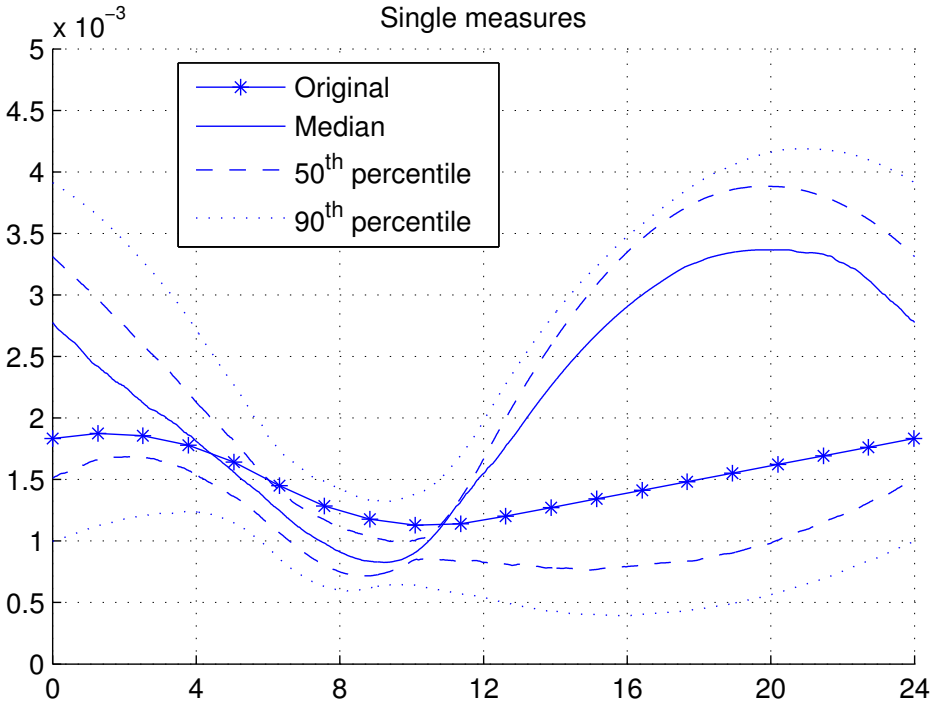

FIGURE 7.7: *50^{th} and 90^{th} percentiles for recovered insulin sensitivity profiles using pre-meal measures only. The black line shows the true insulin sensitivity profile.*

variability induced by sparse and noisy data. Figure 7.8 shows the level of improvement associated with increasing the dataset from 1 to 4 days. N=1000 simulations were run for each period with 10% noise on both BG and nutrition. Bias, as suggested by asymmetric error distributions, was slightly increased with longer periods, and 4 days worth of data showed the largest reduction in the width of the error distribution. The sparsity of data and high noise was reflected in the wide error band.

7.3.5 Effect of measurement noise

Figure 7.9 shows the increasing error in S_I as noise in BG is increased from 0% to 20% for 4 days of data. Noise in meal size was set to 20%, and N=1000 iterations were run for each BG noise level. The effect of noise in nutrition is significant even without noise in BG measurements. Additionally, an increased data set can offset noise to the extent

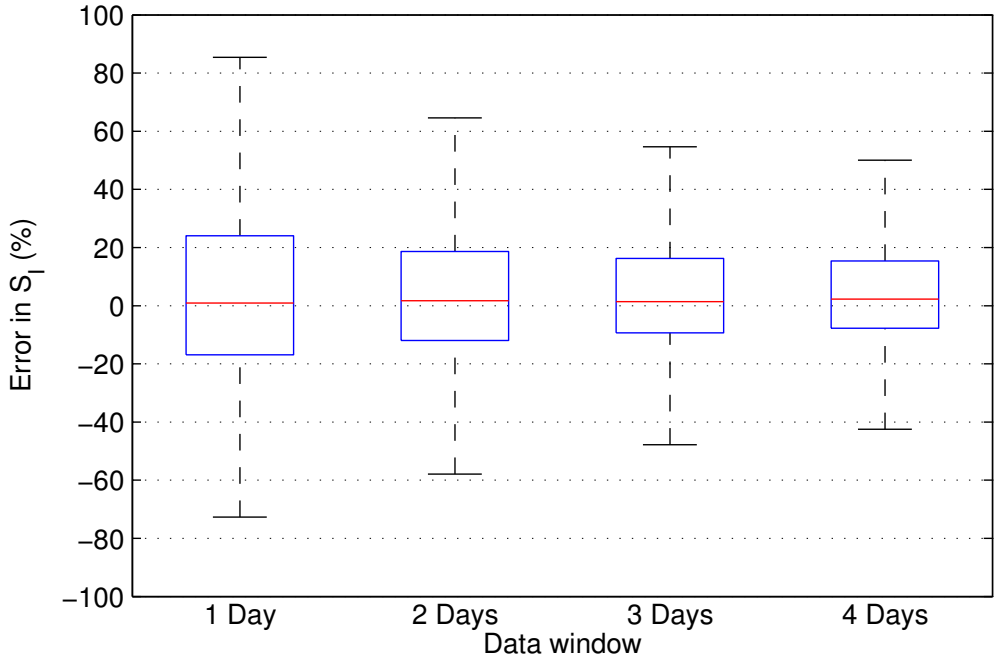

FIGURE 7.8: *Effect of increased measurement windows.*

that 20% noise on BG and nutrition with 4 days of data has a smaller IQR than 1 day of 10% noise on both factors, as seen in Figure 7.8. However, increasing the nutrition noise level appears to increase the offset.

7.4 Discussion

Chapter 2 demonstrated that an insulin sensitivity profile can be identified using real data and the presented methodology in an ICU setting. This setting provides an upper limit on data quality, with highly regulated inputs and intensive oversight. Moving beyond this setting involves increasing noise and decreasing measurement density, but the individuals in question are more metabolically stable. This chapter focuses on the properties of the diurnal S_I profile recovered using this methodology under these conditions.

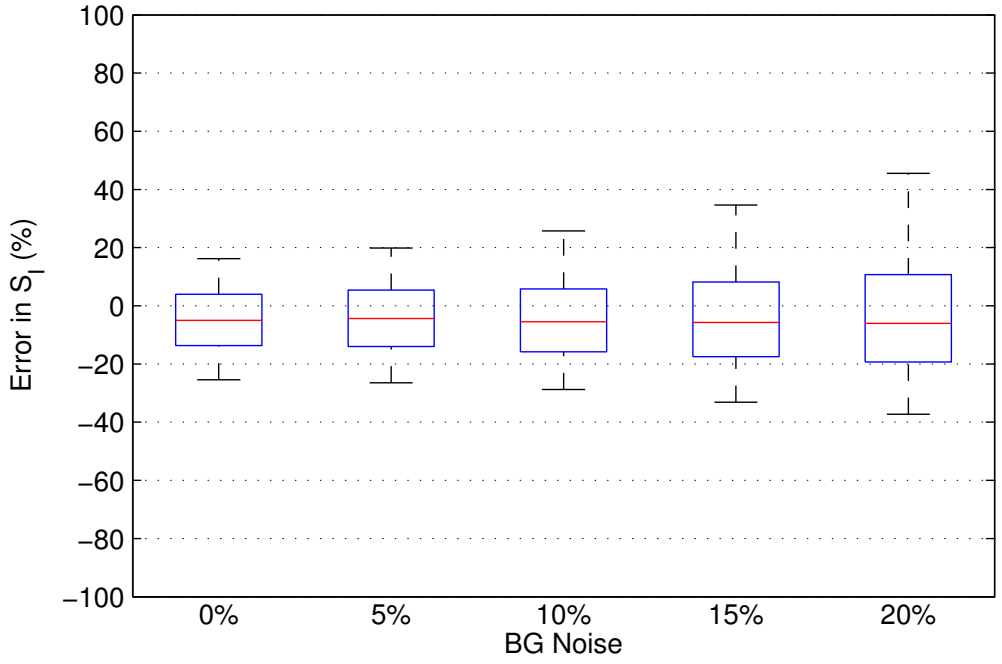

FIGURE 7.9: *Effect of increased measurement noise.*

This *in-silico* testing demonstrates that the insulin sensitivity profile tracks the true profile used when generating the virtual data. The simulation work is not intended as a proof of concept, as neither the scenario (singular T1DM virtual patient with identical daily routines) or noise sources (only BG and nutrition) can be considered representative. However, this work builds confidence in the stability of the methodology, and the inherent ability to retrieve the original signal using a noisy dataset and the model-based assumptions. It also gives an understanding of how the day-to-day insulin sensitivity profile might vary as a function of noise, as opposed to changes in diurnal rhythms themselves. Furthermore, the low error using 4 days of data supports the validity of the insulin sensitivity profiles fit in Chapter 6.

The methodology is not intended as a descriptive modelling process, but instead is intended to be used in a decision-support context. With this in mind, the true endpoint has not been addressed in this work, namely how noise in the data translates into altered

recommendations. Consequently, use of criteria such as prediction error would only be a surrogate for this translation, and would be misleading. This omission is fully justified, as virtual trials without clinical data rely too heavily on model-based assumptions, and bias the results in favour of the algorithm. A non-parametric methodology would have to be adopted, where a bank of appearance profiles from nutrition and insulin were taken from literature and superimposed to generate compartmental solutions that can then be processed by the fitting methodology. Any other approach disguises structural assumptions, and even such a methodology may be impossible due to the non-linearity of the physiological processes. Taken in context, however, this work demonstrates that the insulin sensitivity profile fitted using the presented methodology is not simply a fanciful result, even in the face of high noise.

The *in-silico* work is therefore vital, and it is important the underlying assumptions are both understood and discussed. Firstly, insulin appearance profiles are unmodified in any way. As no variation in the time or size of any plasma insulin peak has been considered, robustness to this error has not been investigated. The fitting procedure thus uses the "true" plasma insulin profile, which is permissible under the original intent of demonstrating the validity of the fitting methodology. For similar reasons, the kinetics of nutrition appearance in plasma were not varied. To add noise into the nutrition compartment the size of each meal (as seen by the fitting procedure) was modified. This process reflects the situation in practice, where carbohydrate counting (and therefore the recorded meal size) is notoriously inaccurate. With regards to the kinetics of insulin and nutrition, mismodelled dynamics will appear as coloured noise in the G_x term, and may be corrected for in practice. Further work would be required to investigate this possibility. The final, and most important, assumption is that plasma glucose follows the kinetics described by the model. This assumption is not inconsequential, and the

reasons for both including and mistrusting this assumption should be plain to all. In practice, this assumption will be negated by comparing the outputs of the decision support procedure using this model to independent decisions made by clinicians, and the resulting outcomes. The validation of model-based prediction thus hinges on real-world outcomes and observations, and a fully *in-silico* study was deemed inadequate.

The ability to track the true insulin sensitivity profile despite bias in the steady-state conditions is one of the major positive outcomes of this work. Perhaps the most important part of insulin therapy is basal insulin replacement, which, as intended, depresses equilibrium glucose concentrations. The consequence is that the fitting procedure either uses an incorrect basal glucose, or adopts a model-based equilibrium point. Steady-state BG relies on both G_b and Q_b, where G_b can be estimated by morning BG readings, and Q_b can be taken directly from the corresponding compartmental solution. Despite the fitting procedure not having access to the "true" set point of $G_b = 8.0; Q_b = 0.0$, the resulting bias shown by Figures 7.8 and 7.9 was negligible.

Finally, use of multiple days of data was shown to help mitigate the effect of high noise and sparse data. Using pre-meal BG only was possible, but the comparison of Figures 7.6 and 7.7 demonstrated reduced accuracy, and Figure 7.5 showed much weaker convergence profiles. However, using both pre- and post- meal BG, multiple days of data improve the fitted insulin sensitivity such that the S_I profile recovered using 1 day of data with 10% noise on BG and nutrition was approximately equivalent to 4 days of data with double this noise level. Naturally, if day-to-day insulin sensitivity varies dramatically in a manner that cannot be statistically adjusted for, the assumption of a static, underlying insulin sensitivity will be invalid and final application impossible. However, current decisions made in day-to-day management of diabetes are made on historical data, and thus truly unpredictable glycaemic responses are unlikely.

7.5 Summary

The presented results prove the validity of the fitting procedure, and demonstrate the stability and accuracy even in the face of sparse data and high noise. Additionally, techniques such as collating multiple days of data can mitigate the effect of high noise. Fitting is even possible using only 3 BG measurements a day, though convergence will take longer, and accuracy reduced. Limitations and assumptions were thoroughly discussed, and while further work is required to investigate how noise translates into modified predictions, the strength of these *in-silico* results suggests further development is warranted.

Chapter 8

Conclusions and Future Work

This body of work lays the foundations for two progressions of model-based heuristic control. Future work should focus on the implementation of these progressions in STAR, and in a new STAR-like algorithm for inpatient/outpatient management of diabetes. Stability and utility of both the fitting and prediction methodologies have been demonstrated throughout, and models have been re-derived to cope with the new scope and likely inputs.

The key contribution of Chapter 2 is a new fitting methodology that no longer requires a regular, rigid piecewise-constant S_I profile. This progression uses an SDE to prevent the regularised basis compromising predictive capability, and despite the added complexity can be interpreted as a generalisation of the original fitting method. Inclusion of an SDE improves fitting around unmodelled dynamics, and further analysis of trends in this noise profile may shed light on areas where the model can be improved. Further analysis of the *b-spline* basis profile should also be carried out to justify the optimal knot width for use in real-time control.

Implementing an SDE complicated prediction, as two independent parameters now exist. Additionally, the G_x profile was irregular and the S_I profile continuous, requiring separate treatment when generating a prediction. Finally, relatively simple non-parametric prediction was desired, as low computational burden may allow predictions to be updated with patient-specific data, a key weakness in STAR. Each of these aims was met in Chapter 3, and a marked improvement in predictive capability was demonstrated by comparing with the original stochastic method. While the results in this chapter are conclusive in demonstrating an improvement for irregular data, future work should focus on developing a structured method for updating each of the PDF matrices with patient data in real time. Quantifying the improvement in performance and/or safety for longer stay patients would be an important step for justifying the added complexity of patient-specific prediction.

Moving model-based heuristic control beyond the ICU requires models that apply for both settings. In particular, types of exogenous forcing must be adequately modelled before model-based predictions can be generated. To meet this goal, the circulating insulin/glucose system model was re-derived with a new structure in Chapter 4. The new model showed much stronger descriptive capability when simulating both insulin infusions and boluses, and insulin clearances were restricted to physiologically relevant rates for each site. The new model was used in conjunction with a unified subcutaneous insulin absorption model to describe the absorption of 4 major subcutaneous insulin preparations in Chapter 5. The resulting model included subcutaneous insulin degradation at the local injection site within the reported range, and thus the two re-derived models can adequately describe subcutaneous dynamics as well as IV infusions and boluses.

Chapter 6 then unified the new models and fitting methodologies into a methodology for recovering diurnal S_I profiles from real-world "diary" style data. The validity of these

profiles was then investigated in a large monte-carlo simulation in Chapter 7. This chapter investigated the ability of the overall structure to recover diurnal S_I profiles in the presence of sparse data and noise. Results from each stage in the simulation were used to select convergence criteria and optimal measurement times, as well as elucidate the effect of measurement density, measurement noise, and quantify the improvement associated with increased data. Overall, this simulation demonstrated that typical "diary" style data can be used to identify relevant parameters despite extremely high uncertainty and sparse, noisy measurements.

8.1 Future direction

The first focus should be on improving the STAR algorithm. While the algorithm is currently working well, Chapter 3 demonstrates the negative effect irregular data has on prediction. The new fitting and prediction methods of Chapters 2 and 3 provide a solution, and have been demonstrated to provide more consistent predictions. Thus, this work provides an opportunity to iteratively improve STAR, and potentially allow patient-specific stochastic model predictions.

Additionally, the results presented in this work validate the S_I profile that can be fitted from typical diabetic "diary" data. Future work should thus focus on development of a decision support algorithm that implements these methodologies, generates predictions, and uses these predictions to optimise both prandial and basal subcutaneous insulin regimes. This development should focus on an in-patient, hospital ward setting to validate any algorithms, as high supervision relative to an outpatient setting will provide much improved safety. The methodologies developed here have the potential to provide

all the tools necessary to develop a low-cost solution for managing BG in an outpatient setting.

Bibliography

[1] American Diabetes Association. Diagnosis and classification of diabetes mellitus. *Diabetes Care*, 36 Suppl 1:S67–S74, Jan 2013.

[2] Michael Brownlee. The pathobiology of diabetic complications: a unifying mechanism. *Diabetes*, 54(6):1615–1625, Jun 2005.

[3] Saikrishna Yendamuri, Gerard J. Fulda, and Glen H. Tinkoff. Admission hyperglycemia as a prognostic indicator in trauma. *J Trauma*, 55(1):33–38, Jul 2003. doi: 10.1097/01.TA.0000074434.39928.72. URL http://dx.doi.org/10.1097/01.TA.0000074434.39928.72.

[4] K. C. McCowen, A. Malhotra, and B. R. Bistrian. Stress-induced hyperglycemia. *Crit Care Clin*, 17(1):107–124, Jan 2001.

[5] J. P. Flatt. Use and storage of carbohydrate and fat. *Am J Clin Nutr*, 61(4 Suppl): 952S–959S, Apr 1995.

[6] H Freeze. *Essentials of Glycobiology*, chapter 6. Cold Spring Harbor Laboratory Press, 2009. URL http://www.ncbi.nlm.nih.gov/books/NBK20703/.

[7] J. E. Gerich, C. Meyer, H. J. Woerle, and M. Stumvoll. Renal gluconeogenesis: its importance in human glucose homeostasis. *Diabetes Care*, 24(2):382–391, Feb 2001.

[8] J. E. Gerich, M. Lorenzi, S. Hane, G. Gustafson, R. Guillemin, and P. H. Forsham. Evidence for a physiologic role of pancreatic glucagon in human glucose homeostasis: studies with somatostatin. *Metabolism*, 24(2):175–182, Feb 1975.

[9] M. Roden, G. Perseghin, K. F. Petersen, J. H. Hwang, G. W. Cline, K. Gerow, D. L. Rothman, and G. I. Shulman. The roles of insulin and glucagon in the regulation of hepatic glycogen synthesis and turnover in humans. *J Clin Invest*, 97(3):642–648, Feb 1996. doi: 10.1172/JCI118460. URL http://dx.doi.org/10.1172/JCI118460.

[10] A. R. Saltiel and C. R. Kahn. Insulin signalling and the regulation of glucose and lipid metabolism. *Nature*, 414(6865):799–806, Dec 2001. doi: 10.1038/414799a. URL http://dx.doi.org/10.1038/414799a.

[11] Frank B. Hu. Globalization of diabetes: the role of diet, lifestyle, and genes. *Diabetes Care*, 34(6):1249–1257, Jun 2011. doi: 10.2337/dc11-0442. URL http://dx.doi.org/10.2337/dc11-0442.

[12] Philip E. Cryer, Stephen N. Davis, and Harry Shamoon. Hypoglycemia in diabetes. *Diabetes Care*, 26(6):1902–1912, Jun 2003.

[13] James Stephen Krinsley. Association between hyperglycemia and increased hospital mortality in a heterogeneous population of critically ill patients. *Mayo Clin Proc*, 78(12):1471–1478, Dec 2003. doi: 10.4065/78.12.1471. URL http://dx.doi.org/10.4065/78.12.1471.

[14] Donald E G. Griesdale, Russell J. de Souza, Rob M. van Dam, Daren K. Heyland, Deborah J. Cook, Atul Malhotra, Rupinder Dhaliwal, William R. Henderson, Dean R. Chittock, Simon Finfer, and Daniel Talmor. Intensive insulin therapy and mortality among critically ill patients: a meta-analysis including nice-sugar study data. *CMAJ*, 180(8):821–827, Apr 2009. doi: 10.1503/cmaj.090206. URL http://dx.doi.org/10.1503/cmaj.090206.

[15] Moritoki Egi, Rinaldo Bellomo, Edward Stachowski, Craig J. French, and Graeme Hart. Variability of blood glucose concentration and short-term mortality in critically ill patients. *Anesthesiology*, 105(2):244–252, Aug 2006.

[16] James S. Krinsley. Glycemic variability: a strong independent predictor of mortality in critically ill patients. *Crit Care Med*, 36(11):3008–3013, Nov 2008. doi: 10.1097/CCM.0b013e31818b38d2. URL http://dx.doi.org/10.1097/CCM.0b013e31818b38d2.

[17] Sean M. Bagshaw, Rinaldo Bellomo, Michael J. Jacka, Moritoki Egi, Graeme K. Hart, Carol George, and A. N. Z. I. C. S C. O. R. E Management Committee . The impact of early hypoglycemia and blood glucose variability on outcome in critical illness. *Crit Care*, 13(3):R91, 2009.

[18] Dawn E. DeWitt and Irl B. Hirsch. Outpatient insulin therapy in type 1 and type 2 diabetes mellitus: scientific review. *JAMA*, 289(17):2254–2264, May 2003.

[19] W Kenneth Ward, Jessica R. Castle, and Joseph El Youssef. Safe glycemic management during closed-loop treatment of type 1 diabetes: the role of glucagon, use of multiple sensors, and compensation for stress hyperglycemia. *J Diabetes Sci Technol*, 5(6):1373–1380, Nov 2011.

[20] G. van den Berghe, P. Wouters, F. Weekers, C. Verwaest, F. Bruyninckx, M. Schetz, D. Vlasselaers, P. Ferdinande, P. Lauwers, and R. Bouillon. Intensive insulin therapy in critically ill patients. *N Engl J Med*, 345(19):1359–1367, Nov 2001. doi: 10.1056/NEJMoa011300. URL http://dx.doi.org/10.1056/NEJMoa011300.

[21] James Stephen Krinsley. Effect of an intensive glucose management protocol on the mortality of critically ill adult patients. *Mayo Clin Proc*, 79(8):992–1000, Aug 2004. doi: 10.4065/79.8.992. URL http://dx.doi.org/10.4065/79.8.992.

[22] J Geoffrey Chase, Geoffrey Shaw, Aaron Le Compte, Timothy Lonergan, Michael Willacy, Xing-Wei Wong, Jessica Lin, Thomas Lotz, Dominic Lee, and Christopher Hann. Implementation and evaluation of the sprint protocol for tight glycaemic control in critically ill patients: a clinical practice change. *Crit Care*, 12(2):R49, 2008. doi: 10.1186/cc6868. URL http://dx.doi.org/10.1186/cc6868.

[23] Frank M. Brunkhorst, Christoph Engel, Frank Bloos, Andreas Meier-Hellmann, Max Ragaller, Norbert Weiler, Onnen Moerer, Matthias Gruendling, Michael Oppert, Stefan Grond, Derk Olthoff, Ulrich Jaschinski, Stefan John, Rolf Rossaint, Tobias Welte, Martin Schaefer, Peter Kern, Evelyn Kuhnt, Michael Kiehntopf, Christiane Hartog, Charles Natanson, Markus Loeffler, Konrad Reinhart, and German Competence Network Sepsis (SepNet) . Intensive insulin therapy and pentastarch resuscitation in severe sepsis. *N Engl J Med*, 358(2):125–139, Jan 2008.

[24] Simon Finfer, Dean R. Chittock, Steve Yu-Shuo Su, Deborah Blair, Denise Foster, Vinay Dhingra, Rinaldo Bellomo, Deborah Cook, Peter Dodek, William R. Henderson, Paul C. Hbert, Stephane Heritier, Daren K. Heyland, Colin McArthur, Ellen McDonald, Imogen Mitchell, John A. Myburgh, Robyn Norton, Julie Potter, Bruce G. Robinson, and Juan J. Ronco. Intensive versus conventional glucose control in critically ill patients. *N Engl J Med*, 360(13):1283–1297, Mar 2009. doi: 10.1056/NEJMoa0810625. URL http://dx.doi.org/10.1056/NEJMoa0810625.

[25] Michael P. Casaer, Dieter Mesotten, Greet Hermans, Pieter J. Wouters, Miet Schetz, Geert Meyfroidt, Sophie Van Cromphaut, Catherine Ingels, Philippe Meersseman, Jan Muller, Dirk Vlasselaers, Yves Debaveye, Lars Desmet, Jasperina Dubois, Aime Van Assche, Simon Vanderheyden, Alexander Wilmer, and Greet Van den Berghe. Early versus late parenteral nutrition in critically ill adults. *N Engl J Med*, 365(6):506–517, Aug 2011. doi: 10.1056/NEJMoa1102662. URL http://dx.doi.org/10.1056/NEJMoa1102662.

[26] Iain Mackenzie, Susan Ingle, Suhail Zaidi, and Simon Buczaski. Tight glycaemic control: a survey of intensive care practice in large english hospitals. *Intensive*

Care Med, 31(8):1136, Aug 2005. doi: 10.1007/s00134-005-2677-2. URL http://dx.doi.org/10.1007/s00134-005-2677-2.

[27] Daleen Aragon. Evaluation of nursing work effort and perceptions about blood glucose testing in tight glycemic control. *Am J Crit Care*, 15(4):370–377, Jul 2006.

[28] J Geoffrey Chase, Steen Andreassen, Karsten Jensen, and Geoffrey M. Shaw. Impact of human factors on clinical protocol performance: a proposed assessment framework and case examples. *J Diabetes Sci Technol*, 2(3):409–416, May 2008.

[29] Jean-Charles Preiser, Philippe Devos, Sergio Ruiz-Santana, Christian Mlot, Djillali Annane, Johan Groeneveld, Gaetano Iapichino, Xavier Leverve, Grard Nitenberg, Pierre Singer, Jan Wernerman, Michael Joannidis, Adela Stecher, and Ren Chiolro. A prospective randomised multi-centre controlled trial on tight glucose control by intensive insulin therapy in adult intensive care units: the glucontrol study. *Intensive Care Med*, 35(10):1738–1748, Oct 2009. doi: 10.1007/s00134-009-1585-2. URL http://dx.doi.org/10.1007/s00134-009-1585-2.

[30] Susan S. Braithwaite, Renee Edkins, Kathy L. Macgregor, Edward S. Sredzienski, Michael Houston, Ben Zarzaur, Preston B. Rich, Bernard Benedetto, and Edmund J. Rutherford. Performance of a dose-defining insulin infusion protocol among trauma service intensive care unit admissions. *Diabetes Technol Ther*, 8(4):476–488, Aug 2006. doi: 10.1089/dia.2006.8.476. URL http://dx.doi.org/10.1089/dia.2006.8.476.

[31] Frederick Chee, Tyrone L. Fernando, Andrey V. Savkin, and Vernon van Heeden. Expert pid control system for blood glucose control in critically ill patients. *IEEE Trans Inf Technol Biomed*, 7(4):419–425, Dec 2003.

[32] Roman Hovorka, Valentina Canonico, Ludovic J. Chassin, Ulrich Haueter, Massimo Massi-Benedetti, Marco Orsini Federici, Thomas R. Pieber, Helga C. Schaller, Lukas Schaupp, Thomas Vering, and Malgorzata E. Wilinska. Nonlinear model predictive control of glucose concentration in subjects with type 1 diabetes. *Physiol Meas*, 25 (4):905–920, Aug 2004.

[33] Jeremy J. Cordingley, Dirk Vlasselaers, Natalie C. Dormand, Pieter J. Wouters, Stephen D. Squire, Ludovic J. Chassin, Malgorzata E. Wilinska, Clifford J. Morgan, Roman Hovorka, and Greet Van den Berghe. Intensive insulin therapy: enhanced model predictive control algorithm versus standard care. *Intensive Care Med*, 35(1): 123–128, Jan 2009. doi: 10.1007/s00134-008-1236-z. URL http://dx.doi.org/10.1007/s00134-008-1236-z.

[34] Liam M. Fisk, Aaron J. Le Compte, Geoffrey M. Shaw, Sophie Penning, Thomas Desaive, and J Geoffrey Chase. Star development and protocol comparison. *IEEE Trans Biomed Eng*, 59(12):3357–3364, Dec 2012. doi: 10.1109/TBME.2012.2214384. URL http://dx.doi.org/10.1109/TBME.2012.2214384.

[35] J Geoffrey Chase, Fatanah Suhaimi, Sophie Penning, Jean-Charles Preiser, Aaron J Le Compte, Jessica Lin, Christopher G Pretty, Geoffrey M Shaw, Katherine T Moorhead, and Thomas Desaive. Validation of a model-based virtual trials method for tight glycemic control in intensive care. *Biomed Eng Online*, 9:84, 2010.

[36] Gretchen Perilli, Christine Saraceni, Michael N Daniels, and Aakif Ahmad. Diabetic ketoacidosis: A review and update. *Current Emergency and Hospital Medicine Reports*, 1(1):10–17, 2013.

[37] J. Geoffrey Chase, Steen Andreassen, Ulrike Pielmeier, Christopher E. Hann, Kirsten A. McAuley, and J.I. Mann. A glucose-insulin pharmacodynamic surface modeling validation and comparison of metabolic system models. *Biomedical Signal Processing and Control*, 4(4):355 – 363, 2009. ISSN 1746-8094. doi: http://dx.doi.org/10.1016/j.bspc.2009.04.002. URL http://www.sciencedirect.com/science/article/pii/S1746809409000433. Special Issue on Biomedical Systems, Signals and Control Extended Selected papers from the {IFAC} World Congress, Seoul, July 2008.

[38] Paul D Docherty, J. Geoffrey Chase, Thomas F Lotz, and Thomas Desaive. A graphical method for practical and informative identifiability analyses of physiological models: a case study of insulin kinetics and sensitivity. *Biomed Eng Online*, 10:39, 2011. doi: 10.1186/1475-925X-10-39. URL http://dx.doi.org/10.1186/1475-925X-10-39.

[39] Christopher E. Hann, J Geoffrey Chase, Jessica Lin, Thomas Lotz, Carmen V. Doran, and Geoffrey M. Shaw. Integral-based parameter identification for long-term dynamic verification of a glucose-insulin system model. *Comput Methods Programs Biomed*, 77(3):259–270, Mar 2005. doi: 10.1016/j.cmpb.2004.10.006. URL http://dx.doi.org/10.1016/j.cmpb.2004.10.006.

[40] Jessica Lin, Normy N. Razak, Christopher G. Pretty, Aaron Le Compte, Paul Docherty, Jacquelyn D. Parente, Geoffrey M. Shaw, Christopher E. Hann, and J. Geoffrey Chase. A physiological intensive control insulin-nutrition-glucose (icing) model validated in critically ill patients. *Comput Methods Programs Biomed*, 102 (2):192–205, May 2011. doi: 10.1016/j.cmpb.2010.12.008. URL http://dx.doi.org/10.1016/j.cmpb.2010.12.008.

[41] Christopher G Pretty. *Analysis, classification and management of insulin sensitivity variability in a glucose-insulin system model for critical illness*. PhD thesis, University of Canterbury, 2012. URL http://hdl.handle.net/10092/6580.

[42] Paul D Docherty, J. Geoffrey Chase, and Timothy David. Characterisation of the iterative integral parameter identification method. *Med Biol Eng Comput*, 50(2): 127–134, Feb 2012. doi: 10.1007/s11517-011-0851-y. URL http://dx.doi.org/10.1007/s11517-011-0851-y.

[43] Carl De Boor. On calculating with B-splines. *Journal of Approximation Theory*, 6 (1):50–62, 1972.

[44] J Geoffrey Chase, Aaron J Le Compte, Fatanah Suhaimi, Geoffrey M Shaw, Adrienne Lynn, Jessica Lin, Christopher G Pretty, Normy Razak, Jacquelyn D Parente, Christopher E Hann, et al. Tight glycemic control in critical care–the leading role of insulin sensitivity and patient variability: a review and model-based analysis. *Computer methods and programs in biomedicine*, 102(2):156–171, 2011. URL http://www.sciencedirect.com/science/article/pii/S0169260710002828.

[45] Christopher G. Pretty, Aaron J. Le Compte, J Geoffrey Chase, Geoffrey M. Shaw, Jean-Charles Preiser, Sophie Penning, and Thomas Desaive. Variability of insulin sensitivity during the first 4 days of critical illness: implications for tight glycemic control. *Ann Intensive Care*, 2(1):17, 2012. doi: 10.1186/2110-5820-2-17. URL http://dx.doi.org/10.1186/2110-5820-2-17.

[46] Tamás Ferenci, Balazs Benyo, Levente Kovács, Liam Fisk, Geoffrey M Shaw, and J Geoffrey Chase. Daily evolution of insulin sensitivity variability with respect to diagnosis in the critically ill. *PloS one*, 8(2):e57119, 2013.

[47] Anders Thorell, Olav Rooyackers, Peter Myrenfors, Mattias Soop, Jonas Nygren, and Olle H. Ljungqvist. Intensive insulin treatment in critically ill trauma patients normalizes glucose by reducing endogenous glucose production. *J Clin Endocrinol Metab*, 89(11):5382–5386, Nov 2004. doi: 10.1210/jc.2004-1118. URL http://dx.doi.org/10.1210/jc.2004-1118.

[48] Nicolaas G Van Kampen. Stochastic differential equations. *Physics reports*, 24(3): 171–228, 1976. URL http://www.sciencedirect.com/science/article/pii/0370157376900296.

[49] Jessica Lin, Dominic Lee, J Geoffrey Chase, Geoffrey M. Shaw, Aaron Le Compte, Thomas Lotz, Jason Wong, Timothy Lonergan, and Christopher E. Hann. Stochastic modelling of insulin sensitivity and adaptive glycemic control for critical care.

Comput Methods Programs Biomed, 89(2):141–152, Feb 2008. doi: 10.1016/j.cmpb.2007.04.006. URL http://dx.doi.org/10.1016/j.cmpb.2007.04.006.

[50] Ror Bellman and KJ Åström. On structural identifiability. *Mathematical Biosciences*, 7(3):329–339, 1970. URL http://www.sciencedirect.com/science/article/pii/002555647090132X.

[51] M. Berger, H. J. Cppers, H. Hegner, V. Jrgens, and P. Berchtold. Absorption kinetics and biologic effects of subcutaneously injected insulin preparations. *Diabetes Care*, 5(2):77–91, 1982.

[52] W. C. Duckworth, R. G. Bennett, and F. G. Hamel. Insulin degradation: progress and potential. *Endocr Rev*, 19(5):608–624, Oct 1998.

[53] Paul D. Docherty, J Geoffrey Chase, Lisa Te Morenga, Thomas F. Lotz, Juliet E. Berkeley, Geoffrey M. Shaw, Kirsten A. McAuley, and Jim I. Mann. A spectrum of dynamic insulin sensitivity test protocols. *J Diabetes Sci Technol*, 5(6):1499–1508, Nov 2011.

[54] G. M. Ward, J. M. Walters, J. Barton, F. P. Alford, and R. C. Boston. Physiologic modeling of the intravenous glucose tolerance test in type 2 diabetes: a new approach to the insulin compartment. *Metabolism*, 50(5):512–519, May 2001. doi: 10.1053/meta.2001.21029. URL http://dx.doi.org/10.1053/meta.2001.21029.

[55] Aleksey V. Matveyenko, David Liuwantara, Tatyana Gurlo, David Kirakossian, Chiara Dalla Man, Claudio Cobelli, Morris F. White, Kyle D. Copps, Elena Volpi, Satoshi Fujita, and Peter C. Butler. Pulsatile portal vein insulin delivery enhances hepatic insulin action and signaling. *Diabetes*, 61(9):2269–2279, Sep 2012. doi: 10.2337/db11-1462. URL http://dx.doi.org/10.2337/db11-1462.

[56] E. Ferrannini, J. Wahren, O. K. Faber, P. Felig, C. Binder, and R. A. DeFronzo. Splanchnic and renal metabolism of insulin in human subjects: a dose-response study. *Am J Physiol*, 244(6):E517–E527, Jun 1983.

[57] R. Rabkin, N. M. Simon, S. Steiner, and J. A. Colwell. Effect of renal disease on renal uptake and excretion of insulin in man. *N Engl J Med*, 282(4):182–187, Jan 1970. doi: 10.1056/NEJM197001222820402. URL http://dx.doi.org/10.1056/NEJM197001222820402.

[58] Jason Wong, J. Geoffrey Chase, Christopher E Hann, Geoffrey M Shaw, Thomas F Lotz, Jessica Lin, and Aaron J Le Compte. A subcutaneous insulin pharmacokinetic model for computer simulation in a diabetes decision support role: validation and simulation. *J Diabetes Sci Technol*, 2(4):672–680, Jul 2008.

[59] Soffia Gudbjrnsdttir, Mikaela Sjstrand, Lena Strindberg, John Wahren, and Peter Lnnroth. Direct measurements of the permeability surface area for insulin and glucose in human skeletal muscle. *J Clin Endocrinol Metab*, 88(10):4559–4564, Oct 2003.

[60] Emma M. Eggleston, Linda A. Jahn, and Eugene J. Barrett. Hyperinsulinemia rapidly increases human muscle microvascular perfusion but fails to increase muscle insulin clearance: evidence that a saturable process mediates muscle insulin uptake. *Diabetes*, 56(12):2958–2963, Dec 2007. doi: 10.2337/db07-0670. URL http://dx.doi.org/10.2337/db07-0670.

[61] P. J. Hurley. Red cell and plasma volumes in normal adults. *J Nucl Med*, 16(1): 46–52, Jan 1975.

[62] T. M. Barratt and M. Walser. Extracellular fluid in individual tissues and in whole animals: the distribution of radiosulfate and radiobromide. *J Clin Invest*, 48(1): 56–66, Jan 1969. doi: 10.1172/JCI105974. URL http://dx.doi.org/10.1172/JCI105974.

[63] B. Linde and G. Chisolm. The interstitial space of adipose tissue as determined by single injection and equilibration techniques. *Acta Physiol Scand*, 95(4):383–390, Dec 1975.

[64] Dylan Thompson, Fredrik Karpe, Max Lafontan, and Keith Frayn. Physical activity and exercise in the regulation of human adipose tissue physiology. *Physiol Rev*, 92 (1):157–191, Jan 2012. doi: 10.1152/physrev.00012.2011. URL http://dx.doi.org/10.1152/physrev.00012.2011.

[65] I. Janssen, S. B. Heymsfield, Z. M. Wang, and R. Ross. Skeletal muscle mass and distribution in 468 men and women aged 18-88 yr. *J Appl Physiol*, 89(1):81–88, Jul 2000.

[66] A Michael Peters, Laura Perry, Claire A. Hooker, Bethany Howard, Mark D J. Neilly, Nagabhushan Seshadri, Ravin Sobnack, Andrew Irwin, Hayley Snelling, Thomas Gruning, Neva H. Patel, Richard S. Lawson, Gregory Shabo, Nigel Williams, Surendra Dave, and Mark C. Barnfield. Extracellular fluid volume and glomerular filtration rate in 1878 healthy potential renal transplant donors: effects of age, gender, obesity and scaling. *Nephrol Dial Transplant*, 27(4):1429–1437, Apr 2012. doi: 10.1093/ndt/gfr479. URL http://dx.doi.org/10.1093/ndt/gfr479.

[67] K. M. Carlisle, M. Halliwell, A. E. Read, and P. N. Wells. Estimation of total hepatic blood flow by duplex ultrasound. *Gut*, 33(1):92–97, Jan 1992.

[68] R. E. Schmieder, A. H. Beil, H. Weihprecht, and F. H. Messerli. How should renal hemodynamic data be indexed in obesity? *J Am Soc Nephrol*, 5(9):1709–1713, Mar 1995.

[69] B. Thorsteinsson. Kinetic models for insulin disappearance from plasma in man. *Dan Med Bull*, 37(2):143–153, Apr 1990.

[70] M. Sjstrand, A. Holmng, and P. Lnnroth. Measurement of interstitial insulin in human muscle. *Am J Physiol*, 276(1 Pt 1):E151–E154, Jan 1999.

[71] M. Sjstrand, A. Holmng, L. Strindberg, and P. Lnnroth. Estimations of muscle interstitial insulin, glucose, and lactate in type 2 diabetic subjects. *Am J Physiol Endocrinol Metab*, 279(5):E1097–E1103, Nov 2000.

[72] E. Van Cauter, F. Mestrez, J. Sturis, and K. S. Polonsky. Estimation of insulin secretion rates from c-peptide levels. comparison of individual and standard kinetic parameters for c-peptide clearance. *Diabetes*, 41(3):368–377, Mar 1992.

[73] L Te Morenga, S. Williams, R. Brown, and J. Mann. Effect of a relatively high-protein, high-fiber diet on body composition and metabolic risk factors in overweight women. *Eur J Clin Nutr*, 64(11):1323–1331, Nov 2010. doi: 10.1038/ejcn.2010.163. URL http://dx.doi.org/10.1038/ejcn.2010.163.

[74] Kirsten A McAuley, Juliet E Berkeley, Paul D Docherty, Thomas F Lotz, Lisa A Te Morenga, Geoff M Shaw, Sheila M Williams, J. Geoffrey Chase, and Jim I Mann. The dynamic insulin sensitivity and secretion test–a novel measure of insulin sensitivity. *Metabolism*, 60(12):1748–1756, Dec 2011. doi: 10.1016/j.metabol.2011.05.009. URL http://dx.doi.org/10.1016/j.metabol.2011.05.009.

[75] Jeremy D. Krebs, Damon Bell, Rosemary Hall, Amber Parry-Strong, Paul D. Docherty, Kristen Clarke, and J Geoffry Chase. Improvements in glucose metabolism and insulin sensitivity with a low-carbohydrate diet in obese patients with type 2 diabetes. *J Am Coll Nutr*, 32(1):11–17, 2013. doi: 10.1080/07315724.2013.767630. URL http://dx.doi.org/10.1080/07315724.2013.767630.

[76] E. Mosekilde, K. S. Jensen, C. Binder, S. Pramming, and B. Thorsteinsson. Modeling absorption kinetics of subcutaneous injected soluble insulin. *J Pharmacokinet Biopharm*, 17(1):67–87, Feb 1989.

[77] G. Nucci and C. Cobelli. Models of subcutaneous insulin kinetics. a critical review. *Comput Methods Programs Biomed*, 62(3):249–257, Jul 2000.

[78] Jiaxu Li and James D. Johnson. Mathematical models of subcutaneous injection of insulin analogues: A mini-review. *Discrete Continuous Dyn Syst Ser B*, 12(2):

401–414, Sep 2009. doi: 10.3934/dcdsb.2009.12.401. URL http://dx.doi.org/10.3934/dcdsb.2009.12.401.

[79] S. Kang, J. Brange, A. Burch, A. Vlund, and D. R. Owens. Subcutaneous insulin absorption explained by insulin's physicochemical properties. evidence from absorption studies of soluble human insulin and insulin analogues in humans. *Diabetes Care*, 14(11):942–948, Nov 1991.

[80] E. W. Kraegen, D. J. Chisholm, and M. J. Hewett. Comparison of plateau insulin levels achieved by intravenous or subcutaneous insulin infusion: evidence for low rates of subcutaneous degradation. *Diabetes Care*, 6(2):118–121, 1983.

[81] R. W. Stevenson, T. I. Tsakok, and J. A. Parsons. Matched glucose responses to insulin administered subcutaneously and intravenously. evidence for subcutaneous inactivation of insulin. *Diabetologia*, 18(5):423–426, May 1980.

[82] Jason Wong, J. Geoffrey Chase, Christopher E Hann, Geoffrey M Shaw, Thomas F Lotz, Jessica Lin, and Aaron J Le Compte. A subcutaneous insulin pharmacokinetic model for computer simulation in a diabetes decision support role: model structure and parameter identification. *J Diabetes Sci Technol*, 2(4):658–671, Jul 2008a.

[83] T. Kobayashi, S. Sawano, T. Itoh, K. Kosaka, H. Hirayama, and Y. Kasuya. The pharmacokinetics of insulin after continuous subcutaneous infusion or bolus subcutaneous injection in diabetic patients. *Diabetes*, 32(4):331–336, Apr 1983.

[84] C. Tarn, E. Teufel, J. Pic, J. Bondia, and H-J. Pfleiderer. Comprehensive pharmacokinetic model of insulin glargine and other insulin formulations. *IEEE Trans Biomed Eng*, 52(12):1994–2005, Dec 2005. doi: 10.1109/TBME.2005.857681. URL http://dx.doi.org/10.1109/TBME.2005.857681.

[85] J. Brange, D. R. Owens, S. Kang, and A. Vlund. Monomeric insulins and their experimental and clinical implications. *Diabetes Care*, 13(9):923–954, Sep 1990.

[86] Food and Drug Administration. Insulin aspart clinical pharmacology and biopharmaceutics review(s). Technical report, Center for Drug Evaluation and Research, July 1999. URL http://www.accessdata.fda.gov/drugsatfda_docs/nda/2000/20-986_NovoLog_biopharmr.pdf.

[87] Thomas Danne, Kerstin Lpke, Kerstin Walte, Wolfgang Von Schuetz, and Mari-Anne Gall. Insulin detemir is characterized by a consistent pharmacokinetic profile across age-groups in children, adolescents, and adults with type 1 diabetes. *Diabetes Care*, 26(11):3087–3092, Nov 2003.

[88] L. Heinemann, R. Linkeschova, K. Rave, B. Hompesch, M. Sedlak, and T. Heise. Time-action profile of the long-acting insulin analog insulin glargine (hoe901) in comparison with those of nph insulin and placebo. *Diabetes Care*, 23(5):644–649, May 2000.

[89] Lutz Heinemann. Variability of insulin absorption and insulin action. *Diabetes Technol Ther*, 4(5):673–682, 2002. doi: 10.1089/152091502320798312. URL http://dx.doi.org/10.1089/152091502320798312.

[90] Thomas F Lotz, J. Geoffrey Chase, Kirsten A McAuley, Dominic S Lee, Jessica Lin, Christopher E Hann, and Jim I Mann. Transient and steady-state euglycemic clamp validation of a model for glycemic control and insulin sensitivity testing. *Diabetes Technol Ther*, 8(3):338–346, Jun 2006. doi: 10.1089/dia.2006.8.338. URL http://dx.doi.org/10.1089/dia.2006.8.338.

[91] A. D. Baron, G. Brechtel, P. Wallace, and S. V. Edelman. Rates and tissue sites of non-insulin- and insulin-mediated glucose uptake in humans. *Am J Physiol*, 255(6 Pt 1):E769–E774, Dec 1988.

[92] O. E. Owen, A. P. Morgan, H. G. Kemp, J. M. Sullivan, M. G. Herrera, and GF Cahill, Jr. Brain metabolism during fasting. *J Clin Invest*, 46(10):1589–1595, Oct 1967. doi: 10.1172/JCI105650. URL http://dx.doi.org/10.1172/JCI105650.

[93] Mayumi L. Prins. Cerebral metabolic adaptation and ketone metabolism after brain injury. *J Cereb Blood Flow Metab*, 28(1):1–16, Jan 2008. doi: 10.1038/sj.jcbfm.9600543. URL http://dx.doi.org/10.1038/sj.jcbfm.9600543.

[94] R. A. Rizza, L. J. Mandarino, and J. E. Gerich. Dose-response characteristics for effects of insulin on production and utilization of glucose in man. *Am J Physiol*, 240(6):E630–E639, Jun 1981.

[95] D. A. F. N. E Study Group. Training in flexible, intensive insulin management to enable dietary freedom in people with type 1 diabetes: dose adjustment for normal eating (dafne) randomised controlled trial. *BMJ*, 325(7367):746, Oct 2002.

[96] A. S. Brazeau, H. Mircescu, K. Desjardins, C. Leroux, I. Strychar, J. M. Eko, and R. Rabasa-Lhoret. Carbohydrate counting accuracy and blood glucose variability in adults with type 1 diabetes. *Diabetes Res Clin Pract*, 99(1):19–23, Jan 2013. doi: 10.1016/j.diabres.2012.10.024. URL http://dx.doi.org/10.1016/j.diabres.2012.10.024.